Manufacture and characterization of porous components based on geopolymers for water purification

Candidate: Mattia Muracchioli

Supervisor: Prof. Paolo Colombo

Co-supervisor: Ing.Giorgia Franchin

Department of Industrial Engineering
University of Padua

This dissertation is submitted for the degree of
MSc Materials Engineering

September 2019

I would like to dedicate this thesis to my mom my sister and my girlfriend …

Declaration

I hereby declare that except where specific reference is made to the work of others, the contents of this thesis are original and have not been submitted in whole or in part for consideration for any other degree or qualification in this, or any other university. This thesis is my own work and contains nothing which is the outcome of work done in collaboration with others, except as specified in the text and Acknowledgements.

Candidate: Mattia Muracchioli
September 2019

Acknowledgements

I would first like to thank my thesis advisor Ing.Paolo Colombo of the Department of Industrial Engineering at University of Padua. The door to Prof. Colombo office was always open whenever I ran into a trouble spot or had a question about my research or writing. He consistently allowed this thesis to be my own work, but steered me in the right the direction whenever he thought I needed it.

I would also like to acknowledge Ing.Giorgia Franchin of the Department of Industrial Engineering at University of Padua as the second reader of this thesis, and I am gratefully indebted to her for her very valuable comments on this thesis.

Finally, I must express my very profound gratitude to my mom to my sister and to my girlfriend for providing me with unfailing support and continuous encouragement throughout my years of study. This accomplishment would not have been possible without them. Thank you.

Author

Mattia Muracchioli

Abstract

The activity of this thesis is mainly focused on the production of geopolymer spheres to be inserted inside the fixed bed column for water purification. The choice of geopolymer as a material is justified by the high adsorption capacities shown. Before the laboratory practice, it was necessary to conduct a deep analysis of the theory works previously carried out, to find the correct composition. Once the starting composition was established, it was necessary to resolve all the problems concerning laboratory practice. Through analysis and adaptations of mathematical models, it has been possible to optimize the choice of the inert medium in which the geopolymerization reaction takes place. Through XRD analysis, searching for peaks of unreacted material, it was possible to optimize the reaction time. SEM images made possible to investigate the dimension of the spheres' porosity and through microanalysis, it was possible to ensure the absence of unwanted substances. Through the pycnometer, it was possible to detect the type of porosity, with the final goal of obtaining almost all open porosity to guarantee permeability characteristics. As of last analysis, adsorption tests were carried out at the laboratories of the University of Turin thanks to the collaboration of Professor Mariella Bruzzoniti. The last activity involved the production of geopolymeric ink for DIW printing to obtain structures able to reduce the pressure losses inside the fixed-bed column. The entire activity of the thesis took place at the laboratories of the industrial engineering department of the University of Padua.

Riassunto

L'attività di questa tesi è principalmente focalizzata sulla produzione di sfere di geopolimero da inserire all'interno di colonne a letto fisso per la depurazione delle acque. La scelta del geopolimero come materiale è giustificata dalle elevate capacità di adsorbimento mostrate. Prima della pratica di laboratorio, è stato necessario condurre un'analisi approfondita degli articoli scientifici relativi ad esperimenti simili svolti in precedenza, per trovare la composizione corretta. Una volta stabilita la composizione iniziale, è stato necessario risolvere tutti i problemi relativi alla pratica di laboratorio. Attraverso analisi e adattamenti di modelli matematici, è stato possibile ottimizzare la scelta del mezzo inerte in cui far avvenire la reazione di geopolimerizzazione. Attraverso analisi XRD, alla ricerca di picchi di materiale non reagito, è stato possibile ottimizzare i tempi di reazione. Le immagini SEM hanno reso possibile lo studio della dimensione della porosità delle sfere e, attraverso la microanalisi, è stato possibile garantire l'assenza di sostanze indesiderate. Tramite il picnometro è stato possibile rilevare il tipo di porosità, con l'obiettivo finale di ottenere quasi tutta porosità aperta per garantire le caratteristiche di permeabilità. Come ultima analisi, sono stati effettuati test di adsorbimento presso i laboratori dell'Università di Torino grazie alla collaborazione della professoressa Mariella Bruzzoniti. L'ultima attività ha riguardato la produzione di inchiostro geopolimerico per la stampa DIW per ottenere strutture in grado di ridurre le perdite di carico all'interno della colonna a letto fisso.
L'intera attività della tesi si è svolta presso i laboratori del dipartimento di ingegneria industriale dell'Università di Padova.

Table of contents

List of figures

List of tables

List of Equations

Chapter 1

Introduction to Geopolymer

This chapter aims to introduce the basic theory of geopolymers. Initially, an overview is provided, with further explanation of the terminology and chemical formulas. Subsequently, a description of the chemical characteristics and the geopolymerization mechanism(alkaline route) is given, by focusing on the description of the siloxonate based molecules, siloxane oligomers and sialate silico-aluminate oligomers. Lastly, an overview of the microstructure and mechanical properties is illustrated.

1.1 Overview of Geopolymers

Geopolymers emerged as a result of attempts to model the geological formation of zeolites. Zeolites are microporous crystalline solids with well-defined structures. Generally, they contain silicon, aluminum, and oxygen in their framework and cations, water and/or other molecules within their pores. Because of their unique porous properties, zeolites are used in a variety of applications such as petrochemical cracking, water softening and purification, and in separation and removal of gases and solvents. Many zeolites occur naturally as minerals and are extensively mined in many parts of the world. Others are synthetic, being made commercially for specific uses, or produced by scientists trying to understand more about their chemistry. Victor Glukhovsky is believed to be the first researcher to attempt to model the geological process of zeolite formation, in the 1950s. Zeolites were synthesized by alkali activation of alumino-silicates present in industrial materials or wastes. These novel binders were initially called ‘soil silicates’ [1]. Some authors believe that zeolitic compounds are the final, stable phase of a long term conversion of primary phases to zeolites. This is in accord with investigations on ancient Roman cement that have indicated the presence of amorphous zeolitic compounds [2]. The outstanding durability of ancient Roman cements and Glukhovsky’s work created interest in the potential to produce new, high strength, durable

cementitious materials. The most comprehensive research in this field was conducted by J Davidovits [3], who first applied the term 'geopolymer' to these alkali-activated alumino-silicates. Geopolymers are produced at low temperature, generally below 100 °C. They consist of chains or networks of mineral molecules linked with covalent bonds. Because they are polymers, they should be referred to with polymer terminology, which is very different from the traditional terminology used by ceramicists. For example, the formula of one major clay mineral, kaolinite, is:

- $Al_2O_3\,2\,SiO_2\,2\,H_2O$
- $Si_2O_5Al_2(OH)_4$

From a geopolymer standpoint, J.Davidovits [4] proposed the following generic formula:

$$[\equiv Si - O - Al - [OH]_2]_n$$

with the covalent aluminum hydroxyl side groups

$$[- Al - [OH]_2]$$

branched to the poly(siloxo) hexagonal macromolecule

$$[\equiv Si - O -]_n$$

This polymeric approach has profound consequences concerning a better understanding of the geopolymerization mechanisms. In particular, metakaolin results from the dehydroxylation of the -OH groups in kaolinite, according to the reaction:

$$Si_2O_5Al_2(OH)_4 \longrightarrow Si_2O_5Al_2O_2 + 2\,H_2O$$

The reactive molecule consists of two different aluminosilicate oxides $2\,Si_2O_2Al_2O_3$, namely:

$$[\equiv Si - O - Al = O]_n$$

$$[\equiv Si - O - Al - O -]_n$$

This suggests strong chemical reactivity, as opposed to the traditional way of writing $2\,Si_2O_2Al_2O_3$. The starting raw materials are:

- rock-forming minerals, alumino-silicates,

- amorphous silica,
- and industrial by-products (alumino-silicates) like coal fly ash, blast furnace slag.

A geopolymer could be made by dissolving an aluminosilicate material such as kaolinite in highly alkaline environment such as NaOH or KOH solutions. Figure 1.1 shows geopolymers to be part of the alkali-activated family of cementitious materials, characterized by low calcium content. Geopolymerisation is a process in which silicon, aluminum, and

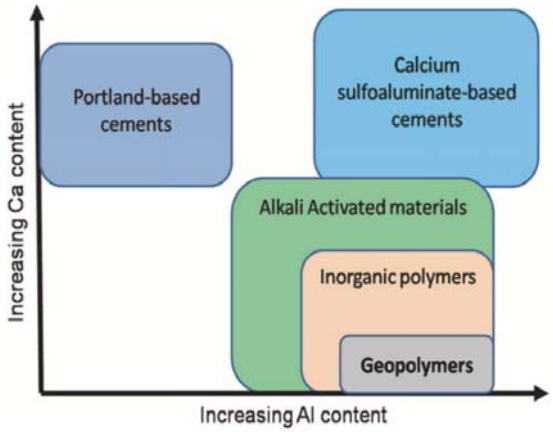

Fig. 1.1 *Overview of geopolymers*

oxygen atoms create a chain of SiO_4 and AlO_4 tetrahedra linked alternatively by shared oxygen atoms. The water to a solid ratio in this process, if no aggregates are used, ranges [5] from 0.3 to 0.4. The products are amorphous to semi-crystalline materials with superior mechanical behaviour [6]. Structural differences and resulting properties of geopolymers can be explained by variation in the source silicon to aluminum amorphous molar ratio, alkali metal cation type and concentration, water content and curing regime amongst other variables in the geopolymer synthesis. The reactants used to form conventional geopolymers are usually metakaolin as the Al-Si source and an activator solution containing reactive silicate anions and alkali cations. The focus of research in this field may be summarised as follows:

- **Al–Si source**: identifying low cost, readily available materials suitable to participate in geopolymerization. It has been shown [7] that a wide range of natural materials and industrial wastes such as kaolin, fly ash, blast furnace slag, alkali- feldspars and tungsten mine waste can be used to make geopolymers
- **alkali activation**: analyzing the effects of pH and alkali ions on process completion and the final properties of the product, e.g. it has been shown that K-feldspars show

increased dissolution in NaOH solution compared with KOH solution, and thus confer higher compressive strength [5]

- **geopolymerisation**: the mechanisms of the reaction have yet to be fully understood; the parameters affecting the process, microstructural reorganization of the source materials and the reaction steps have been studied extensively by analytical methods.

The unique properties of geopolymers such as high early strength, extraordinary durability, resistance to chemical attack, ability to immobilize toxic atoms and environmental benefits such as low energy consumption and carbon dioxide emission in production make geopolymers a strategic material for sustainable development and a serious alternative to Portland cement.

1.2 Geopolymer structure

The following empirical formula has been postulated by Davidovits [8] to describe geopolymers

$$\mathrm{M}_n[-(\mathrm{Si}-\mathrm{O}_2)_z - Al - O]_n \cdot w\mathrm{H}_2\mathrm{O}$$

in wich:

- M is an alkali metal
- z is 1, 2 or 3
- n is the degree of polymerisation

Based on the Si/Al ratio, three monomeric units may be defined:

- Polysialate: **SiO_2/Al_2O_3=2** (Si-O-Al-O-)
- Polysialatesiloxo **SiO_2/Al_2O_3=4** (Si-O-Al-O-Si-O-)
- Polysialatedisiloxo **SiO_2/Al_2O_3=6** (Si-O-Al-O-Si-O-Si-O-)

These structures are composed of AlO_4^- e SiO_4^- tetrahedra. Cations of alkali or alkali earth metals (Na^+, K^+, Ca^{2+}) are required in the structure to balance the negative charge. By dissolving an aluminosilicate powder in alkali solution such as NaOH, first AlO_4^- e SiO_4^- tetrahedra are created and, according to the concentration of silicon in the solution, one of the above monomers is formed. The molecular arrangements in some geopolymer frameworks are

shown in Fig 1.7. A reaction mechanism for geopolymerization proposed by Davidovits [9] involves the chemical reaction of precursors such as aluminosilicate oxides (Al^{3+} in IV-fold coordination) with alkali polysilicates, resulting in polymeric Si–O–Al bonds. To emphasise the IV-fold coordination of Al in these Al-Si minerals, these configurations are usually written as $(Si_2O_5Al_2O_2)_n$ rather than $2\,SiO_2Al_2O_3$. The fabrication of $(Si_2O_5Al_2O_2)_n$ is carried out by:

(i) calcining aluminosilicate hydroxides $Si_2O_5Al_2(OH)_4$

$$2\,Si_2O_5Al_2(OH)_4 \Longrightarrow (2\,Si_2O_5Al_2O_2)_n + 4\,H_2O$$

or

(ii) condensation of SiO and Al_2O vapors:

$$4\,SiO(vapor) + 2\,Al_2O(vapor) + 4\,O_2 \Longrightarrow (Si_2O_5Al_2O_2)_n$$

with also production of:

- $2\,SiO + O_2 \Longrightarrow 2\,SiO_2$ (Condensed Silica Fume)
- $Al_2O + O_2 \Longrightarrow Al_2O_3$ (Corundum)

The structure of geopolymers can be amorphous or semi-crystalline, depending on the condensation temperature. Amorphous polymers are obtained at 20– 90°C, whereas semi-crystalline polymers are obtained at 150–1200°C [10].

1.3 Geopolymerization

In the 1950s Glukhovsky [11]. proposed a general mechanism for the alkali activation of materials primarily comprising silica and reactive alumina. The Gluhhovsky model divides the process into three stages:

(i) destruction–coagulation;

(ii) coagulation– condensation;

(iii) condensation–crystallization.

Figure 1.2 presents a highly simplified reaction mechanism for geopolymerization. The reaction mechanism shown in Fig 1.2 outlines the key processes occurring in the transformation of a solid aluminosilicate source into a synthetic alkali aluminosilicate. It should be noted that though processes are presented linearly are largely coupled and occur concurrently. Dissolution of the solid aluminosilicate source by alkaline hydrolysis produces aluminate and silicate species. It is important to note that the dissolution of solid particles at the surface resulting in the liberation of aluminate and silicate (most likely in a monomeric form) into the solution has always been assumed to be the mechanism responsible for conversion of the solid particles during geopolymerization. This assumption does have almost overwhelming scientific merit based on the literature describing alkaline dissolution, and so is shown in Fig 1.2 Despite this, the actual process of particle to gel conversion has never been confirmed in the highly alkaline and poorly solvated conditions prevailing during geopolymer synthesis. Without the benefit of conclusive mechanistic understanding of solid particle conversion, surface dissolution will be assumed in the simplistic mechanistic model described here. Once in solution, the species released by dissolution are incorporated into the aqueous phase, which may already contain silicate present in the activating solution. A complex mixture of silicate, aluminate and aluminosilicate species is thereby formed, and the speciation equilibria within these solutions have been studied extensively [12]. Dissolution of amorphous aluminosilicates is rapid at high pH, and this quickly creates a supersaturated aluminosilicate solution. In concentrated solutions, this results in the formation of a gel, as the oligomers in the aqueous phase form large networks by condensation. This process releases the water that was nominally consumed during dissolution. As such,

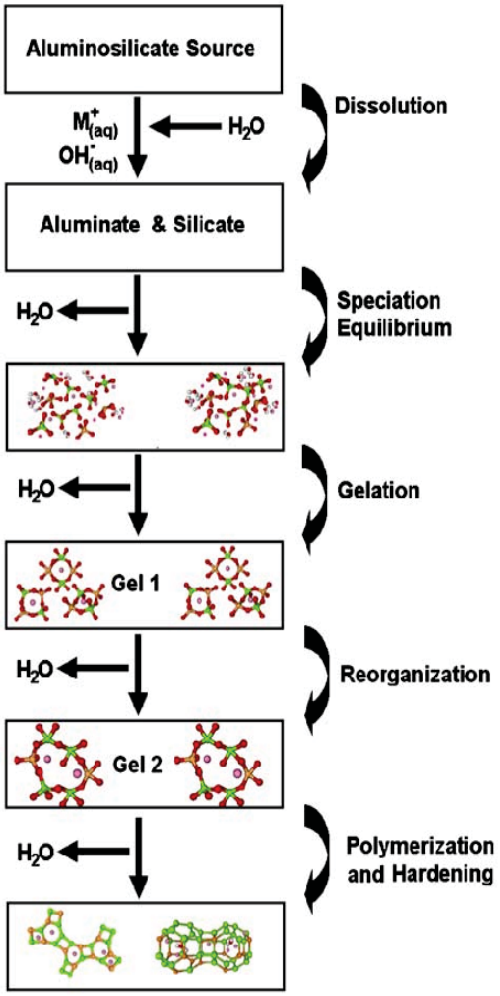

Fig. 1.2 *Conceptual model of geopolymerization*

water plays the role of a reaction medium but resides within pores in the gel. This type of gel structure is commonly referred to as biphasic, with the aluminosilicate binder and water forming the two phases. The time for the supersaturated aluminosilicate solution to form a continuous gel varies considerably with raw material processing conditions and solution composition and synthesis conditions [13]. Despite this, some systems never gel. These are typically dilute, and the concentration of dissolved silicon and aluminum is observed to oscillate due to the slow response of the system far from equilibrium [14]. After gelation the system continues to rearrange and reorganize, as the connectivity of the gel network increases, resulting in the three-dimensional aluminosilicate network commonly attributed to geopolymers. This is depicted in Fig 1.2 by the presence of multiple 'gel' stages, consistent with recent experimental observations [15] and numerical modeling for both metakaolin and fly ash-based geopolymers [16]. Figure 1.2 describes the activation reaction as an outcome of two successive and controlling stages. Nucleation, or the dissolution of the aluminosilicate material and formation of polymeric species, is highly dependent on thermodynamic and kinetic parameters and encompasses the two first steps proposed by Glukhovsky. Growth is the stage during which the nuclei reach a critical size and crystals begin to develop. These processes of structural reorganization determine the microstructure and pore distribution of the material, which are critical in determining many physical properties [17].

J.Davidovits [4] made a distinction between two synthesis routes:

- in alkaline medium (Na^+, K^+, Li^+, Ca^{2+}, Cs^+ and the like);
- in acidic medium with phosphoric acid and organic carboxylic acids.

The alkaline route is the most important in terms of commercial applications.

1.3.1 Geopolymer ceramic-like synthesis in alkaline medium: poly(sialate) based on poly(silicone) terminology

In 1937, W.L. Bragg published a method for classifying all kinds of silicates and their crystal structures based on the concept of the ionic theory by Linus Pauling. The fundamental unit is a tetrahedral complex consisting of a small cation such as Si^{4+}, or Al^{3+} in tetrahedral coordination with four oxygens (Pauling's first rule). Many textbooks explain the geometry of the SiO_4- tetrahedron and other mineral structures as determined by the relative sizes of the different ions. This ionic coordination representation is no longer adapted to the requirements of geopolymer chemistry as this is governed by covalent bonding mechanisms.

The differences between the ionic concept (coordination) and the covalent bonding are profound. See Fig. 1.3

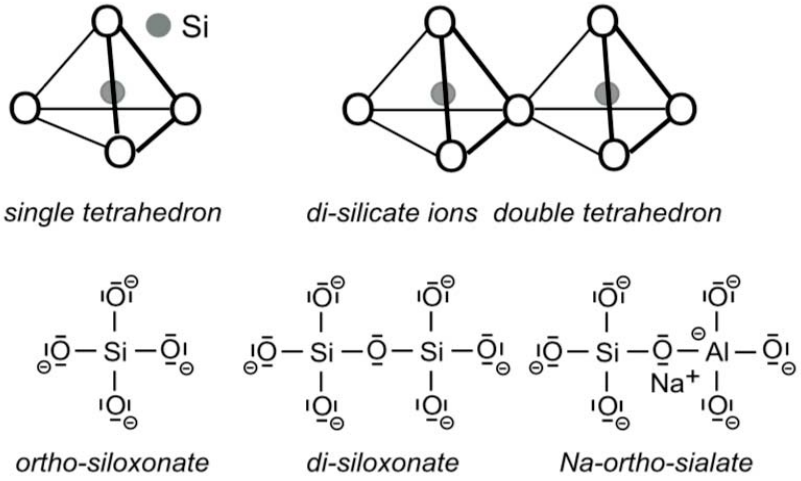

Fig. 1.3 *Top, tetrahedron structure; bottom, covalent bonding.*

The double tetrahedron structure (coordination) shares one oxygen anion O^{2-}, whereas, in the Si-O-Si- molecular structure, the covalent bond is achieved through Si and O sharing one of their electrons. This results in a stronger bond within the structure. The American mineralogist and geochemist G.V. Gibbs and his team [18] studied the polymeric bond Si-O-Si-O. As result, they have concluded that a silica polymorph like quartz can be viewed as a giant molecule bound together by essentially the same forces that bind the atoms of the Si-O-Si skeleton into a small siloxane molecule. The term "giant molecule" used by G.V. Gibbs is equivalent to the definition of "geopolymer" and the wording "small siloxane molecule" describes the organosilicon polymer compounds. There are direct structural analogies between poly(siloxonates) silicates, poly(sialates) silico-aluminates and poly(methylsiloxane) silicone molecules. Sialate is an abbreviated form for alkali silicon-oxo-aluminate, the alkali being sodium-potassium lithium calcium and the term poly(sialate) covers all geopolymers containing at least one (Na, K, Li, Ca)(Si-O-Al), (Na,K,Li,Ca)—sialate unit [19]. What is important here is the exact identity in shape and structure between siloxonate based molecules (alkali silicates), siloxane oligomers and sialate, silico-aluminate, oligomers. Fig. 1.4 shows the structures for monomers, dimers, trimers, tetramers and pentamers of poly(siloxonate), poly(methylsiloxane) and poly(sialate) respectively. Because of its amphoteric character, the Al atom is either trivalent (in acidic medium) or tetravalent (in alkaline medium) according to the reaction

$$Al(OH)_3 + OH^- \Longrightarrow [Al(OH)_4]^-$$

There is very often misunderstanding between the chemical tetravalence of Al and the tetracoordination of Al with surrounding oxygens. Tetravalence describes a chemical mechanism (covalent or polar bonding), whereas tetracoordination shows the crystallographic positions of the atoms, independently of the forces that govern their intra connection: ionic, covalent, van der Waals, hydrogen bonds (physical characteristic). The mix up is due to the general tetrahedral representation after Bragg that does not differentiate between AlO_4 tetravalence and IV-fold coordination with oxygen. According to Bragg's method, the sialate network consists of SiO_4 and AlO_4 tetrahedra linked alternatively by sharing all the oxygens (Fig. 1.3).

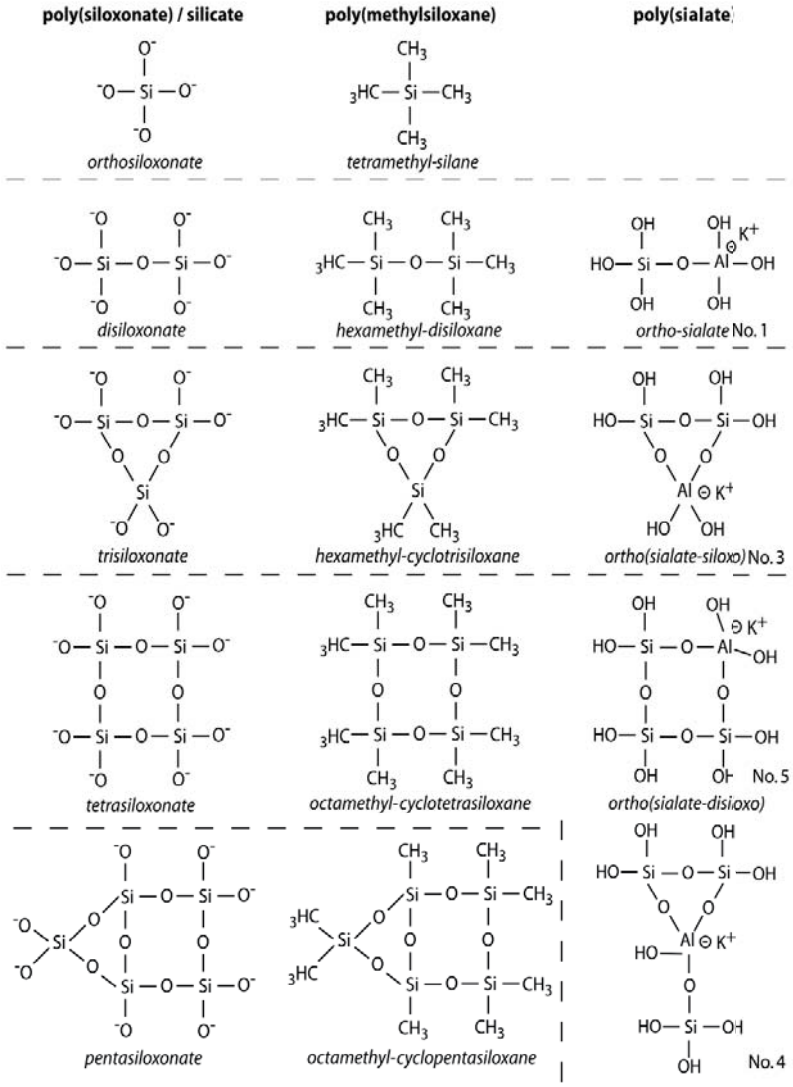

Fig. 1.4 *Molecular structures of poly(siloxonate), poly(methy-siloxane) and poly(sialate) oligomers. The caption "No." for sialate oligomers refers to the molecules isolated in solution and displayed in Fig. 1.8.*

In Fig.1.5a the Al atom in the kaolinite molecule is trivalent -O-Al-$(OH)_2$. After dehydroxylation into metakaolinite, it is still chemically trivalent but becomes tetracoordinate with its surrounding oxygens and is chemically unstable. In Fig.1.5b, alkalinization of kaolinite produces a tetravalent, chemically stable Al unit. It is obvious that, in the latter case, Al is also tetracoordinate with O and OH, but this physical characteristic does not play any major role in the chemical mechanism of geopolymerization.

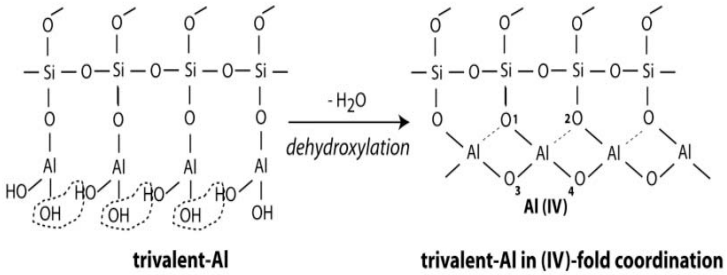

(a) *Al trivalent*

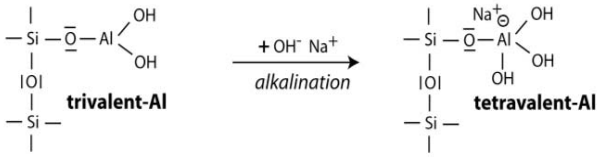

(b) *Al tetravalent*

Fig. 1.5 *Trivalent and tetravalent Al atom.*

Another point of concern is numerous scientific papers displaying a misleading structural representation of metakaolin. See the incorrect model in Fig. 1.6. First, in the Al-O-Al layer, the Al^{3+} atom is represented as being chemically tetravalent (AlO_4), in the same way as the Si-O-Si network with its tetravalent Si^{4+} configuration. The oxygen atom is also trivalent O^{3-}, which is nonsense because it is chemically bivalent. This is a major error, namely the confusion between chemical valence and physical coordination. In fact, for metakaolin, the Al atom is trivalent Al^{3+}, but Al is tetracoordinate, Al(4), pentacoordinate, Al(5) and even hexacoordinated Al(6) to oxygens. The reactive molecule comprises two Al-oxide types.

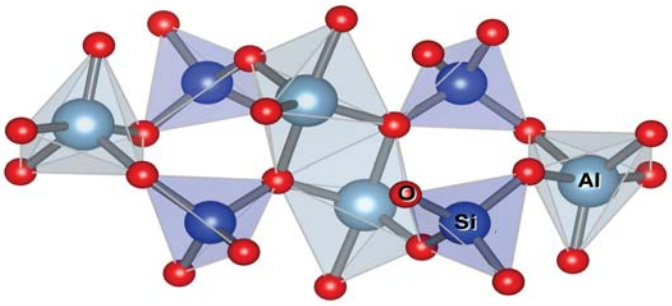

Fig. 1.6 *Wrong model for metakaolin structure: tetravalent aluminum and trivalent oxygen.*

An important issue in sialate based geopolymerization relates to its reaction mechanism. At the beginning of geopolymer research and afterward, for at least 25 years, it was assumed that the geochemical syntheses occurred through hypothetical oligomers (dimer, trimer). Further polycondensation of these hypothetical building units provided the actual structures of the three-dimensional macromolecular edifice, see Fig. 1.7.

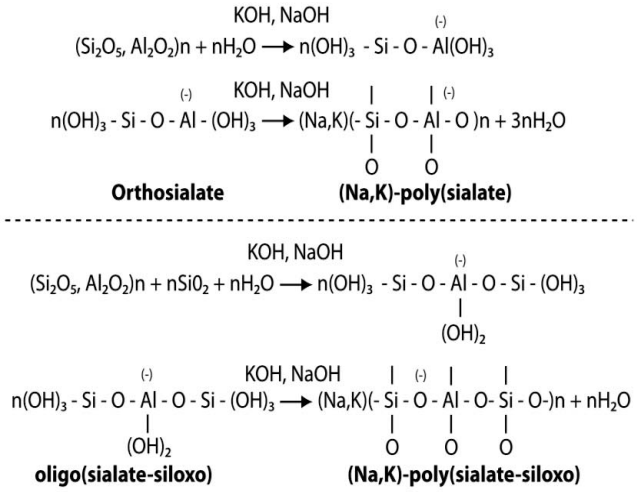

Fig. 1.7 *Reaction mechanism for sialate and sialate-siloxo species, described as hypothetical by Davidovits in 1988*

The most important contribution to a better understanding of the reaction mechanism is the paper by North and Swaddle [20]. Using Si and Al NMR spectroscopy, they suspected the presence of solute species with Si-O-Al sialate linkages in concentrated solutions. One major improvement in their research was that their study was carried out at low temperature, at 5°C and below. Indeed, it was discovered that the polymerization of oligo sialates was taking place on a time scale of around 100 milliseconds, i.e. 100 to 1000 times faster than the polymerization of orthosilicate. At room temperature or higher, the reaction is so fast

that it cannot be detected with conventional equipment. They chose KOH over NaOH used in their previous study because concentrated KOH aluminosilicate solutions resist gelation longer than their NaOH analogs. Owing to the very weak signal of Si, the NMR experiments had to be run up to three days longer to get significant detailed spectra. They successfully detected five solute species, displayed in Fig. 1.8 below, namely two linear molecules and three cycles:

- one ortho-sialate $(OH)_3$-Si-O-Al$(OH)_3$ for Si:Al=1;
- one linear ortho(sialate-siloxo) $(OH)_3$-Si-O-Si$(OH)_{2_}$-O-Al$(OH)_3$, one cycle ortho(sialate-siloxo), for Si:Al=2;
- two cyclesortho(sialate-disiloxo),for Si:Al=3.

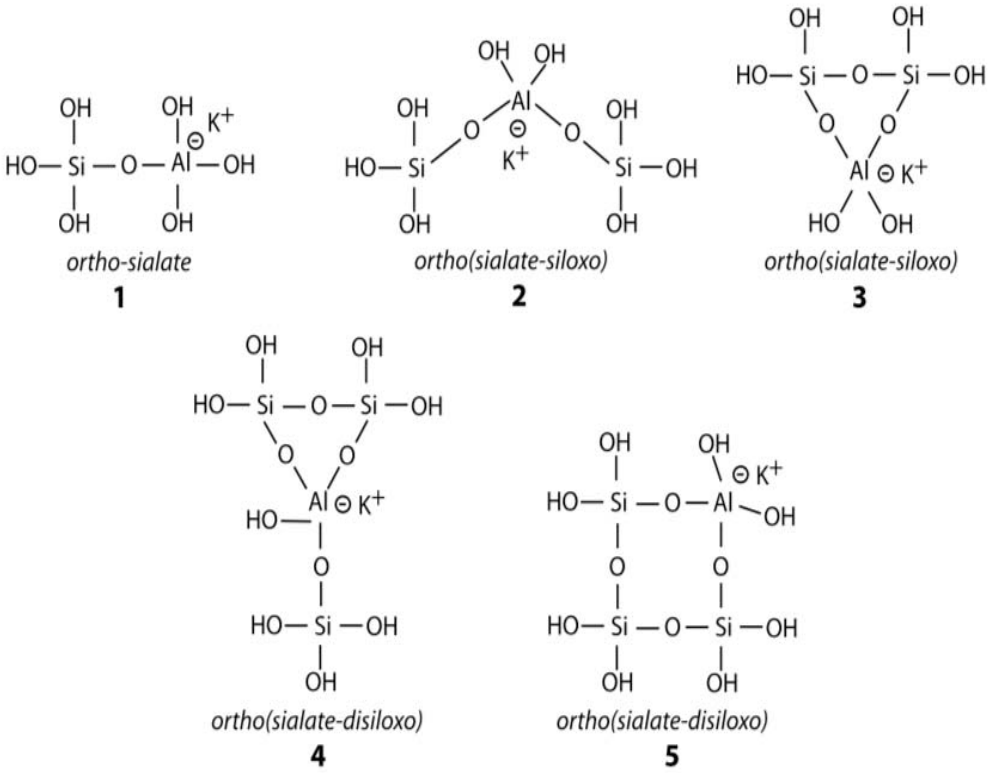

Fig. 1.8 *Five ortho-sialate oligomers isolated in KOH solutions, after North and Swaddle (2000)*

The hypothetical oligomers outlined in geopolymer synthesis were no longer virtual molecules. As a matter of fact, they exist in soluble forms and are stable in concentrated

solutions at high pH. Swaddle's study confirmed our polymerization mechanisms tentatively reported earlier with linear oligo-sialate, oligo(sialate disiloxo) and rings or cycles, as starting geopolymer building units.

1.4 Kinetics of geopolymerization

Determining the key parameters in the kinetics of geopolymerization is essential to better control setting time and microstructural development of geopolymeric gels. Geopolymerisation consists of dissolution and hydrolysis followed by a condensation step in an alkaline silicate plus alumino-silicate system. Experimental techniques such as calorimetry have been frequently used by researchers [21] to investigate geopolymerization kinetics. This technique is useful in determining the reactivity of calcined materials in alkali environments and so could help to optimize calcination. Rahier et al. [22] used quasi isothermal modulated differential scanning calorimetry to observe the changes in heat flow and heat capacity during the setting of geopolymeric gels. They showed that the reaction consists of at least two steps:

- dissolution
- polymerization

and that the second step is autocatalytic. It has been shown that the rate of condensation between silicate species is lower than that between aluminate and silicate species [23] [24]. The role of Al_2O_3 and SiO_2 in geopolymerization and its kinetics has been studied by De Silva et al [25]. They concluded that the geopolymerization kinetics and set rate of geopolymeric gel are controlled principally by Al_2O_3, whereas the Si content is responsible for later strength development of the product. Similar results have been reported by Provis et al. [26], who also showed that high silica systems react more slowly with a 'pause' in the latter stages of the reaction before a further reaction occurs. The mechanism of Al speciation in accelerating the condensation step of geopolymer formation using the calculation of the partial charge of aluminate and silicate species has been investigated by Weng et al. [27], who concluded that varying the particle size of metakaolin has a significant effect on the properties of hardened geopolymer. They reported that milled metakaolin powders with high specific surface area have shorter setting time, higher strength and a more homogeneous microstructure due to improved Al availability, as predicted by the partial charge model. Recently, Provis at al. [28] have developed a model based on the work of Faimon [29] to study the chemical reaction sequence and kinetics of geopolymerization. They propose the reaction sequence for geopolymerization indicated in Fig. 1.9. By postulating reactions for each step and corresponding kinetic expressions for each reaction, assuming that the

stoichiometry of the reaction predicts the kinetics, they developed a comprehensive kinetic model for geopolymerization. Applying the model to experimental data from the literature, they showed that the model could be used to determine the rate of geopolymerization reaction and setting time for a wide range of Si/Al ratios in raw materials.

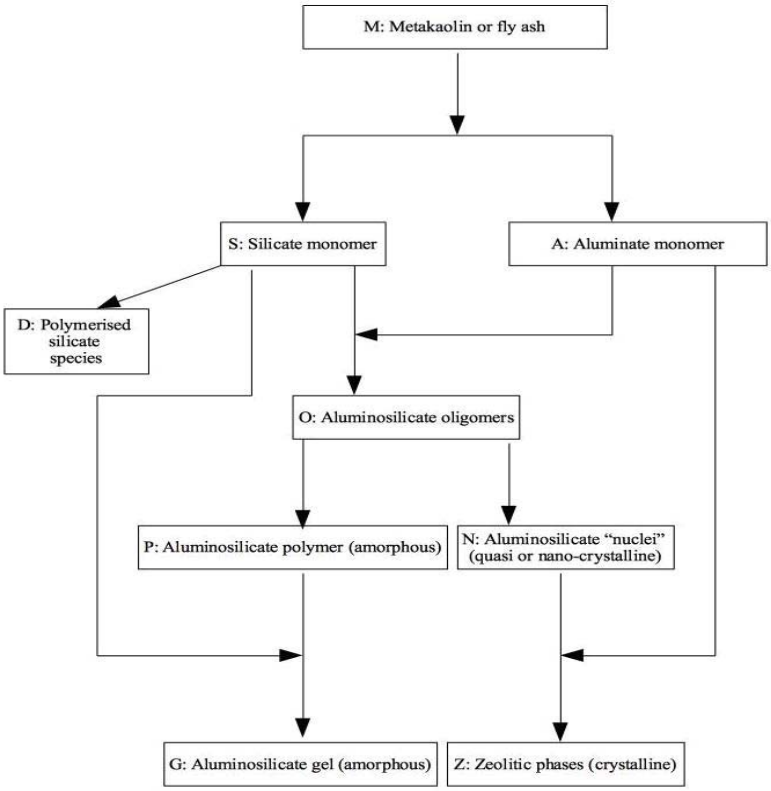

Fig. 1.9 *Proposed reaction sequence for geopolymerization*

1.5 Geopolymer microstructure

A polymer is a macromolecule with definite size and molecular weight. A gel, on the other hand, designates an indefinite amorphous compound with unresolved dimension. Kriven et al. [30] used TEM (transmission electron microscopy) to investigate the microstructure of fully reacted potassium-poly(sialate-siloxo) type geopolymers. It consists of nanoparticles ranging from 5 to 15 nm in dimension(50 to 150 A°) separated by nanoporosity, the features of which are of the order of 3 to 10 nm.

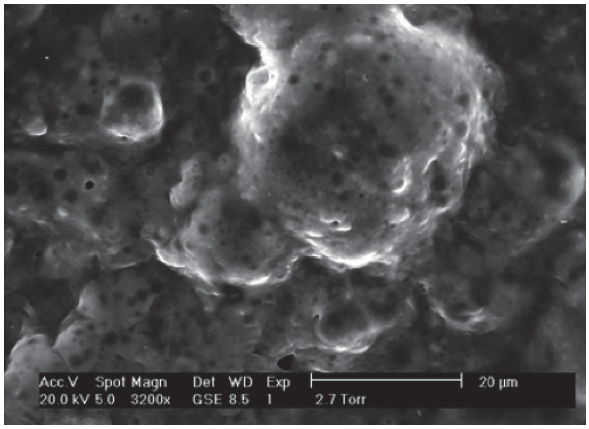

Fig. 1.10 *ESEM micrograph of K-PSS geopolymeric cement matrix*

Figure 1.10 shows an ESEM micrograph of the hardened K-PSS7 geopolymeric cement matrix [31]. It can be seen that the microstructure of geopolymeric products is sponge-like. No crystal with a regular shape is observed in the bulk geopolymeric cement matrix. Zhang and Li also performed EDXA on the whole region shown in the ESEM micrograph to determine its chemical composition after polycondensation reaction. The oxide molar ratios of SiO_2 / Al_2O_3 and K_2O / Al_2O_3 are 4.28 and 1.06, respectively, which are close to the theoretical values of K-PSS geopolymeric matrix (SiO_2 / Al_2O_3 = 4.0 and K_2O / Al_2O_3 = 1.0). Then they heated the room temperature samples slowly over 4 h to 1000°C. The nanosized microstructure was still stable after reaching 1000°C and subsequent furnace stabilization to$\approx$ 990°C. Selected area diffraction (SAD) indicated that the fully reacted regions are still amorphous. No evidence of sintering or "grain growth" was observed. The nano-particulates represent a characteristic feature of the geopolymer matrix and their dimensions suggest the presence of a macromolecule of definite size, and therefore, definite molecular weight. Sindhunata et al. [32] studied the microstructure of fly ash-based geopolymer matrix and found that its structure resembles aluminosilicate particulates of 5 – 20 nanometers in dimension, which are connected and form nanochannels and pores, as reported by Kriven et al. (2003) for K—poly(sialate-siloxo) geopolymer. It is the accumulation of these nanoparticles, or individual particulates, that forms the geopolymer matrix. They are sometimes called precipitated particles and their dimensions are similar to those of micelles made of surfactant molecules, which result from the self-aggregation of small surfactant molecules in water. However, the temperature stability of the geopolymer nanoparticles strongly supports the presence of giant molecules. In other words, it is in favor of the polymeric model. Fig. 1.11 shows the very small dimension of this geopolymer nanoparticulate, when compared to other spherical structures, colloidal silica, silica fume and fly ash.

The core of these nanoparticulate geopolymers is made of aluminosilicate frameworks that are similar to those of rock-forming minerals. Yet, there are major differences. In 1994, J.Davidovits simulated a theoretical structure for K- poly(sialate-siloxo) (K)-(Si-O-Al-O-Si-O) that was consistent with the NMR spectra. It is displayed in Fig. 1.12a and does not show the presence of water in the structure. This is demonstrated by the fact that Al MAS NMR spectroscopy of all(Na, K)-poly(sialate-siloxo) (Na, K)-(Si-O-Al-O-Si-O) showed Al chemical shifts in the range of 55 ppm from $[Al(H_2O)_6]^{3+}$ identical to the spectrum displayed in Fig. 1.12b, which indicates that the aluminum is of the $AlQ_4(4Si)$ type and is tetrahedrally coordinated, or more exactly tetravalent. The absence of any other resonance and the extremely narrow peak at 55 ppm, excludes any residual singular building units of low molecular weight such as dimers and trimers. (Na, K)-poly(sialate-siloxo) (Na,K)—(Si-O-Al-O-Si-O) are true threedimensional framework silico-aluminates with polymeric building units.

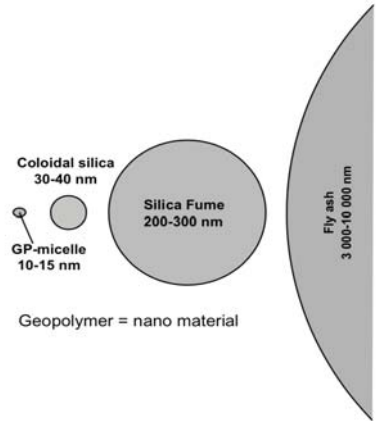

Fig. 1.11 *Dimension of different geopolymeric micelle compared*

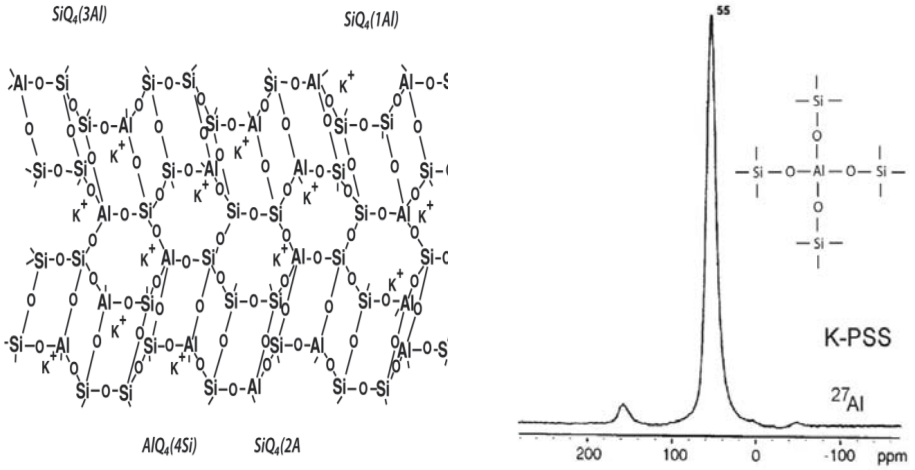

(a) **(b)**

Fig. 1.12 *(a) 3D structural model for fully reacted K poly(sia- late-siloxo), (b) right Al MAS-NMR spectra for K poly(sialate-siloxo) K PSS*

Water is present only at temperatures below 150°C– 200°C, essentially in the form of -OH groups associated with SiQ_3(3Si,1OH) and SiQ_2(2Si,2OH) species (Fig. 1.13). These -OH groups are located essentially on the surface of the nanoparticles, and each particulate is surrounded with some physically bonded water and some siloxonate hydrate molecules. Nevertheless, scientists working on low-temperature applications, such as cement and waste management, try to pinpoint cation hydration and water molecules like for Portland cement. One model first proposed by Barbosa et al. [33] and Rowles [34] only shows incompletely reacted geopolymer.

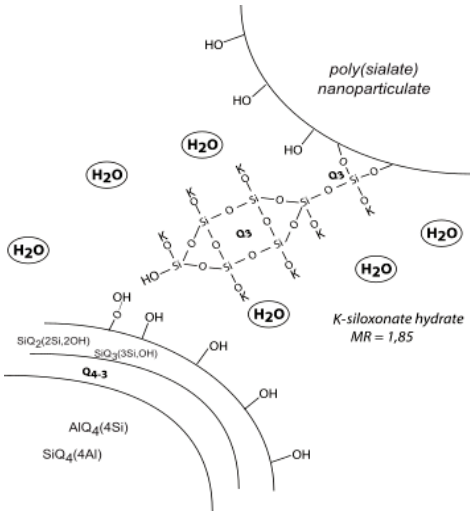

Fig. 1.13 *Simplified structure of K nano-poly(sialate) particulates with siloxonate molecule between the particulates*

The geopolymerization mechanism shown in Fig. 1.14 starts with oligomer condensation into a ribbon-like small molecule. This intermediary stage involves several Si-OH groups together with H_2O molecule and also free NaOH resulting from the geopolymerization. It is coined NASH (sodium aluminosilicate hydrate) or KASH (potassium aluminum silicate hydrate) by some cement scientists and generalized to the final geopolymer structure, which is wrong. The free NaOH is fully consumed during the polycondensation step into the 3D network. The reasoning of the cement scientists is only valid for the first stage of alkalinization (which they call alkali activation) as exemplified by the Al NMR spectra shown in Fig. 1.15. The major resonances at 74/65 ppm in alkali-activated slag can be assigned to AlQ_2(2Si,2OH) and AlQ_3(3Si, OH) species. The Al spectrum demonstrates that in opposition to alkali-activated slag, the Al in (Ca, K) geopolymers is entirely chemically connected, i.e. the cations Na^+ and K^+ are trapped within the structure, with no -OH group inside the particulates, providing long term stability and corrosion resistance. To call them

NASH (sodium aluminosilicate hydrate) or KASH (potassium aluminosilicate hydrate) is inappropriate and generates confusion.

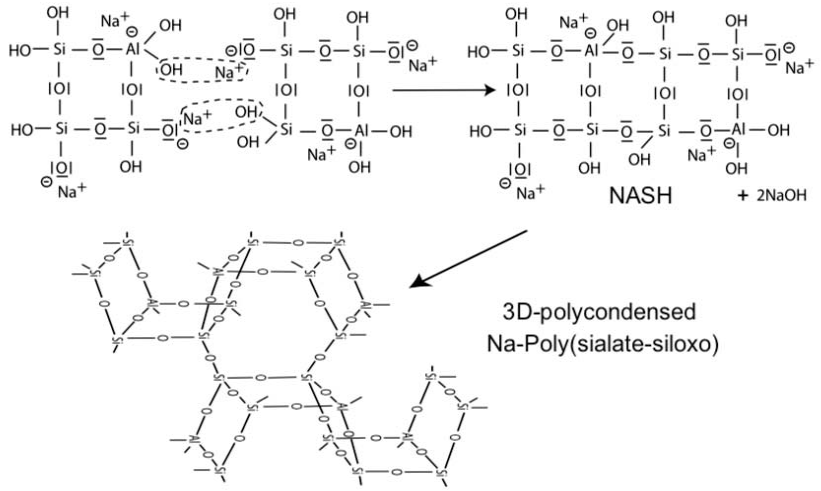

Fig. 1.14 *Geopolymerization with intermediary oligo-sialate-hydrate formation, top part right, wrongly called NASH/ KASH by cement scientists. This hydrated molecule polycondenses into a fully reacted 3D geopolymer network.*

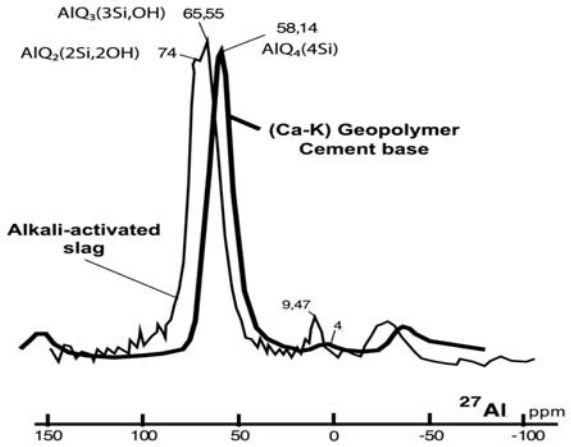

Fig. 1.15 *Al NMR spectrum of hardened geopolymeric Cement Base, evolution from alkali activated slag towards geopolymer cement*

1.6 Mechanical properties of geopolymers

Mechanical behavior is a basic property in assessing engineering material for a specific application. For geopolymers as novel cementitious materials, compressive strength is an important factor. Ever since their invention in the 1950s, the better compressive strength, setting time and durability of geopolymers over conventional cement have been perceived as advantages. However, the compressive behavior of geopolymers varies according to the raw materials and processing method used. To obtain a geopolymer with high compressive strength, a high strength gel phase and a high ratio of gel to nonpolymeric phases are required. These factors relate directly to the type and molar ratios of oxides in the Al-Si source, type, and pH of alkali solution and solubility of raw materials in the activator solution. Davidovits [3] introduced three 'key parameters' for producing high strength geopolymers. Based on research on kaolinite-based geopolymers, he defined:

- $0.2 < Na_2O / SiO_2 < 0.28$
- $3.5 < SiO_2 / Al_2O_3 < 4.5$
- $15 < H_2O / Na_2O < 17.5$

Zuhua et al [35] investigated the role of structural water in the compressive strength of kaolinite geopolymers. They showed that the final strength of products increases by increasing the calcination temperature of kaolinite. This result seems to be due to the higher activity of the clay calcined at higher temperature and also a lower structural water content (which has a negative effect on the strength of the product). Given the importance of the dissolution of Al-Si species in alkali solution and of the polymerization reaction, it is unsurprising that the characteristics of the alkali solution directly affect the microstructural reorganization of the calcined clay and so the final mechanical properties of the product. It has been shown [36] that flexural strength, compressive strength and apparent density of geopolymers increase as NaOH solution concentration increases from 4 to 12 mol and the higher the concentration of NaOH, the higher the amorphous content of the products. Although the dissolution of Al-Si species increases on increasing the concentration of alkali solution, excessive amounts of NaOH or KOH in the aqueous phase decrease the SiO_2 / Na_2O ratio and so inhibit polycondensation. Therefore, there is a limit for alkali hydroxide concentration in the activator solution to obtain a high strength gel phase. It has been also shown [37] that KOH provides more inorganic polymer precursors than NaOH since the larger K_z cation favors the formation of longer silicate oligomers, with which $[Al(OH)_4]^-$ prefers to bind; thus better setting and higher compressive strength is acquired(Fig. 1.16).

Using alkali solution composed of alkali hydroxide and dissolved silicate is beneficial for compressive strength relative to alkali hydroxide alone. Dissolved silica not only balances the SiO_2 / Al_2O_3 and Na_2O / SiO_2 ratios in the mixture but also catalyses polycondensation by providing $[SiO_4]^-$ monomers and by initiating polymerisation between $[AlO_4]^-$ and $[SiO_4]^-$ tetrahedral units. Therefore, higher compressive strength may be obtained using an activator composed of soluble silicate and alkali hydroxide. It should be noted that, again, there is a limit for the addition of silicates to the mixture $(Si/Al = 1.90)$ and very high ratios of Si/Al are not advisable due to the negative effect on mechanical properties. High Si/Al ratios increase the porosity of the structure and also the content of unreacted species, and these factors directly decrease the compressive strength of the geopolymer.

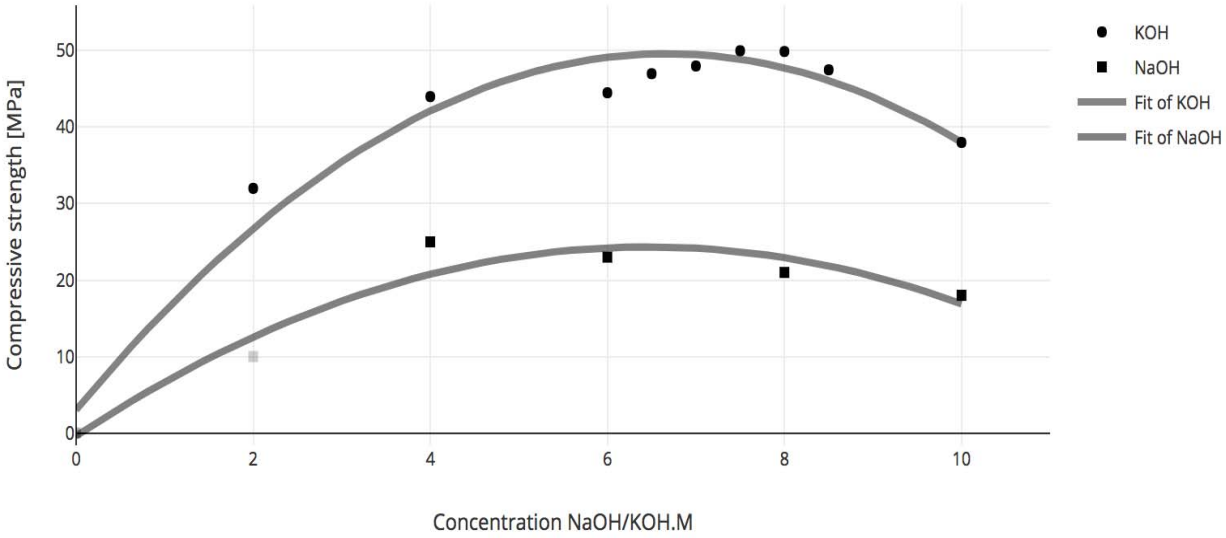

Fig. 1.16 *Effect of alkali hydroxide concentration on compressive strength of geopolymers aged for 7 days*

The presence of calcium compounds such as CaO and $Ca(OH)_2$ has been shown [38] to improve the compressive strength of geopolymers; here the effect of $Ca(OH)_2$ is more pronounced. Precipitation of calcium silicate hydrate or calcium silicate aluminate phases and catalysis of the dissolution of Al-Si particles in alkali solution have been proposed as two reasons for the enhanced mechanical behavior observed in geopolymers produced by the addition of calcium compounds to raw materials.

Chapter 2

Geopolymers as effective adsorbents

This chapter aims to contextualize the choice of geopolymers as adsorbents materials. Initially, an overview of zeolites is provided, with further explanation of differences with geopolymer. Subsequently, a description from a physical point of view, of the adsorption mechanism is given, by focusing on the ion exchange and the cation selectivity. Lastly, a mathematical model, from which we obtain parameters capable of describing both the adsorption mechanism and allows us a comparative analysis of the various data, is illustrated.

2.1 Natural zeolites

We mentioned in chapter 1 that geopolymers emerged as a result of attempts to model the geological formation of zeolites and because of that, they have many features in common. Therefore it becomes important to understand better what zeolites are and the reason why they are widely used in the wastewater treatment. Nowadays, the world is facing a water crisis due to lacking clean drinking water. With the fast development of various industries, a huge quantity of wastewater has been produced from industrial processes and was discharged into soils and water systems. Wastewater usually contains many pollutants such as cationic and anionic ions, oil and organics, which have poisonous and toxic effects on ecosystems. Removal of these contaminants requires cost-effective technologies and a variety of techniques have been developed in the past decades in dealing with wastewater treatment. Currently, adsorption is believed to be a simple and effective technique for water and wastewater treatment and the success of the technique largely depends on the development of an efficient adsorbent. Since the original discovery of zeolitic minerals in a volcanogenic sedimentary rock, zeolitic tuffs have been found in many areas of the world and in the past decades have found a variety of applications in adsorption, catalysis, building industry, agriculture, soil remediation, and energy. Natural zeolites are hydrated aluminosilicate minerals of a porous structure with valu-

able physicochemical properties, such as cation exchange. There are many natural zeolites identified in the world. Clinoptilolite, mordenite, phillipsite, chabazite, stilbite, analcime, and laumontite are very common forms whereas offretite, paulingite, barrerite, and mazzite, are much rarer. Among the zeolites, clinoptilolite is the most abundant natural zeolite and is widely used in the world. In the zeolite structure, three relatively independent components are found: the aluminosilicate framework, exchangeable cations, and zeolitic water. The general chemical formula of zeolites is

$$\mathrm{M_{x/n}[Al}_x\mathrm{Si}_y\mathrm{O}_{2(x+y)}] \cdot p\mathrm{H_2O}$$

where:

- M is Na, K, Li and/or Ca, Mg, Ba, Sr
- n is cation charge
- $y/x = 1-6, p/x = 1-4$

The primary building block of zeolite framework is the tetrahedron, the center of which is occupied by a silicon or aluminum atom, with four atoms of oxygen at the vertices. Substitution of Si^{4+} by Al^{3+} defines the negative charge of the framework, which is compensated by monovalent or divalent cations located together with water. The aluminosilicate framework is the most conserved and stable component and defines the structure type. The water molecules can be present in voids of large cavities and bonded between framework ions and exchangeable ions via aqueous bridges. The water can also serve as bridges between exchangeable cations. Zeolites are capable of exchanging ions with an external medium, which is the significant characteristic of zeolite. Ion exchange proceeds in an isomorphous fashion. The equilibrium ion exchange is expressed by the following equation:

$$z_B A^{z+_A} + z_A B L_{zB} \Leftrightarrow z_A B^{z+_B} + z_B A L_{zA}$$

where:

- z_A^+ and z_B^+ are the valences of the respective cations
- L is defined as a portion of zeolite framework holding unit negative charge

The ion exchange behavior of natural zeolite depends on several factors, including the framework structure, ion size, and shape, charge density of the anionic framework, ionic charge and concentration of the external electrolyte solution. Among all these factors the most important one, on which the theoretical treatment is concentrated, is the framework

structure, specifically the porosity. Previous work [39] demonstrated that the crystal structure of clinoptilolite has a 3-dimensional aluminosilicate framework, which specific structure causes the developed system of micropores and channels occupied by water molecules and exchangeable cations. According to the results of X-ray diffraction (XRD) studies, clinoptilolite unit cell parameters are as follows:

- $a = 17.66\,\text{Å}$
- $b = 17.963\,\text{Å}$
- $c = 7.400\,\text{Å}$
- $\beta = 116°47'$

Two-dimensional channel system is formed in the clinoptilolite minerals (parallel to a and c axes) row based on the features of the aluminosilicate framework structure. There are two channels running parallel to each other and to the c axis: a channel consisting of a 10-member (tetrahedron) ring of the size of $a = 4.4$ Å to 7.2 Å and a channel consisting of an 8-member ring with the size of $a = 4.1$ Å to 4.7 Å and a channel run parallel to a axis consisting of an 8-member ring with the size of $a = 14.0$ Å to 5.5 Å. However, these data are ambiguous and cannot clear the problem of identifying the clinoptilolite framework structures and porous parameters. Pore sizes of the aluminosilicate framework of the clinoptilolite are also indefinite. Further work conducted by Nabiollah Mansouri et.al [40] investigate physical and structural properties of the clinoptilolite pores. In particular, they observed two types of porosities:

- Primary porosity
- Secondary porosity

The primary porosity, which is connected with the clinoptilolite framework structure, can be defined as microporosity presented by nanotube system of the clinoptilolite 3-dimensional aluminosilicate framework. Mesoporosity and macroporosity form the secondary porosity. The mesoporosity is formed by slot pores determined mainly by cleavability of the zeolite crystallite. The macropores consist of pores of various forms which are located between blocks of the zeolite crystallite and other minerals in the clinoptilolite rock. Both because of the porosity and their nature of exchanging ions, the zeolites exhibit high performance in adsorption of cations in an aqueous solution such as ammonium and heavy metals. However these materials are not good adsorbents for adsorption of anionic ions and organics. Surface modification using cationic surfactant can change the surface charge of natural zeolite,

making them applicable for adsorption of anions and organics. Modification of natural zeolites using some heavy metals can also make them for inorganic anion adsorption by surface precipitation.

2.2 Differences between Zeolite and Geopolymer

Geopolymers, despite having a tendency to ion exchange similar to zeolites, differ from those in particular due to the crystalline structure and the type of porosity, in particular, the size of the pore. As can be seen from the image below, the zeolites have an XRD pattern typical of crystalline materials whereas the geopolymers can be considered as an amorphous or semi-crystalline material.

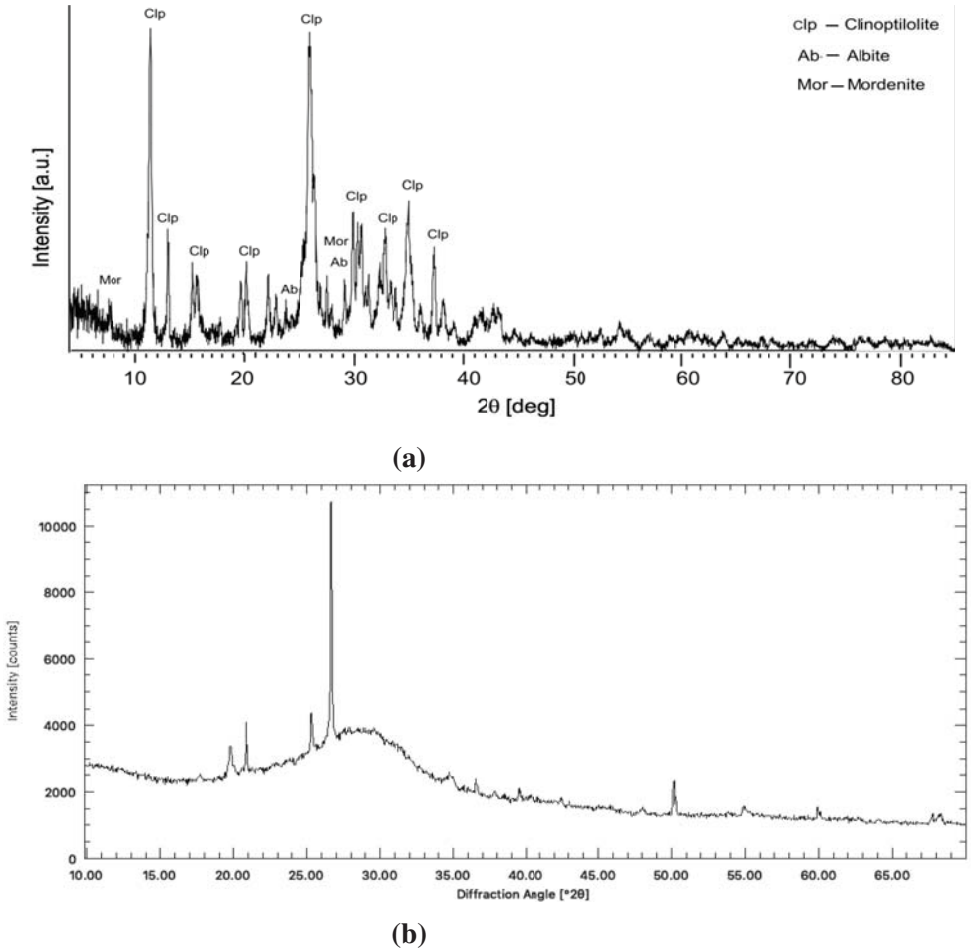

Fig. 2.1 *XRD Patterns of Zeolite **(a)** and Geopolymer **(b)***

Regarding the porosity, there are various categories of pore sizes described in the literature. A summary of the most frequently used pore size classifications is presented in Table 2.1.

Classification	Specified types of pores, d [nm]			
	Macro-	Meso-	Micro-	Supermicro-
IUPAC	>50	2 ÷ 50	<2; (0.4 ÷ 2)	0.7 ÷ 2
Dubinin	>200 ÷ 400	(200 ÷ 400) >d >(3 ÷ 3.2)	<1.2 ÷ 1.4	(3 ÷ 3.2) >d >(1.2 ÷ 1.4)
Cheremskoj	>2000	-	2000 >d >200	-
Kodikara	104 ÷ 106	-	103 ÷ 3 × 104	25 ÷ 103

Table 2.1 *Summary of the most frequently used pore size classifications*

In the zeolitic structure, the porosity is micro/meso-type whereas in geopolymers is mainly macro / meso. The difference in microstructure affects also the reaction conditions. The following table shows the main differences in the synthesis process

Classification	Zeolite syntesis	Geopolymerisation
Reagent	Solution of Al complex + solution of Si complex	Starting material source of Si-Al complex + alcaline solution + silicate
First step	Nucleation into the solution	Leaching of Al-Si solid into paste
Following step	Growth of crystals in solution	Diffusion and condensation of Al and Si complexes in paste
Temperature	90 –300 °C	Ambient
pH	6-11	14
Products	Crystalline zeolite	Blend of gel and materials before Al-Si

Table 2.2 *Syntesis processes of zeolite and geopolymer*

Interestingly that the two synthesis processes take place at extremely different temperatures; in particular the synthesis of geopolymers takes place at room temperature. This characteristic, together with the tendency to ion exchange (common to both), makes the geopolymers and in particular their absorption mechanism, worthy of a more depth study.

2.3 Wastewater treatment: Solidification/Stabilization & Adsorption mechanism

Since the origin of the term geopolymer to define those materials synthesized by the alkali activation of aluminosilicate monomers at ambient temperature, studies about geopolymers have been widely spread. Nevertheless, while these studies continue, others have explored new applications as immobilizations of waste, radioactive and toxic materials and as adsorbent. Water and wastewater treatment processes produce various sludges, spent ion exchangers, catalysts, and highly concentrated effluents, which pose frequently disposal problems due to the hazardous components and chemical instability. One option for treating these water treatment residues (WTR) is the solidification/ stabilization (S/S), which allows safe landfilling or utilizing obtained solid materials. The definition of S/S is the process of mixing waste with a binder to convert it into a monolithic solid and thus reduce the likelihood of release of hazardous components to the environment. Typically, S/S mechanisms are divided into two categories:

- physical encapsulation
- chemical stabilization

However, a clear cut separation is not meant as these mechanisms can work in conjunction and the exact determination of mechanism is difficult; figure 2.2 shows a schematic representation of the immobilization process.

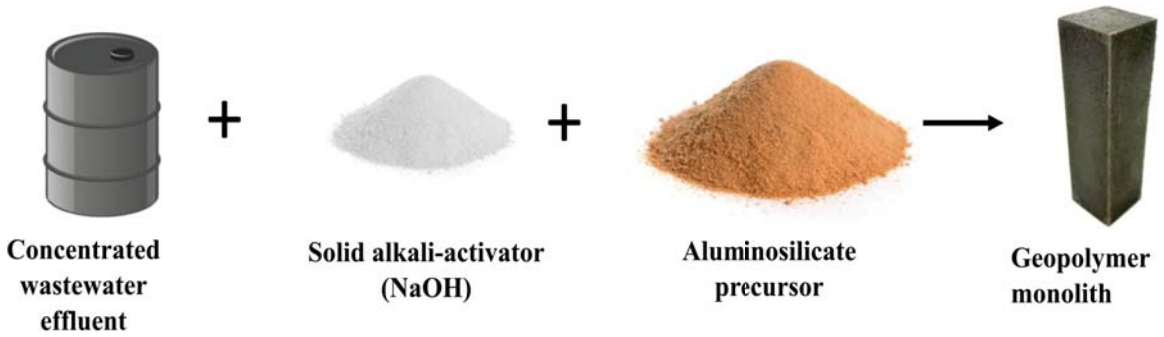

Fig. 2.2 *Schematic presentation solidification/ stabilization of concentrated wastewaters*

Physical encapsulation takes place on a micrometric scale and is, therefore, more characteristic of zeolitic structures than of geopolymeric ones due to the difference in the size of the porosity. Chemical stabilization occurs on the nanoscale. Metal(loid)s can react with other reactive compounds in the mixture and become part of the aluminosilicate structure,

for example by replacing silicon atoms; however since it is not a mechanism of our interest, we will not go into it further.

Another important approach, as we have already mentioned, for the removal of heavy metal ions is adsorption. Adsorption of wastewater by zeolite is feasible due to its unique three-dimensional network structure, with fixed-sized pores and paths that allow only certain heavy metals to pass through. Similar to zeolite, geopolymer, an inorganic polymer, have a three-dimensional polymeric structure and pores formed by the condensation of aluminosilicate mineral powder in addition to an alkali solution at room temperature. The geopolymer synthesis process is simpler than that of zeolite (see Table 2.2). Therefore, wastewater treatment using a geopolymer as an adsorbent should be more feasible, and thus merits further examination. Adsorption(Fig 2.3) is a process that occurs when a gas or liquid solute accumulates on the surface of a solid or a liquid (adsorbent), forming a molecular or atomic film (the adsorbate). This process differs from absorption, in which a fluid (the absorbate) is dissolved by or permeates a liquid or solid (the absorbent), respectively. Furthermore, adsorption is a surface phenomenon, whereas absorption involves the whole volume of the material. The main sorption mechanism of geopolymers is thought to be ion-exchange similar to zeolites which occurs at both interlayer and surface sites. Ion exchange is a chemical reaction where an ion carrier material (ion exchanger) exchanges their ions with others disposed of in solution (counterions). Even though the ion exchanger is not dissolved, the ion exchanger must have an open network structure to let ions be dissolved in the aqueous solution. The ion exchangers can be cationic, anionic or amphoteric in accordance with the charge of the balancing ion, and the number of ions exchanged should be equal to the proportion of free counterions in solution in agreement with the stoichiometric ratio of exchange. In the case of geopolymers, which are Xray amorphous materials formed by non localized but well distributed negative tetrahedral silicate and aluminate units, they can be considered as cationic exchangers. Their negatively charged structure, balanced by alkali metals such as Na^+ or K^+, can be completely hydrated and mobilized. This gives a lower bonding strength in comparison with zeolites and eases to be ion-exchanged when

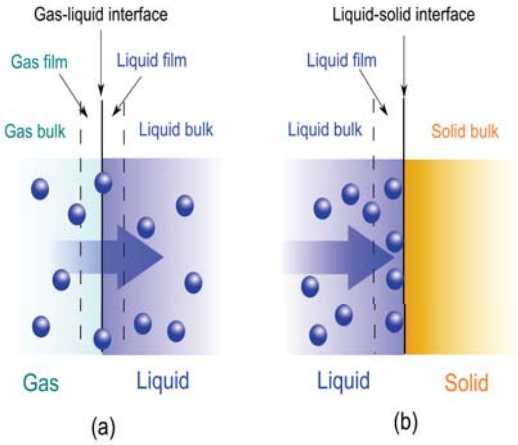

Fig. 2.3 *Sorption Mechanism*

they are in contact with solutions of chloride or nitrate of the desired cation. The maximum number of possible exchangeable cations, known as theoretical ion exchange capacity (TEC), is equal to the negative charge of the geopolymer network and can be measured by elemental analysis of aluminum. Nevertheless, it is not always possible to ion exchange the total amount of available exchangeable cations (TEC value), and a real exchange capacity (REC value) should be determined by an ion-exchange method. The general procedure of ion exchange can be formulated by the following equations:

$$Na^+G^- + M^+Y^- \longrightarrow M^+G^- + Na^+ + Y^-$$

When the geopolymer, represented as $Na^+ G^-$ (ion exchanger), is ionized in an aqueous solution, the released cation (Na^+ or K^+) diffuses inside the material, transfers through the interphase boundary and finally arrives to the solution. If a salt MY is also dissolved in the solution (M^+ and Y^- ions), the Na^+ in geopolymer is replaced by an equivalent amount of counterion M^+ due to the electroneutrality requirement. Clearly, from a microstructural point of view, these cations will tend to occupy the empty spaces typical of both zeolitic and geopolymeric structure as can be seen from the following image

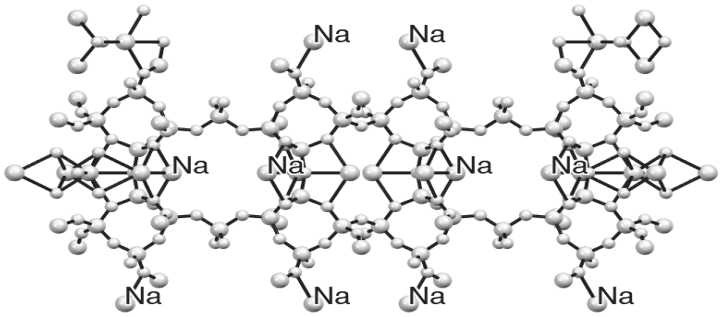

(a) *Clinoptilotite where Na^+ exchange occurs*

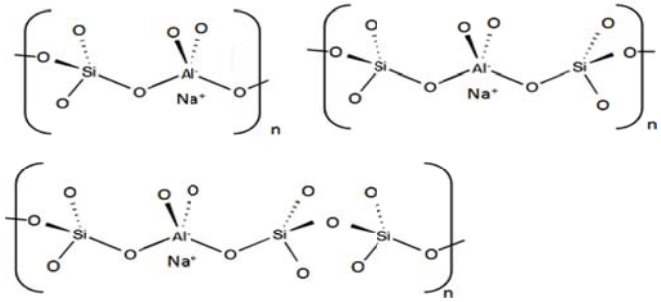

(b) *sialate geopolymer, sialate-siloxo geopolymer, sialate-disiloxo geopolymer*

Fig. 2.4 *Position of the cation in the zeolite **(a)** and in gopolymer **(b)***

2.4 Effect of ion exchange over geopolymers & cations selectivity

We saw in the previous section, how the adsorption mechanism in geopolymers is vehiculated by the cation exchange. However, cations have different dimension so it is clear that geopolymers show different absorption capacities depending on the cation considered. It is important, before proceeding with a more detailed study of the cationic selectivity, consider the effect of ion exchange over geopolymers.

2.4.1 Effect of ion exchange

An important study on the effect of ion exchange over geopolymers was conducted by Joseé Ramoón et.al [41]. They analyzed an ion exchanging between a geopolymer and a solution composed by NH_4Cl,$(NH_4)_2TiO_2(C_2O_4)_2$ and $(CH_3)_4NBr$ 0.1M to guarantee a larger proportion of free counterions in solution so a complete ion exchange.

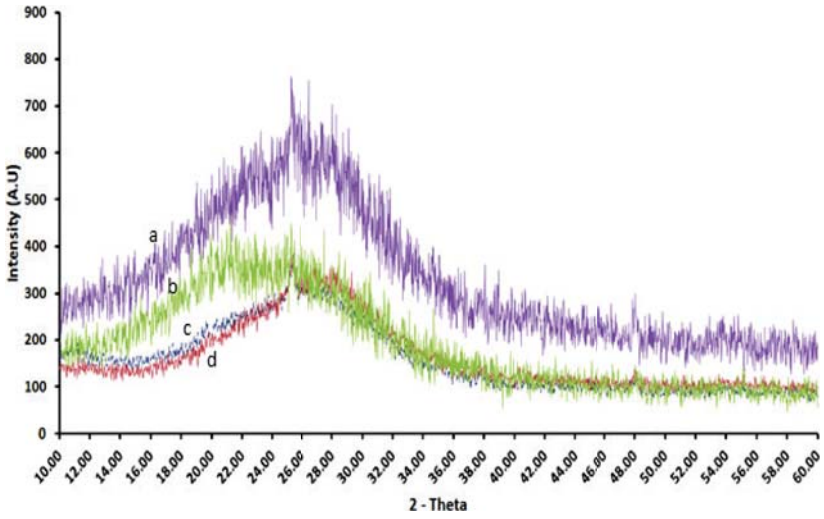

Fig. 2.5 *XRD pattern of* ***(a)*** *former geopolymer,* ***(b)*** *geopolymer ion exchanged with* $(NH_4)_2TiO_2(C_2O_4)_2$, ***(c)*** *geopolymer ion exchanged with* NH_4Cl *and* ***(d)*** *geopolymer ion exchanged with* $(CH_3)_4NBr$

As we can see from Figure 2.5, the amorphous structure of the geopolymer remains after ion-exchanged (hump: $2\Theta = 28$). This conclusion is further demonstrated by FT-IR analysis; as shown in figure 2.6, the vibration modes corresponding to amorphous sodium aluminosilicate ($1645.44, 878.56 cm^{-1}$), symmetric stretching of Si-O-Al, Si-O-Si ($706.9 cm^{-1}$) and flexion of Si-O-Si and O-Si-O ($571.73 cm^{-1}$) remained as a former geopolymer. The only

modifications observed between spectra were those ascribed to vibration modes representative of their counterions. Whenever a geopolymer is synthesized, the three coordinated

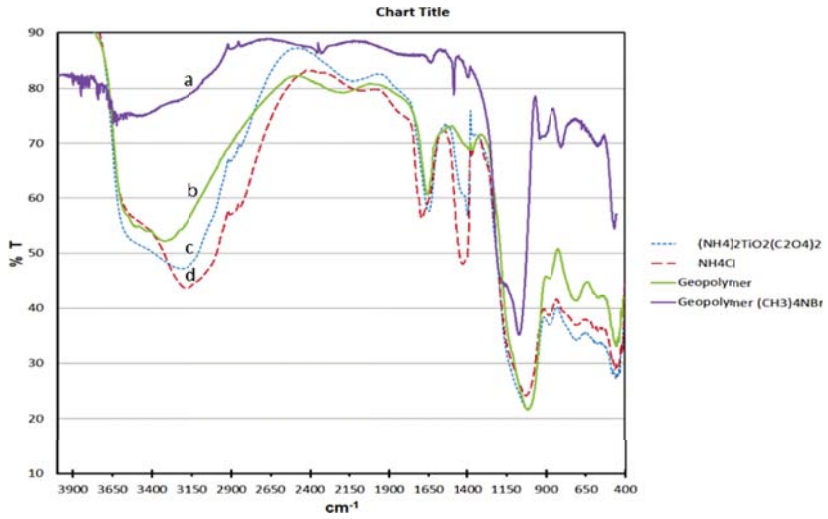

Fig. 2.6 *FT-IR Analysis of geopolymer and geopolymer ion exchanged with differnt cation*

aluminum in metakaolin, Al(IV), Al(V) and Al(VI) (chemical shift: 49-80, 35-40 and -5-15 ppm, respectively), are transformed into Al(IV) to form the geopolymer structure. As it can be observed in Figure 2.7, this structure remained in all ion exchanged samples, and in some occasions, Al(V) and AI(VI) arose at 30 ppm and 2 ppm as in the case of $(CH_3)_4NBr$ because of the size of the counterion mainly.

In conclusion, the ion exchange does not change the structure of the geopolymer that remains amorphous. This can be explained by the fact that the cations exchanged do not take part in the lattice but remain in the empty spaces (see also Fig 2.4).

2.4.2 Cations selectivity

Successful application of geopolymers as adsorbents would require a detailed understanding of these materials and their structure and its relationship to various aspects of their properties. However, there is still a lack of knowledge on the local structure/arrangement of the geopolymer network as well as on the structure/properties relationship. Knowledge of the structure and local arrangement of the geopolymer network is lacking because of the absence of long-range ordering of these materials and limits on the application of diffraction techniques for this purpose (see also Fig 2.1b). As we have seen in the previous section, Si and Al nuclear magnetic resonance (NMR) and Fourier transform infrared (FTIR) spectroscopy

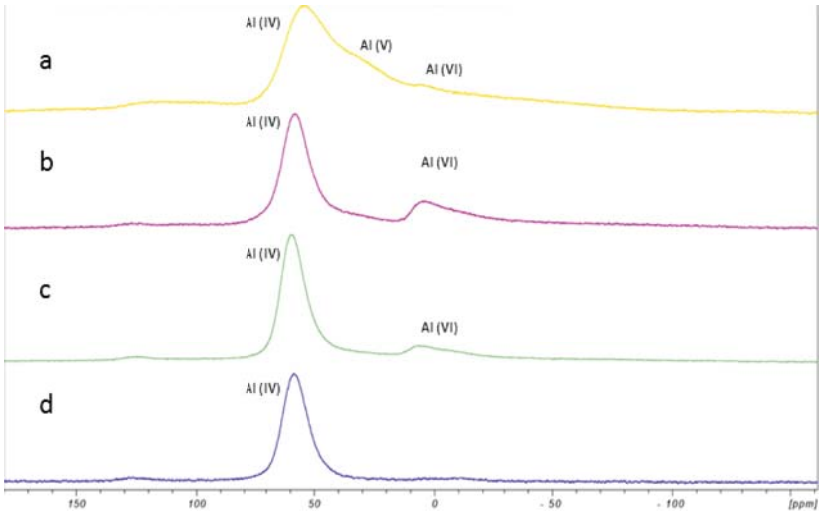

Fig. 2.7 *Al MAS NMR of* ***(a)*** *geopolymer ion exchanged with* $(CH_3)_4NBr$, ***(b)*** *geopolymer ion exchanged with* NH_4Cl, ***(c)*** *geopolymer ion exchanged with* $(NH_4)_2TiO_2(C_2O_4)_2$ *and* ***(d)*** *former geopolymer.*

have been successfully used to characterize amorphous alumosilicate materials and also to represent a basic method for the study of geopolymers. Accordingly, several structural parameters that could influence the properties of the geopolymer material and eventually limit its potential application for a specific purpose are not known. In particular, knowledge of the size and shape of the alumosilicate rings that control access of guest species into the geopolymer and of the local structures accommodating the charge compensating cations is essential for the potential application of geopolymer materials in waste management, adsorption, catalysis, etc., and these parameters could probably affect the geopolymer's mechanical properties. Many sophisticated methods have been developed and used for obtaining their detailed structural characterization. Among other things, the size of the channel/ring and the accessibility of framework Al atoms can be conveniently tested by ion exchange of cations/cationic complexes of various dimensions. Oleg Bortnovsky et.al [42] have been attempted to adapt the methods that have been successfully used for characterization of microporous zeolites to the new field of geopolymer materials, in particular, they analyzed the absorption of two different cations:

- Co^{2+}
- Cs^{+}

Sample	Atomic ratio of the pure geopolymeric phase			
	Si/Al	Na/Al	Cs/Al	Co/Al
Na-Geo	1.6	1.1	-	-
Cs-Geo	1.8	0.0	0.56	-
Co-Geo/I	2.0	0.03	-	0.59
Co-Geo/II	2.0	0.86	-	0.12

Table 2.3 *Chemical Composition of the Geopolymer Phase*

As we can see from the Table 2.3 there are a complete replacement of the Na^+ ions of the as-prepared geopolymer by Co^{2+}(residual Na/Al$\leq$ 0.03, Co/Al $\geq$ 0.5; i.e. close to 100% of the total ion capacity). This also suggests homogeneous distribution of Co^{2+} ions in the geopolymer matrix. On the other hand, only partial exchange has been obtained for larger Cs^+ ions (Cs/Al = 0.56; i.e. about 50% of the total ion capacity)

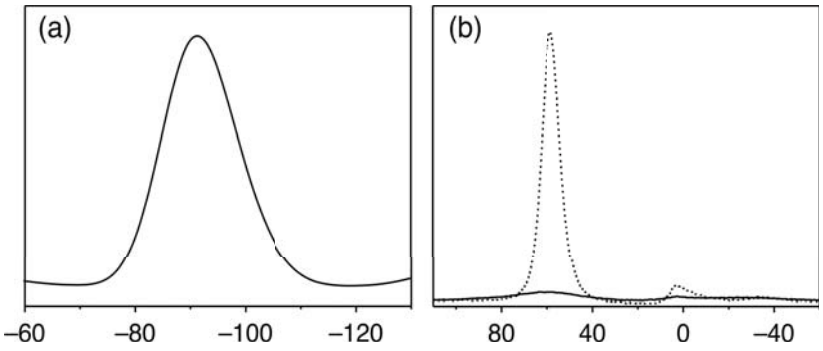

Fig. 2.8 ***(a)****Si mass angle spinning nuclear magnetic resonance (MAS NMR) spectrum of Na-geopolymer.* ***(b)*** *Al MAS NMR spectrum of Na-geopolymer(dotted line) and of Co-geopolymer/I with Co/Al 0.59 (continuous line).*

The Si and Al MAS NMR spectra of the Na-sample, as well as the Al MAS NMR spectra of the Co-geopolymer (Co/ Al 0.59), are depicted in Fig.2.8. Si resonance in the spectrum of the Na-geopolymer at around 90 p.p.m. corresponds to tetrahedrally coordinated Si atoms and indicates the exclusive presence of tetrahedral Si in the Na-sample. In the case of Al MAS NMR, two resonances were observed for the Na-sample. The band at 59 p.p.m. predominates in the spectrum and indicates that more than 95% of the Al atoms

exhibit tetrahedral coordination. The weak signal at 4 p.p.m. corresponds to the octahedrally coordinated Al and can be attributed to the traces of unreacted metakaolinite and mullite. As follows from Fig.2.8b, in the case of the Co-exchanged geopolymer, the intensity of the Al resonance at 59 p.p.m. decreased dramatically (about eight times). This could be explained by a strong paramagnetic effect of the Co^{2+} ions in close vicinity of the Al atoms, following their role as a charge balancing cations of the negative charge of the framework Al. Both NMR and ion exchange experiments indicate that the whole inner volume of the ground geopolymer materials can easily communicate with the outer environment. Thus, it should be suggested that the leaching properties of geopolymers are controlled by the kinetics of the transport rather than by the thermodynamic stability of the local structure, possibly accommodating environmentally important cations/species. As has been stressed, Co^{2+} and Na^{+} could be exchanged in the vicinity of all the Al atoms in the geopolymer network at room temperature, a property of the geopolymer matrix closely similar to zeolites. It is generally accepted that Co^{2+} and Na^{+} aqueous complexes cannot penetrate through the six-membered rings of zeolites at room temperature. Accordingly, by analogy, this indicates that all the Al atoms of the geopolymer network are accessible through eight-membered (eight Al or Si atoms) or larger alumosilicate rings. However, Cs^{+} ions, which are too large to penetrate through the zeolite eight-membered rings, were exchanged in the vicinity of only 50% of the Al atoms present. Thus, it can be suggested that access to approximately one-half of the Al atoms of the geopolymer is through eight-membered rings, while access to the second half of the Al ions is controlled by 10 membered or larger rings. We have therefore demonstrated, as the size of the cations and any complexes forming in the aqueous solution, is a very important parameter, especially as regards the application of geopolymers as absorbents. However, since the adsorption mechanism is purely superficial, in the synthesis of the geopolymer, surfactants can be added to increase the specific surface and thus obtain a greater adsorption performance. It is therefore clear how the study of the cationic selectivity must also take into account the overall porosity and the contact time consequently, the theoretical treatment becomes much more difficult; for this reason most of the knowledge we have today about the cationic selectivity of geopolymers derive from empirical data of specific adsorption tests for different ions and different contact times. Table 2.4 summarizes most of these data.

Adsorbate	Adsorption capacity (mg/g)
Cu(II)	152
Pb (II)	118.6
Cs^+	15.24
NH_4^+	21.07
Zn(II)	74.53
Ni(II)	42.61
Cd(II)	26.246
Co(II)	69.23
Mn(II)	72.34

Table 2.4 *Adsorption capacity of a typical metakaolin-based-geopolymer for different cations at room temperature for 8h*

2.5 Adsorption Isotherms: Modeling & Interpretations

So far we have treated and discussed the effectiveness of geopolymers as adsorbents only from a physical point of view, through the analysis of the microstructure and quantitative data. For completeness of analysis, it is, therefore, necessary to introduce one or more mathematical models able to describe the adsorption phenomena, thus allowing a comparative analysis of the data also from a qualitative point of view. The solid phase is known as adsorbent and the liquid phase (the solvent, normally water) contains one or more compounds to be adsorbed (the adsorbates). Due to unbalanced forces, the adsorbate is attracted to the adsorbent surface, and consequently, the degrees of freedom and the surface free energy are reduced [43]. The transference of the adsorbate from the liquid phase to the solid phase continues until the equilibrium to be reached between the amount of adsorbate linked in the adsorbent and the amount of adsorbate remaining in the solution. The affinity degree

between the adsorbent and adsorbate determines this distribution in liquid and solid phases. In operational terms, some configurations are possible for an adsorption process, for example, discontinuous batch adsorption, continuous stirred-tank reactor (CSTR), fixed bed adsorption, expanded bed adsorption, fluidized bed adsorption, simulated moving bed adsorption, and others. For this work, we will only consider the fixed bed configuration. In this type of configuration, a solution with initial adsorbate concentration C_0 (normally named influent) is pumped at a flow rate Q, through a column with Z height, which is packed with a certain amount m of adsorbent. During the operation, the adsorbate is transferred from the solution to the adsorbate surface. As a consequence, the solution is clarified, achieving an output concentration of C_t. The equilibrium is attained when the bed saturation occurs C_t=C_0.

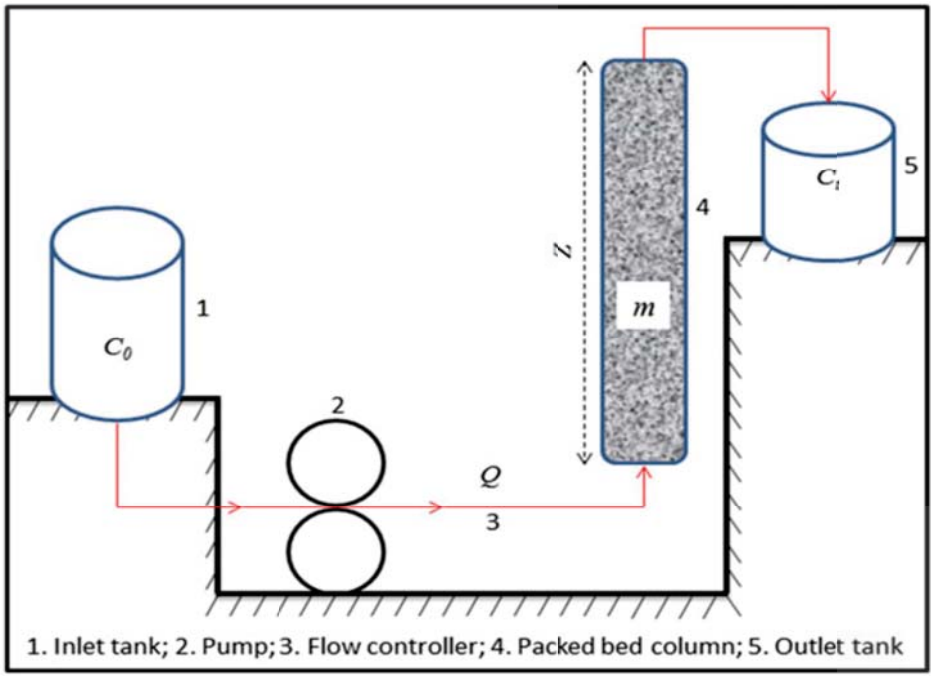

Fig. 2.9 *Schematic representation of a fixed adsorption operation*

The fixed bed systems are useful and fundamental to scale up adsorption operations. The real operational conditions, such as flow rate and bed height, can be simulated, and parameters for scale-up can be obtained. To develop an adsorption operation, in discontinuous batch or fixed-bed systems, the first step is the adsorbent choice and the second is the obtainment of the adsorption isotherms. Since we have already seen the reasons for the choice of the geopolymer as an adsorbent, only the isothermal analysis remains to determine its effectiveness. Adsorption isotherms are a relation between the amount of adsorbate adsorbed in the adsorbent (q_e) and the amount of adsorbate remaining in the liquid phase (C_e) when

the two phases are in dynamic equilibrium at a determined temperature. In liquid-phase adsorption systems, the isotherm curves are important due to the following aspects:

- From the isotherm parameters, it is possible to obtain the maximum adsorption capacity of a determined adsorbent under different experimental conditions. The maximum adsorption capacity is indicative of the adsorbent quality.
- Also from the isotherm parameters, it is possible to obtain information about the energetic, steric, and affinity viewpoints.
- The isotherm shape can provide information about the interaction mechanism that occurs between the adsorbent and the adsorbate.
- In terms of the adsorption rate modeling, a local equilibrium is generally considered, to solve the partial differential equations. This local equilibrium is mathematically described by the adsorption isotherms.
- Thermodynamic adsorption parameters, such as standard Gibbs free energy change (ΔG^0), standard enthalpy change (ΔH^0), and standard entropy change (ΔS^0), can be found from the isotherms. These parameters are fundamental to verify the spontaneity and nature of the adsorption operation.

Since the construction methods of adsorption isotherms are standardized, we will focus our attention solely on the classification of these curves and on two main mathematical models able to describe the parameters related to equilibrium (Langmuir Model) and kinetics (Pseudo Second-Order Model).

2.5.1 Classification of the equilibrium isotherms

As described above, the equilibrium isotherms show the amount of adsorbate that can be absorbed by the adsorbent (q_e) in relation to the equilibrium concentration of the adsorbate in the fluid phase (C_e). These are critical parameters in the adsorption system design. Furthermore, the shape of the equilibrium curve helps to explain certain phenomena associated with the interaction between the adsorbate and adsorbent. Therefore, the isotherm shape not only provides information on the affinity between the molecules but also reflects the possible mode of interaction between adsorbate and adsorbent [43]. The classification of liquid-solid adsorption isotherms describes a system [43] and suggests how their form can be used to diagnose the adsorption mechanism, in order to obtain information regarding the physical nature of the adsorbate and the adsorbent surface and also to measure the specific surface

area of the adsorbent. In this classification, the equilibrium curves are identified according to the initial slope into four main classes, and subgroups are described for each class, based on the shapes of the upper parts and slope changes. Figure 2.10 shows the classification proposed by Giles [44].

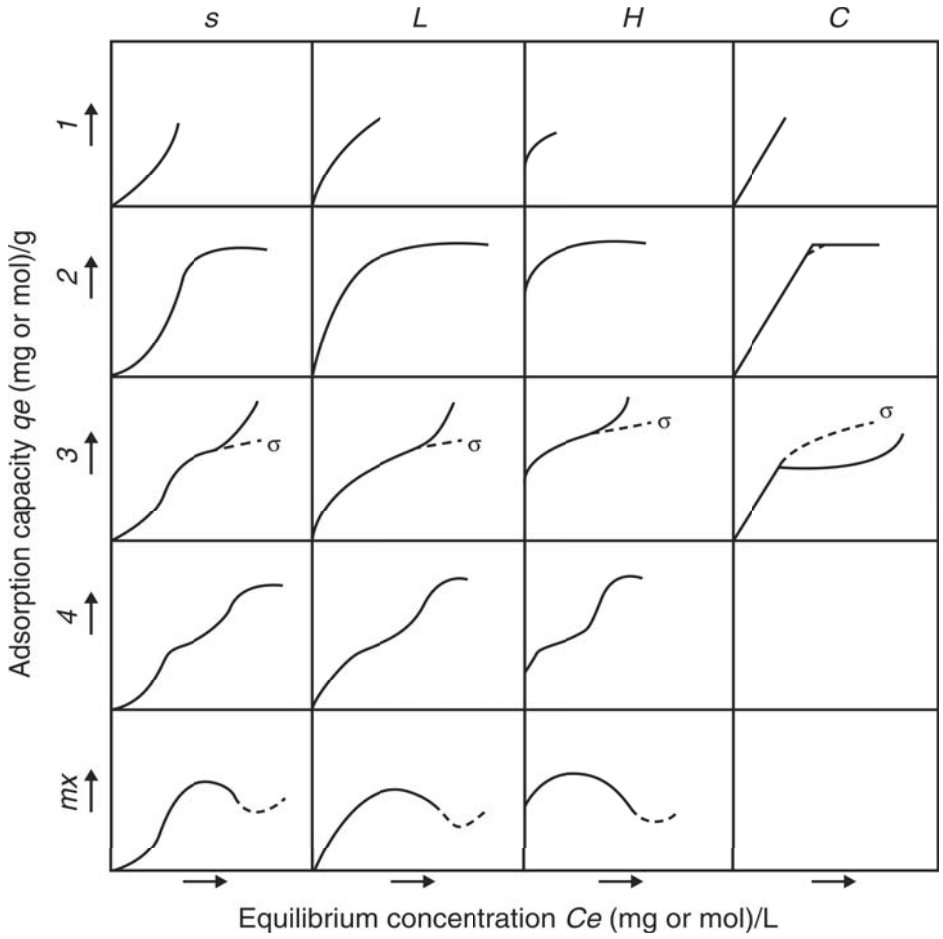

Fig. 2.10 *Adsorption isotherm classification*

The main classes are:

- S curves or vertical orientation isotherm
- L curves or normal or "Langmuir" isotherms
- H curves or high-affinity isotherms
- C curves or constant partition isotherm

According to the work of T.W. Cheng [45] the isotherms relating to the geopolymers follow an L(2)-type trend which represents the normal or Langmuir isotherms. The initial

shape of the equilibrium curve follows the basic premise that the higher the solute concentration, the greater the adsorption capacity until the number of adsorption site clearance is limited, occurring competition between solute molecules for the available sites. Usually, it is indicative that the molecules are adsorbed flat on the surface or, sometimes, of vertically oriented adsorbed ions with particularly strong intermolecular attraction. Thus they have one of the following characteristics:

- the adsorbed molecules are more likely to be adsorbed flat
- are systems with high polar solute and substrate.

This isotherm type indicated that the adsorption occurs due to relatively weak forces, such as van der Waals forces. The subclass 1 occurs when the adsorption sites were not fully occupied, or there was not a completely vertical orientation of the molecules of the solvent. The subclass 2 indicates that there is no intermolecular interaction between the solute, forming a long plateau, indicating a saturation of the adsorbent monolayer. In this case, a high energy barrier should be overcome before the additional adsorption can occur on new sites after the surface has been saturated to the first degree. Therefore, the solute has a high affinity for the solvent, but low affinity for the layer of solute molecules already adsorbed. In subclass 3, a short plateau must mean that the adsorbed solute molecules expose a surface, which has nearly the same affinity for more solute as the original surface possessed. This indicates that the solute in the solution has some intermolecular interaction with the solute in the adsorbent surface, leading to the formation of multilayers. The subclasses 4 are attributed to the development of a fresh surface in which adsorption can occur. The second plateau represents the complete saturation of the new surface. This additional layer may occur when

- A proportion of the original surface may be uncovered by reorientation of the molecules already adsorbed, due to intermolecular interactions
- formation of new surfaces in crystalline solids, generating new adsorption sites
- already exposed parts that allow the formation of two layers, for example, due to the formation of micelles.

Finally, the mx subclass occurs occasionally when a fall in slope occurs after the first inflection. This is probably due to the association of the solutes in solution; with an increase in concentration, the solute–solute attraction begins to increase more rapidly than the adsorbent–solute attraction.

2.5.2 Langmuir Model

The adsorbent and the adsorbate are in dynamic equilibrium, and the fractional coverage of the surface depends on the concentration of the adsorbate. The extent of surface coverage is normally expressed as the fractional coverage, Θ (Langmuir 1918):

$$\Theta = \frac{Number\ of\ adsorption\ sites\ occupied}{Number\ of\ adsorption\ sites\ available} \tag{2.1}$$

In the dynamic adsorption equilibrium, the adsorption and desorption rates are the same, so:

$$A(aq) + M(surface) \Leftrightarrow AM(surface)$$

The rate of surface coverage due to adsorption is proportional to the solution concentration C_A of A and the number of vacant sites $N(1-\Theta)$, where N is the total number of sites and can be expressed as

$$\frac{d\Theta}{dt} = k_a C_A N(1-\Theta) \tag{2.2}$$

The change of Θ due to desorption is proportional to the number of adsorbed species $N\Theta$, so

$$\frac{d\Theta}{dt} = -k_d N\Theta \tag{2.3}$$

where the kinetic constants are ka for adsorption and kd for desorption. At equilibrium, there is no change in the composition in both phases (the sum of these two rates is equal to zero), and solving for Θ results in the Langmuir isotherm:

$$\Theta = \frac{K_L C_e}{1 + K_L C_e} \tag{2.4}$$

where the Langmuir constant (KL) is

$$K_L = \frac{K_a}{K_d} \tag{2.5}$$

Considering the exchange of molecules between adsorbed and liquid phase, the fraction covered can be considered the relation between the adsorption capacity at equilibrium (q_e) and the maximum adsorption capacity, which occur when all sites of the monolayer are occupied (q_m)

$$\Theta = \frac{q_e}{q_m} \tag{2.6}$$

Therefore the Langmuir equation becomes:

$$q_e = \frac{q_m K_L C_e}{1 + K_L C_e} \tag{2.7}$$

In practice, the constant k_L is associated with increased affinity of the adsorbate by adsorbent, since k_L represents the inverse of the equilibrium concentration in the liquid phase when the adsorption capacity reaches 50% of the monolayer adsorption capacity (or $f(1/k_L) = 0.5q_m$, where f is the function of the Langmuir isotherm). Therefore, k_L increase leads to a higher initial slope of the adsorption isotherm. On the other hand, qm is associated with the curve plateau formation and complete saturation of the monolayer adsorbate. q_m is in the order from unity to tens of milligrams per gram in the case of monatomic ion adsorption and the order from hundreds to thousands of milligrams per gram for dyes and larger molecule adsorption. However, the maximum monolayer adsorption capacity can vary due to many factors, such as the chemical structure of the adsorbate and adsorbent, molecular size, and nature of the adsorbent. An important work on isotherms of absorption of geopolymers was conducted by T.W. Cheng [45]. They performed experiments with the applications of geopolymer in a SiO_2 to Na_2O molar ratio of 1.0 alkali solution, at different pH, to adsorb heavy metals of various concentrations. The experimental data were analyzed using the Langmuir model to obtain the isothermal adsorption curves and the parameters. According to Purkait et al. [46], the expressions of the Langmuir isotherm model are represented as

$$\frac{C_e}{q_e} = \frac{1}{q_m K_L} + \frac{C_e}{q_m} \tag{2.8}$$

A linear equation can be obtained by plotting C_e / q_e versus C_e. The maximal amount of heavy metal ion adsorption q_m and the Langmuir constant K_L were determined from the intercept and the slope of the plot. All the related parameters are listed in Table 2.5 and represented in the Figure 2.11.

The data obtained show that the metakaolin based geopolymer has excellent adsorption ability. Its adsorption dynamics fit the pseudo-second-order kinetic model well and the isothermal curve was superior for fitting the Langmuir model, suggesting that heavy metal ions perform as a single molecule layer for geopolymer adsorption. The results reveal that the geopolymer adsorption reaction for heavy metal ions is endothermic, and implies that the adsorption is an ionic reaction when heavy metal ions exchange with Na^+ in the geopolymer. Furthermore, a higher pH (for example, pH 4–5) can increase the number of heavy metal ions adsorbed on the geopolymer.

pH	Heavy metal	Langmuir model		
		q_m (mg/g)	K_L (1/mg)	R^2
<2	Pb^{2+}	8.13	0.2031	0.998
	Cu^{2+}	3.61	0.6852	0.996
	Cr^{3+}	4.69	0.2586	0.995
	Cd^{2+}	3.36	1.5225	0.998
4.0	Pb^{2+}	147.06	0.1135	0.994
	Cu^{2+}	48.78	0.0258	0.993
	Cr^{3+}	19.94	0.1580	0.998
	Cd^{2+}	67.57	0.4485	1.000

Table 2.5 *Langmuir parameters for different heavy metals*

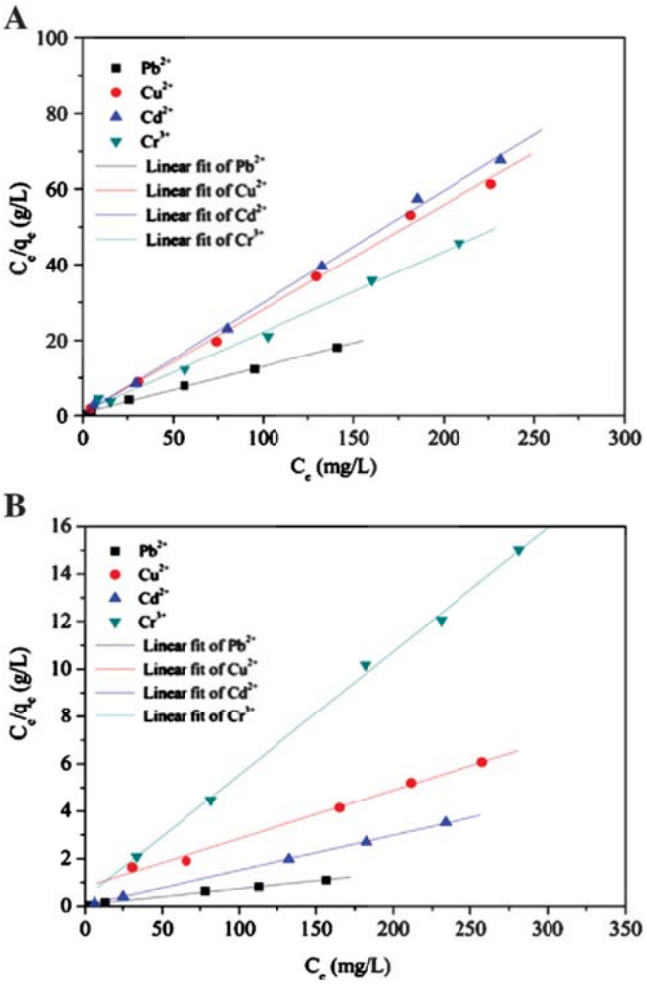

Fig. 2.11 *Langmuir isotherm for the adsorption of heavy metals onto geopolymer.* ***(a)*** $pH = 2$ *and* ***(b)*** $pH = 4$

Chapter 3

From the production of spheres to 3D printing

This chapter aims to explain the reason behind the choice of spherical geometry first and then the evolution through a more complex geometry with the use of 3D print technology. Initially, an overview of the specific surface area calculations is provided, with a further link with the adsorption mechanism. Subsequently, a description of the pressure drop phenomena inside the fixed bed column is given, by focusing on the Ergun equation and its adaptability in the description of load losses on a solid lattice. Lastly, a brief introduction to 3D printing technology is illustrated.

3.1 The reasons behind the choice of spherical geometry

We saw in Chapter 2 the reasons that led a study and therefore the use of geopolymers in the field of purification of wastewater exploiting their excellent characteristics as an adsorbent substrate. In common practice, it is always chosen to insert the adsorbent substrate in a spherical shape. Why? The general structure of a bed of particles can often be characterized by the specific surface area of the bed S_B [47] and the fractional voidage of the bed e. S_B is the surface area presented to the fluid per unit volume of bed when the particles are packed in a bed. Its units are $(length)^{-1}$. e is the fraction of the volume of the bed not occupied by solid material and is termed the fractional voidage, voidage, or porosity. It is dimensionless. Thus the fractional volume of the bed occupied by solid material is $(1-e)$. S is the specific surface area of the particles and is the surface area of a particle divided by its volume.

Its units are again $(length)^{-1}$. For a sphere, for example:

$$S = \frac{\phi d^2}{\phi d^3/6} = \frac{6}{d} \tag{3.1}$$

The table 3.1 shows some values of S, S_B and e for various geometries.

	Solid constituents		**Porous mass**	
No.	**Description**	**Specific surface area** $S(m^2/m^3)$	**Fraction voidage, e (-)**	**Permeability coefficient B** (m^2)
	Spheres			
1	0.794 mm diam.	7600	0.393	6.2×10^{-10}
2	1.588 mm diam.	3759	0.405	2.8×10^{-9}
	Cubes			
3	3.175 mm	1860	0.190	4.6×10^{-10}
4	3.175 mm	1860	0.425	1.5×10^{-8}
	Cylinders			
5	3.175 mm $\times$ 3.175 mm diam.	1840	0.401	1.1×10^{-8}
6	3.175 mm $\times$ 6.35 mm diam.	1585	0.397	1.2×10^{-8}
	Discs			
7	3.175 mm diam. $\times$ 1.59 mm	2540	0.398	6.3×10^{-9}

Table 3.1 *Properties of beds of some regular-shaped materials*

It can be seen that S and S_B are not equal due to the voidage which is present when the particles are packed into a bed. If point contact occurs between particles so that only a very small fraction of surface area is lost by overlapping, then:

$$S_B = S(1-e) \tag{3.2}$$

As can be seen from the data shown in table 3.1, the specific surface area for a spherical geometry is greater than that of any other geometry. It is therefore evident that a larger surface area is preferable in adsorption processes since these are superficial phenomena.

Taking up the Languimir model (already described in paragraph 2.5.2) becomes even easier to understand this correlation; it is based on 4 important assumptions:

- The surface containing the adsorbing sites is a perfectly flat plane with no corrugations (assume the surface is homogeneous)
- The adsorbing gas adsorbs into an immobile state.
- Each site can hold at most one molecule of A (mono-layer coverage only).
- There are no interactions between adsorbate molecules on adjacent sites.

Fig. 3.1 *Representation of the Langmuir assumptions*

Figure 3.1 is a simple graphic representation of the assumptions made by Langmuir for the development of its adsorption isotherms. It is therefore clear that an increase in the surface corresponds to an increase in the adsorption capacity independent of the type of material used and it is precisely for this reason that in most applications spherical geometry is preferable. At this point, it would seem that the choice of spheres with the smallest possible diameter is the ideal condition we would like to have. However this is not true; it is necessary to consider another important phenomenon (described in the next section) that occurs inside the fixed-bed columns, that is the pressure drop.

3.2 Pressure drop

The flow of fluids through beds composed of stationary granular particles is a frequent occurrence in the chemical industry and therefore expressions are needed to predict pressure drop across beds due to the resistance caused by the presence of the particles. The first experimental work on the subject was carried out by Darcy in 1830 when he examined the rate of flow of water from the local fountains through beds of sand of various thicknesses. It was shown that the average velocity, as measured over the whole area of the bed, was directly proportional to the driving pressure and inversely proportional to the thickness of the bed.

This relation, often termed Darcy's law, has subsequently been confirmed by several works and can be written as follows:

$$u_c = K\frac{-\Delta P}{l} \tag{3.3}$$

where:

- $-\Delta$P is the pressure drop across the bed
- l is the thickness of the bed
- u_c is the average velocity of flow of the fluid
- A is the total cross-sectional area of the bed
- V is the volume of fluid flowing in time t
- K is a constant depending on the physical properties of the bed and fluid

The linear relation between the rate of flow and the pressure difference leads one to suppose that the flow was streamline. This would be expected because the Reynolds number for the flow through the pore spaces in a granular material is low since both the velocity of the fluid and the width of the channels are normally small. The resistance to flow then arises mainly from viscous drag can then be expressed as:

$$u_c = B\frac{-\Delta P}{\mu l} \tag{3.4}$$

where μ is the viscosity of the fluid and B is termed the permeability coefficient for the bed and depends only on the properties of the bed. The value of the permeability coefficient is frequently used to indicate the ease with which a fluid will flow through a bed of particles or a filter medium. Many attempts have been made to obtain general expressions for pressure drop and mean velocity for flow through packings in terms of voidage and specific surface, as these quantities are often known or can be measured. Alternatively, measurements of the pressure drop, velocity, and voidage provide a convenient way of measuring the surface area of some particulate materials, as described later. The analogy between streamline flow through a tube and streamline flow through the pores in a bed of particles is a useful starting point for deriving a general expression. The equation for streamline flow through a circular tube is:

$$u = \frac{d_t^2}{32\mu}\frac{-\Delta P}{l_t} \tag{3.5}$$

where:

- μ is the viscosity of the fluid
- u is the mean velocity of the fluid
- d_t is the diameter of the tube
- l_t is the length of the tube

If the free space in the bed is assumed to consist of a series of tortuous channels, equation 4.5 may be rewritten for flow through a bed as:

$$u_1 = \frac{d\prime_m^2}{K\prime\mu}\frac{-\Delta P}{l\prime} \tag{3.6}$$

where:

- $d\prime_m$ is some equivalent diameter of the pore channels
- $K\prime$ is a dimensionless constant whose value depends on the structure of the bed
- $l\prime$ is the length of the channel
- u_1 is the average velocity through the pore channels

For equation 4.6 to be generally useful, an expression is needed for d_m, the equivalent diameter of the pore space. Kozeny [48] proposed that d_m may be taken as:

$$d\prime_m = \frac{e}{S_B} = \frac{e}{S(1-e)} \tag{3.7}$$

where:

$$\frac{e}{S_B} = \frac{volume\ of\ voids\ filled\ with\ fluid}{wetted\ surface\ area\ of\ the\ bed} \tag{3.8}$$

Then taking $u_1 = \frac{u_c}{e}$ and $l\prime \propto l$, equation 4.6 becomes:

$$u_c = \frac{1}{K_C}\frac{e^3}{S_B^2}\frac{1}{\mu}\frac{-\Delta P}{l} \tag{3.9}$$

K_C is generally known as Kozeny's constant and a commonly accepted value for K_C is 5. Equation 4.9 applies to streamline flow conditions, though Carman [49] and others have extended the analogy with pipe flow to cover both streamline and turbulent flow conditions through packed beds. In this treatment a modified friction factor $\frac{R_1}{\rho\mu_1^2}$ is plotted against a

modified Reynolds number R_{e1}. This is analogous to plotting $\frac{R}{\rho\mu^2}$ against R_e for flow through a pipe. The modified Reynolds number R_{e1} is obtained by taking the same velocity and characteristic linear dimension d'_m as were used in deriving equation 4.9. Thus:

$$R_{e1} = \frac{\mu_c \rho}{S(1-e)\mu} \tag{3.10}$$

The friction factor, which is plotted against the modified Reynolds number, is $\frac{R_1}{\rho\mu_1^2}$ where R_1 is the component of the drag force per unit area of particle surface in the direction of motion. R_1 can be related to the properties of the bed and pressure gradient as follows. Considering the forces acting on the fluid in a bed of unit cross-sectional area and thickness l, the volume of particles in the bed is $l(1-e)$ and therefore the total surface is $Sl(1-e)$. Thus the resistance force is $R_1 Sl(1-e)$. This force on the fluid must be equal to that produced by a pressure difference of P across the bed. Then, since the free cross-section of fluid is equal to e:

$$\frac{R_1}{\rho\mu_1^2} = \frac{e^3}{S(1-e)} \frac{-\Delta P}{l} \frac{1}{\rho\mu_c^2} \tag{3.11}$$

Carman found that when $\frac{R_1}{\rho\mu_1^2}$ was plotted against R_{e1} using logarithmic coordinates, his data for the flow through randomly packed beds of solid particles could be correlated approximately by a single curve (curve A, Figure 3.2, whose general equation is:

$$\frac{R_1}{\rho\mu_1^2} = 5R_{e1}^{-1} + 0.4R_{e1}^{-0.1} \tag{3.12}$$

From equation 4.16 it can be seen that for values of R_{e1} less than about 2, the second term is small and, approximately:

$$\frac{R_1}{\rho u_1^2} = 5R_{e1}^{-1} \tag{3.13}$$

As the value of R_{e1} increases from about 2 to 100, the second term in equation 4.16 becomes more significant and the slope of the plot gradually changes from -1.0 to about $\frac{-1}{4}$. Above R_{e1} of 100 the plot is approximately linear. The change from complete streamline flow to complete turbulent flow is very gradual because flow conditions are not the same in all the pores. Thus, the flow starts to become turbulent in the larger pores, and subsequently in successively smaller pores as the value of R_{e1} increases. Probably, the flow never becomes completely turbulent since some of the passages may be so small that streamline conditions prevail even at high flow rates. the curve B in figure 3.2 represents the Sawistowski equation that describes the flow of a fluid through hollow bed packing; we do not proceed to a further description of this model as it is not of interest to our case study.

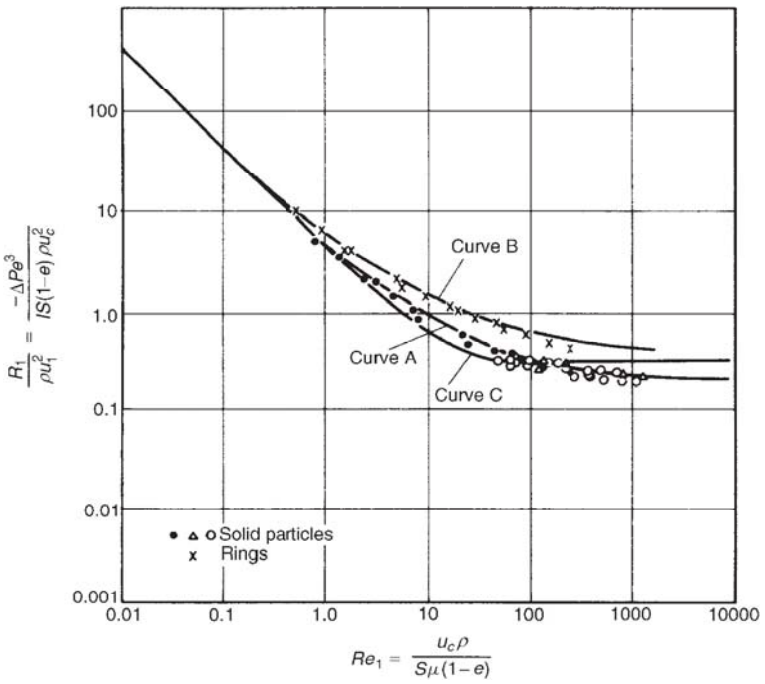

Fig. 3.2 *Carman's graph*

For flow through random packings packed columns, Ergun [48] obtained a good semi-empirical correlation for pressure drop:

$$\frac{-\Delta P}{l} = 150\frac{(1-e)^2}{e^3}\frac{\mu u_c}{d^2} + 1.75\frac{1-e}{e^3}\frac{\rho u_c^2}{d} \tag{3.14}$$

This equation is plotted in the fig 3.2 as curve C.The form of equation 4.21 is somewhat similar to that of equations 4.16 and 4.17, in that the first term represents viscous losses which are most significant at low velocities and the second term represents kinetic energy losses which become more significant at high velocities. Now we rewrite the equation3.14 in terms of Ergun friction factor f_{Erg}

$$f_{Erg} = \frac{\Delta p}{L\rho v_s^2} D\frac{\varepsilon^3}{(1-\varepsilon)} = \frac{150}{Re_{Erg}} + 1.75 \tag{3.15}$$

where:

- f_{Erg} is the Ergun frictional factor
- Δp is the pressure drop across the bed
- L is the length of the bed (not the column)

- D is the diameter of the particles
- ρ is the density of the fluid
- μ is the dynamic viscosity of the fluid
- v_s is the superficial velocity (i.e. the velocity that the fluid would have through the empty tube at the same volumetric flow rate)
- ε is the void fraction of the bed (bed porosity at any time)

It, therefore, becomes quite clear that a reduction in diameters would lead to an increase in terms of load losses within the fixed bed columns, thus making greater pressures in revenue necessary. Thus the choice of the diameter resulted in a trade-off between the adsorption capacity and the load losses.

- A reduction in diameter leads to an increase in surface area and therefore to an increase in adsorption capacity
- On the contrary, a reduction in the diameter leads to an increase in the load losses

Fortunately, there is another way to increase the surface area, ie to increase the porosity of the material used. This is exactly what was used in the laboratory procedures used for this thesis but we will discuss it in more detail in chapter 5.

3.2.1 Pressure drop structured bed

We saw in the previous section how the pressure drop inside the fixed bed column is an extremely important parameter that must be taken into consideration. Over the last few years, the use of structured bed packings is preferred over granulated materials in applications where load losses must be minimized, still guaranteeing a high specific surface area. The low pressure drop is probably the main advantage to take in account because permits perform reactions at a very high space velocity (low contact time) and in this way, increase in some cases the selectivity and/or use of a high length over diameter ratio reactors. Nevertheless, chemical

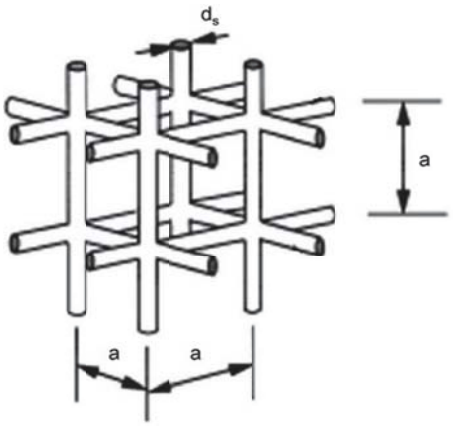

Fig. 3.3 *Cubic cell mode*

engineering parameters are still not completely clear for the scientific community and many approaches are attempted to solve this problem. Pressure drop measurement presented in the literature [50] confirmed that foam matrices follow the Forscheimer relationship. The pressure drop is the sum of viscous and inertial terms and Ergun model may simulate these results. But, the major problem in the foam pressure drop estimation is to reliably define structural properties of the cellular medium to define the equivalent particle diameter (d_p) necessary to use the well known Ergun's equation. These considerations can also be extended, with good approximation, to the particular geopolymeric structures that we will see then be produced through 3D printing. As we have seen in section 3.2, Ergun's equation has been successfully employed in the literature to predict the pressure drop of granular media. Ergun's equation for an incompressible fluid, through a rigid and homogeneous porous medium, is given by

$$\frac{-\Delta P}{l} = 150\frac{(1-e)^2}{e^3}\frac{\mu u_c}{d^2} + 1.75\frac{1-e}{e^3}\frac{\rho u_c^2}{d}$$

The major problem in the foam pressure drop estimation is to reliably define the structural properties of the cellular medium to replace the equivalent particle diameter (d_p). Different geometrical models for the foam structure presented in the literature are very complex and empirical equation must be used to fit the data; consequently, we consider only the cubic cell model presented by Giani et.al [51] with the assumption that the cellular structure is made of solid cylindrical filaments (struts) connected in the three dimensions as a regular cubic lattice (3.3). Richardson used external surface areas (a_c) to compare the pressure drop of the ceramic foams with the spherical particles [50]. The total volume V_0 is given by

$$V_0 = b^3 \tag{3.16}$$

The overall volume of the struts V_S can be calculated as a function of the foam void fraction (ε):

$$V_S = (1-\varepsilon)V_0 \tag{3.17}$$

However, V_S can be calculated as the overall volume of the cylinders (struts) included in the unit cell. Assuming that the intersection volume of the strut is of second order, V_S is well estimated by

$$V_S = \frac{12}{4}\pi(\frac{d_s}{2})^2 b \tag{3.18}$$

Combing Eqs (3.16) and (3.17) the following expression is obtained for d_s from the pitch (a) and porosity (ε)

$$d_S = \frac{a[(4/3\pi)(1-\varepsilon)]^{1/2}}{1-[(4/3\pi)(1-\varepsilon)]^{1/2}} \tag{3.19}$$

The external specific surface area per unit cell volume is then computed as

$$a_c = \frac{4}{d_s}(1-\varepsilon) \tag{3.20}$$

For comparing foams and particles, the external specific surface area per unit bed volume of spherical particles is used. ac is given by the following equation:

$$a_c = \frac{6}{d_p}(1-\varepsilon) \tag{3.21}$$

Finally, the substitution of (3.20) in (3.21) gives the relationship between strut and particle diameter for a porous medium with the same porosity:

$$d_p = \frac{6}{4}d_s \tag{3.22}$$

Eqs. (3.19) and (3.22) lead to the particle diameter equivalent to the cellular structure based only on the size of its mean window (a) and the foam porosity. Once the porosity (ε) is quantified, Ergun's equation can be used to estimate the pressure drop in the foam. This analogy between foams and bed of spherical particles has no physical meaning due to the high void inside the virtually packed bed. However, allows the direct determination of the estimation of the pressure drops in a very simple and reliable way for further studies. This proposed model was used by Lacroix et.al [52] to fit the experimental data with a correct estimation as shown in figure 3.4. The results obtained by their works clearly show that pressure drops of foams are much lower than the ones of a packed bed of spheres(fig 3.5)

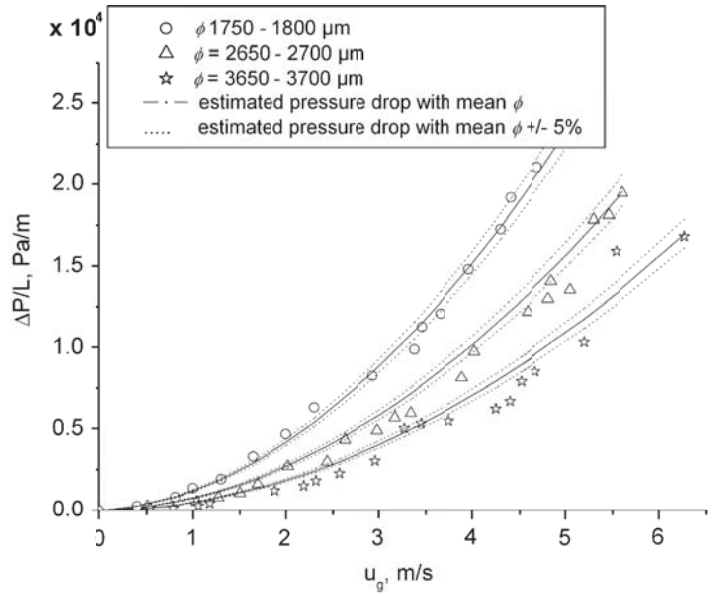

Fig. 3.4 *Pressure drop measurement and estimated results*

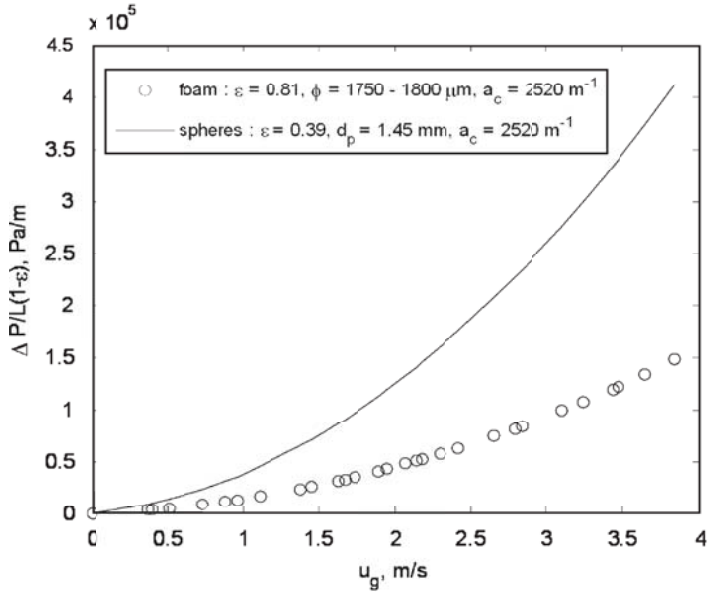

Fig. 3.5 *Comparison of pressure drop between foam and real packed bed*

Although this model has been used for the description of foam, therefore not applicable for the description of the 3D geopolymeric structures treated in this work (or at least not without some considerations), it is, however, a demonstration of how effectively the use of structured packed bed leads to a reduction in load losses.

3.3 Additive manufacturing

As seen in the previous chapters, the high adsorption capacities of the geopolymers have made it an ideal material for the constitution of the adsorbent substrate inside the fixed-bed column. However, subsequent analyses have highlighted the need for a change of geometry of these substrates to minimize the pressure losses within these systems. An effective way of producing geopolymer-based structures capable of providing this new need is additive manufacturing. Additive manufacturing (AM), also designated as solid freeform fabrication (SFF), Rapid Prototyping (RP), or 3D printing, describes a class of technologies in which a part is directly generated from a virtual model by adding material to form the part. AM is defined by ASTM F2792-12a (Standard Terminology for Additive Manufacturing Technologies) as the "process of joining materials to make objects from 3D model data, usually layer upon layer, as opposed to subtractive manufacturing methodologies, such as traditional machining". According to the philosophy of AM, the choice of a 3D computer graphic, 3D model, and material system are sufficient to build apart. Consequently, it is possible to generate parts with arbitrary geometries without the need of adapting the typical manufacture process itself. Preferably, parts ready to use, that is, possessing the final physical properties of the desired object, are generated using AM technologies, but also the manufacture of semifinished parts, requiring additional processing, has turned out to be technically and economically feasible. The material (feedstock) is typically fed into the process as a powder/granulated, paste or suspension, that is, the material is in a state optimized for the layer deposition process. In the manufacturing process itself, the material is used to build up the desired object and it is simultaneously transferred into a state possessing its final physical properties, or at least a mechanical strength sufficient to transfer the built object to further processing steps. According to the needs of the particular material used, the desired geometry or the purpose of the object being built, an entire set of AM technologies has been developed. Polymeric, metallic, and ceramic materials can be all processed by these technologies. The initial motivation for the development of RP technologies, that is, technologies for the manufacturing of individual products without any requirement for dedicated tooling, was to reduce the time to market of new products by shortening the period between design, testing, and implementation. While in the '80s and '90s, the basic technologies for AM were developed and flexibility in design was the priority, nowadays the physical properties of the parts generated are a major concern. Accordingly, the terminology for this class of technologies shifted gradually from RP to AM. The direct deposition of ceramic slurries is arguably the most used AM technology for the generation of porous structures. It consists of the extrusion through a nozzle of a viscous ceramic paste in the form of a filament. The control of the rheological

properties of the filament is essential to prevent deformation of the part after extrusion and sagging of the filaments, especially when the geometry includes spanning features as in most porous components. The technique was originally patented and developed by Cesarano at the Sandia National Laboratories in the USA. In Robocasting, a ceramic suspension with a high solid loading undergoes a transformation from a pseudoplastic to a dilatant behavior when extruded in air, triggered by minimal drying of the slurry. Drying in air, however, limits the minimum diameter of the printing nozzle to about 500 μm, otherwise clogging is experienced. To overcome these issues, inks have been developed which have a reversible gel transformation and are deposited in a nonwetting (often oil) bath. Briefly, they behave like a viscous gel when loaded in the printing head, but as they are extruded the shear stress breaks the gel structure and the viscosity decreases of several orders of magnitude. After extrusion, the fluid undergoes quick gelation increasing again the viscosity to a level before shearing which prevents deformation of the filament. This behavior can be achieved by controlled flocculation of a ceramic suspension (e.g., by a change in pH, ionic strength of the solvent, addition of polyelectrolytes) to form a gel, or by using gelling additives, for example, by using an inverse thermo-reversible gel. Another possibility is the formulation of a ceramic ink containing a polymeric binder and plasticizer (e.g., PVB and PEG), which can be added up to 23 wt% (relative to the ceramic phase). For fine lattice structures, defects generated by debinding were not reported. These variations in Robocasting have been mostly denominated DIW technologies. Typical nozzle sizes are in the range 100–1000 μm and, after drying, the material has a high green density (up to 60%), which allows achieving almost complete densification upon sintering. The combination of fine and dense filaments makes the technology particularly attractive for the production of components suitable for several applications, based on structural and functional ceramics. The ideal rheology for a DIW ink is that of a Bingham pseudoplastic fluid, i.e. a fluid who shows initial yield

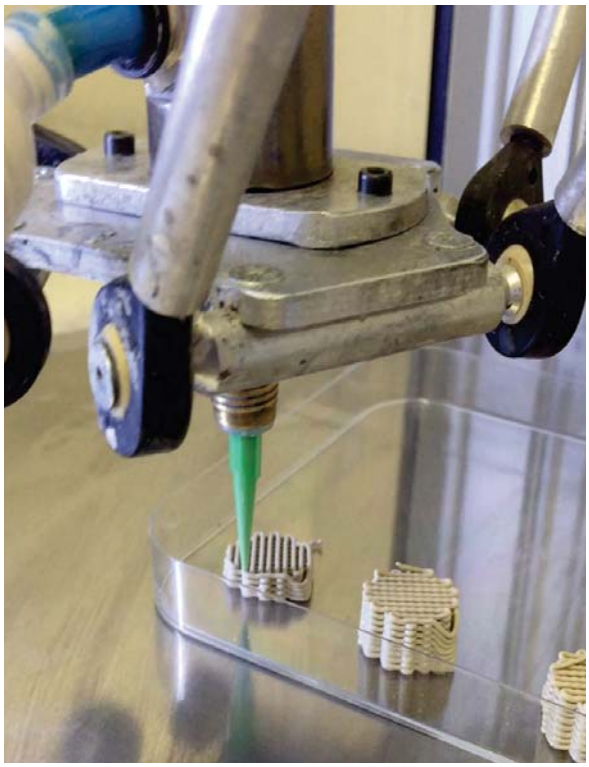

Fig. 3.6 *Direct ink writing laboratory process*

stress and whose viscosity decreases with the increasing shear rate. In this way, the ink can be easily extruded at low pressure but can retain its shape once deposited, even in case of suspended struts. However, DIW of geopolymeric inks is a particularly challenging task, because the inks are subjected to ongoing (polycondensation/geopolymerization) reactions which continuously modified their rheological properties over time. Time has been involved as the 4th dimension in so-called 4D printing technologies to produce objects able to change their configuration or function depending on external stimuli [53]; geopolymeric slurries could be good candidates as smart materials for 4D printing once their reaction over time could be effectively controlled. An important study concerning the development of a geopolymeric ink was carried out by Giorgia Franchin et.al [54] at the laboratories of the University of Padua. They compared several inks with different water content and different kinds and amounts of additives to determine which parameters enable the optimal extrusion as well as the retention of the produced shape.

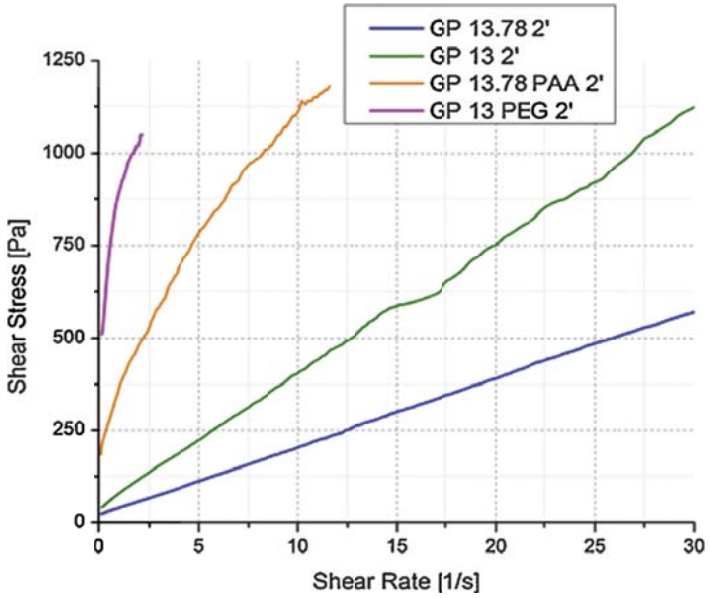

Fig. 3.7 *Flows curves from steady rate sweep test performed on the four inks*

As can be seen from the figure 3.7 shear thinning behavior was confirmed for pure geopolymer mixtures GP 13.78 and GP 13, as an initial decrease in the viscosity values were detected at low shear rates. The rapid destruction of freshly formed aluminosilicate bonds due to the increasing stress likely responsible for such behavior. GP 13.78 PAA had higher yield stress and viscosity values; the slope of the flow curve decreased with the increasing shear rate also at higher values, testifying a more significant shear thinning behavior. Sample GP 13 PEG possessed even higher yield stress and viscosity possibly due to its lower water content. They also performed dynamic oscillation tests to asses whether the inks had a

transition to low rigidity system at higher shear stress values.

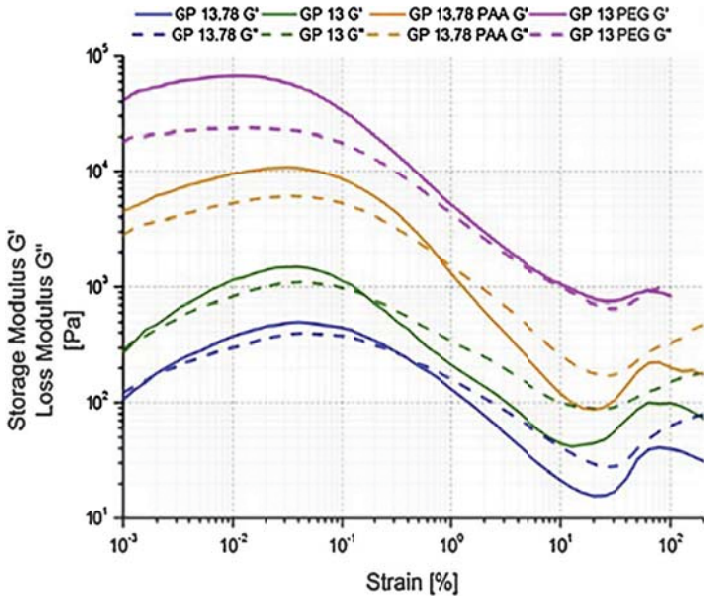

Fig. 3.8 *Dynamic strain sweep test performed on the four inks*

The behavior showed in figure 3.8 could be classified as type IV in the LAOS system, and could be explained if a reversible gel nature was assumed: the geopolymer network in formation was responsible for the elastic component, but the microstructural arrangement of the material could still be gradually destroyed by stresses above the yield stress, allowing the flow. Based on the results of this works, all inks could potentially be employed for DIW of geopolymeric lattices with such unsupported features. This is an extremely important result both from an environmental point of view and from an economic point of view, making the geopolymers of the ideal candidates for the massive application in the field of water purification

Chapter 4

Experimental

This chapter deals with the main materials used for the production of geopolymer spheres and the main equipment used for their characterization.

4.1 Materials

The raw materials used to create the starting geopolymeric mixture were mainly metakaolin, an alkaline solution prepared with the correct molar ratios in the laboratory, water, and foaming agent. As a metakaolin powder it was used ARGICAL1200S® with the following composition:

Chemical composition	**(%)**
SIO_2	55
Al_2O_3	39
Fe_2O_3	1,8
TiO_2	1,5
$K_2O + Na_2O$	1
$CaO + MgO$	0,6

Table 4.1 *ARGICAL1200S® chemical composition*

3 main alkaline solutions have been used respectively:

- An alkaline sodium-based solution
- An alkaline potassium-based solution
- An alkaline mixed solution (with both sodium and potassium)

The use of 3 different alkaline solutions allowed not only a greater amount of data, but also the possibility to test mostly the dependence of some fundamental properties, such for example the adsorption capacity, on the size of the ions present within the geopolymer lattice. The alkaline solutions were prepared starting from 205K® (with a molar ratio $\frac{K_2O}{SiO_2} = 3.295$)as source of K ion and BritesilC205® (with a molar ratio $\frac{Na_2O}{SiO_2} = 2.05$) as Na source. The procedure used to prepare these solutions will be discussed in the next section. As the foaming agent was used the sodium dodecyl sulfate (SDS) diluted in water. The use of this agent has the only purpose of increasing the specific surface area thanks to the enhancement of the porosity (see Chapter 3 for a more detail explanation). The PEG was used as an inert medium to create a hydrophobic surface for obtaining the spherical surface (the reasons for this choice will be described in more detail in chapter 5).

4.2 Laboratory equipment used

The main instruments used for the experimental tests and the realization of the samples are reported below

4.2.1 X-Ray powder diffraction

Fig. 4.1 *BRUKER©D8 ADVANCE instrument for powder diffractometry.*

For X-ray diffraction, the BRUKER©D8 ADVANCE instrument is used for powder diffractometry. This technique is very important for the study of the solid-state of materials since it allows to recognize the crystalline phases that make up the sample. The instrument exploits the phenomenon of diffraction, associated with the deviation of the wave propagation trajectory when they encounter an obstacle in their path. The effects due to diffraction occur when the electromagnetic wavelength at a precise frequency is made to affect the material sample. The source of the diffractometer, which consists of an X-ray beam with a power of 2 kW (40 kV, 40 mA), emits waves at a known frequency so that the interaction with matter produces

heat, photon emission, fluorescence, absorption, and scattering (coherent or incoherent). It is the incoherent scattering phenomenon that is responsible for the diffraction effects. The electrons infracted become secondary sources of X radiation having the same wavelength as the incident radiation. The interaction with a crystalline material has the consequence that the diffused beams are recombined constructively only in certain directions. In diffractometry, X-rays are exploited, since their wavelength is comparable to the spacing between the atoms of a crystal, therefore they are the right source for diffraction on an interatomic scale. When these waves interact with the atoms of the sample, they behave as a diffraction lattice, producing deviated rays only for particular angles. It is possible, through the detector, to measure these angles and to obtain the spacing value of the diffraction grating, or the distance between the nuclei of the material atoms. In the pattern, the peak obtained represents the diffraction event and its height is directly proportional to the event intensity of the event itself. In laboratory practice, however, since geopolymer is an amorphous material, the use of this equipment does not provide useful data from the structural point of view but allows us to observe peaks due to unreacted material (that must be avoided). Furthermore, as we will see in the next section, it allows us to verify that the inert medium used for the creation of a hydrophobic surface is not present within our material index of the absence of interaction.

4.2.2 Pycnometer

Fig. 4.2 *MICROMETRICSTM™ACCUPYC 1330*

To perform density measurements on samples and powders a helium pycnometer is used MICROMETRICS™ACCUPYC 1330. Gas expansion pycnometer is also known as constant volume gas pycnometer. The simplest type of gas pycnometer (due to its relative lack of moving parts) consists of two chambers, one (with a removable gas-tight lid) to hold the sample and the second chamber of fixed, known (via calibration) internal volume – referred to as the reference volume or added volume. The device additionally comprises a valve to admit a gas under pressure to one of the chambers, a pressure measuring device – usually a transducer – connected to the first chamber, a valved pathway connecting the two chambers, and a valved vent from the second of the chambers. In practice the sample may occupy either chamber, that is gas pycnometers can be constructed

such that the sample chamber is pressurized first, or such that it is the reference chamber that starts at the higher pressure. The working equation of a gas pycnometer wherein the sample chamber is pressurized first is as follows:

$$V_s = V_c + \frac{V_r}{1 - \frac{P_1}{P_2}} \tag{4.1}$$

where:

- V_s is the sample volume
- V_c is the volume of the empty sample chamber (known from a prior calibration step)
- V_r is the volume of the reference volume (again known from a prior calibration step)
- P_1 is the first pressure (i.e. in the sample chamber only)
- P_2 is the second (lower) pressure after expansion of the gas into the combined volumes of sample chamber and reference chamber.

While pycnometers (of any type) are recognized as density measuring devices they are in fact devices for measuring volume only. Density is merely calculated as the ratio of mass to volume; mass being invariably measured on a discrete device, usually by weighing. The volume measured in a gas pycnometer is that amount of three-dimensional space which is inaccessible to the gas used, i.e. that volume within the sample chamber from which the gas is excluded. Therefore, the volume measured considering the finest scale of surface roughness will depend on the atomic or molecular size of the gas. Helium, therefore, is most often prescribed as the measurement gas, not only is it of small size, it is also inert and the most ideal gas. Closed pores, i.e. those that do not communicate with the surface of the solid, are included in the measured volume. Helium may, however, demonstrate some measurable permeability through low-density solids (polymers and cellulosic materials predominantly) thus interfering with the measurement of solid volume. In such cases larger molecule gases such as nitrogen or sulfur hexafluoride are beneficial. Adsorption of the measuring gas should be avoided, as should excessive vapor pressure from moisture or other liquids present in the otherwise solid sample.

4.2.3 Direct Ink Writing Printer

Fig. 4.3 *Direct Ink Wrting Printer 20x40 Delta Turbo*

For the realization of scaffolds using the DIW technique, the Delta Turbo 20x40 printer is used, produced by the Italian company Wasp (Massa Lombarda, Italy). The ink was transferred into a plastic syringe, which served as a cartridge for direct ink writing. Each syringe can contain up to 30 mm^3 of ink. The lateral (XY) resolution of the printer is 120μm; the Z resolution is 4μm. The syringe base system can mount conical nozzles of various sizes (Nordson Italia S.p.a., Segrate, IT) ranging from 100 to 1500μm. After extrusion, it is possible to choose whether to keep the substrate in the air or in immersion in a hydrophobic liquid (typically oil) to limit drying and clogging issues. The printer is equipped with a display from which it is possible to adjust not only the flow speed but also the height at which to position the extruder. The final shape of the product to be produced is designed using the Solid Works®software and subsequently transferred to the internal memory of the printer through the appropriate accommodation for the external SSD memory.

4.2.4 Scanning Electron Microscopy (SEM)

Scanning electric microscopy is a technique which is useful to analyze the surface and topography of a material. SEM functioning is based on the possibility to detect the effects produced by the interaction of electrons with the matter. Typically, a beam of accelerated free electrons, called primary electrons, is focused on the sample by a system of lenses. The interaction between the electrons and the matter lead to different signals which can be treated and amplified to produce a pixel in the screen and create an image. SEM apparatus consists of an electron source, an accelerator system, electromagnetic lenses for beam focusing, detectors, electronic system for data conversion and vacuum system.

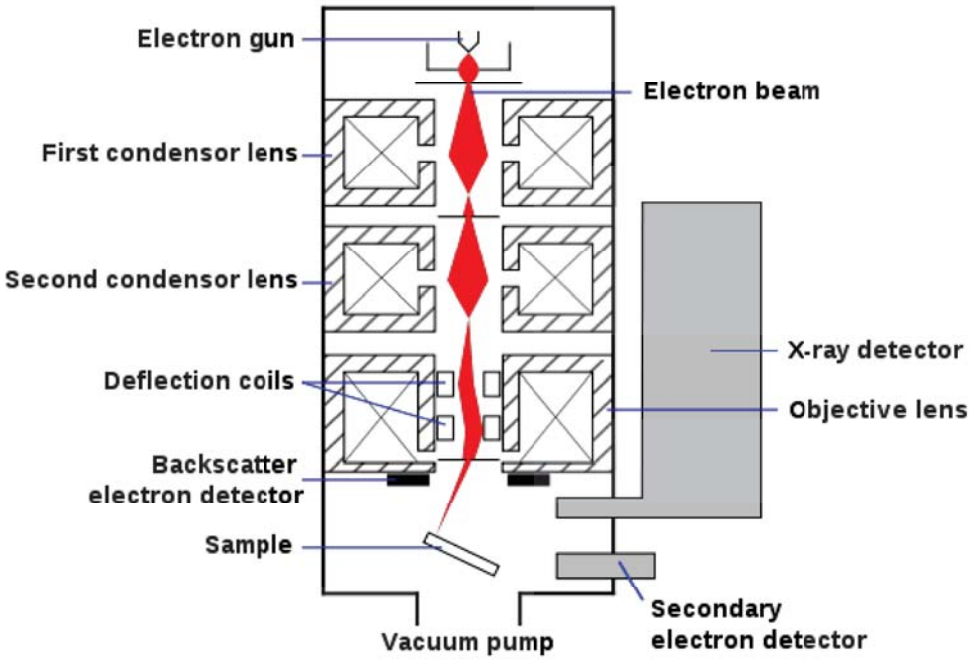

Fig. 4.4 *Schematic Diagram of a SEM*

The main form of signals that are produced by the electronic scansion of the sample are listed below:

- Electronic emission (secondary electrons, back-scattered electrons, Auger electrons)
- Photonic emission (infrared and visible)
- X-ray emission

Each of these forms of the signal provides indications on composition and morphology of the material but the most commonly exploited source is the emission of secondary electrons. Secondary electrons have lower energy (< 50 eV) than back-scattered electrons and they are the result of the interaction between the primary beam and the electron cloud of the material's surface. This interaction leads to the ejection of electrons from the valence band of the specimen's atoms (inelastic scattering). Non-conductive materials like polymers must be coated with high atomic number conductive materials (like gold) to prevent the accumulation of static electric charges on the surface of the sample. The presence of static charges on the surface causes interference with the signals carried by the secondary electrons and deteriorates the image formation. Secondary electrons provide information about the morphological characteristics of the sample surface. The identification of the tridimensional details of the specimen's surface is due to the so-called edge effect. A difference, in contrast,

is revealed by the detector when the secondary electrons are scattered from different areas of the sample surface. Signal brightness is proportional to the number of secondary electrons which tend to change from flat areas to sharp surfaces and edges on the material. When the electron beam impacts the sample perpendicular to the surface a narrow area is irradiated and few electrons escape. As the angle of incidence increases, a larger area interacts with the incident beam, resulting in more electrons being emitted from the sample. In this study, we used the JEOL JSM 6490™SEM model. The equipment is equipped with a detector for backscattered electrons that allows acquiring morphological images correlated to variations in atomic number (Z), these differences are visible through different levels of gray present and localized in the black and white image obtained from the examined area. To characterize these compositional differences it is possible to use the analysis system of the company JEOL™(IXRF SYSTEMS 500) for the measurement of fluorescence X-rays in energy dispersion which allows the simultaneous determination of all the elements present in the area investigated simultaneously with the morphological observation. Even very small surfaces can be analyzed qualitatively and quantitatively, obtaining distribution maps of the elements present in the area in question or concentration profiles of one or more elements along arbitrarily chosen segments. The use of microanalysis, even if not very accurate, served mainly as further proof of the presence or absence on the surface of any trace of residual PEG (medium used for the production of a hydrophobic surface) and ethanol used for washing the spheres.

Chapter 5

Production of geopolymer spheres and 3D printing

This chapter deals with the calculations and procedures used for the production of geopolymer spheres carried out in the laboratories of the University of Padua. The performance of this thesis activity also saw the collaboration of Professor Mariella Bruzzoniti of the University of Turin. The last part of this thesis is the 3D printing of geopolymeric structures, only describing the procedure without the justification of the choices made because due to a lack of time that did not allow the achievement and the study of significant results but only mere empirical results.

5.1 Geopolymer Calculations Composition

The first step in creating geopolymer spheres was the choice of chemical composition. As seen in Chapter 1 a material to be considered a geopolymer must respect certain molar ratios(1.6). Going more specifically, the quantity of Al_2O_3 and SiO_2 influence the mechanical properties and the geopolymerization reaction rate; for the application for which these spheres are designed there is no need for excellent mechanical properties as the most important feature is the adsorption capacity. The reaction rate as discussed in Chapter 1 is mainly influenced by the Alumina molar content.

After these considerations, previous tests were conducted and the following molar ratio was found to be the most suitable:

- Al_2O_3=1 mol
- SiO_2=4 mol
- K_2O=1 mol
- H_2O=18 mol

We used as metakaolin ARGICAL1200S®who has this composition (100g of product):

- SiO_2=55g
- Al_2O_3=39g

so the % weight are:

- SiO_2=0.55
- Al_2O_3=0.39

The number of moles are:

- mol SiO_2= $0,009152937$
- mol Al_2O_3= $0,003825029$
- molar ratio $2,392906367$

As mention in Chapter 4, 3 different types of alkaline solution have been prepared. We reported below only the calculations made for the potassium solution because for the other 2 the procedure is the same. The potassium-based solution is made by mixing potassium silicate, potassium hydroxide, and water. The formula of potassium silicate is:

$$K_2O(nSiO_2) + xH_2O$$

n and x are fixed and depends on the type of potassium silicate. In our case, in the lab we use 205K®so:

- n= 3.295
- x=0.155

The molecolar weights of this potassium silicate is MW($K_2O(nSiO_2)$ with n=3.295 = $94.196 + (3.295 \cdot 60.09) = 292.19$. The H_2O impurity in the 205K®is 15.5%(0.155) of the total weight so the number of H_2O moles inside are 2,974991674 mol. The next step is to calculate how many moles, of each component, the solution and the metakaolin give to the geopolymer.

- Al_2O_3: all moles are given by the metakaolin.
- SiO_2 moles are given either by solution and metakaolin
  - mol SiO_2 given by metakaolin = 2,392906367
  - mol SiO_2 given by the solution = 1,6071
- mol K_2O: all moles are given by the solution. As we have seen before the formula of potassium silicate is $K_2O(3.295SiO_2)$ so
  - 1 mol K_2O= 3.295 mol of SiO_2
  - $1 : 3.295 = x : 1.6071 \rightarrow x = 0,487738998$ (actual mol contained within the solution)
  - $1 - 0,487738998 = 0,812261002$ (mol we need to add in order to reach the desired composition of our geopolymer)
  - we can't add mol of K_2O but we can add mol of KOH. In order to do that we have to keep in mind this reaction:

    $$K_2O + H_2O \rightarrow 2KOH$$

    this means that 1 mol of K_2O corrspond 2 mol of KOH, so instead to add 0,812261002 mol of K_2O we add 1,624522003 mol of KOH ($2 \cdot 0,812261002$)
- mol H_2O: all moles are given by the solution (We neglect the subsequent added moles deriving from the use of diluted SDS as the contribution is extremely small).

By transforming all moles into mass (g) we get:

- Al_2O_3= 101.96 g
- SiO_2:
  - SiO_2 Metakaolin = 143.789361 g
  - SiO_2 Solution = 96.571 g

- K_2O:
  - K_2O Solution = 45.94 g
  - K_2O to add = 76.512
  - KOH to add = 91.145 g
- H_2O:
  - H_2O Solution = 26,14156658 g
  - H_2O to add = 283,5127392 g

The total grams of metakaolin, potassium silicate, water, potassium hydroxide that we have to mix to get the geopolymer composition we fixed are:

- Metakaolin = 261.44 g (remember you have to keep in mind that Al_2O_3 and SiO_2 make up the 94% of the entire metakaolin weight)
- Potassium Silicate= 168,6552683 g
- Water =283,5127392 g
- potassium hydroxide = 91,1454315g

To simplify laboratory practice and to avoid wasting material, it was decided to fix the quantity of solution at 25g; the following table (5.1) shows the quantities of metakaolin and SDS compared to 25 g of alkaline solution which must be mixed together to obtain a geopolymer mixture with the correct molar ratios and which is also in an amount sufficient to allow a quantity to be obtained sufficient number of samples to be used for characterization.

Type of geopolimer	Metakaolin (g)	Solution (g)	SDS (g)
K-based	11,11	25	2,88
Na-based	12,68	25	2,88
Mixed	10,98	25	2,88

Table 5.1 *Grams of substance used to prepare the geopolymer spheres*

5.2 Inert Medium

Once the desired composition of the geopolymer was established, and consequently the number of substances that had to be mixed, the next problem was to find an inert medium in which the geopolymerization reaction occurs and that guaranteed the formation of a hydrophobic surface for obtaining a spherical surface. Researchers at the University of Padua laboratories, supervised by prof. Paolo Colombo, have successfully tested many media among which stand out for effectiveness:

- Olive oil
- PEG
- Silicone oil

Among the following, the use of PEG was chosen due to its greater washability and high availability in the laboratory. However, this choice involves a problem; the creation of the spheres, as we will see in the next section, takes place by falling off the geopolymeric mixture using a pipette inside a beaker containing the PEG. However, the density of the medium within which the geopolymerization reaction takes place must be such as to guarantee a certain viscosity of the mixture before contact with the walls or with the bottom of the container. Viscosities that are too low involve a modification of the final geometry of the spheres which are therefore not perfectly spherical but flattened. It is clear that a rudimentary process such as the one used does not allow good control over the final geometry, but to obtain a more accurate characterization, we have tried to improve all the possible steps. We took into consideration the stokes formula to describe the sedimentation process:

$$\upsilon_{\infty} = \frac{2}{9}\frac{\rho_s - \rho_f}{\mu} \cdot g r^2 \tag{5.1}$$

where:

- υ_{∞} is the sedimentation velocity
- ρ_s is is the mass density of the particles
- ρ_f is is the mass density of the fluid
- μ is is the dynamic viscosity
- g is the gravitational acceleration.
- r is the radius of the spheres

The procedure used in this thesis, however, uses a PEG that is not at room temperature because to guarantee a faster geopolymerization reaction, the whole system is heated through a thermostatic bath at T of 70°C. This involves the need for a PEG density calculation at the working temperature. There are two options available:

- The use of a viscometer for the practical calculation of the PEG viscosity at the temperature of 70°C
- Mathematical interpolations

It was decided to proceed with the mathematic approach because it was faster. From the literature we have the density data for several types of PEG at 20°Cand 98°C; because we heated our system at 70°C to accelerate the reaction, we need a relationship between molecular weight, temperature, and viscosity. However, the interpolation of the data is more complicated since the viscosity data were correlated by using the following equation:

$$ln(v) = A + \frac{B}{T(K) - C} \tag{5.2}$$

where:

- T is the absolute temperature
- v is the kinematic viscosity
- A B and C are values determined by regression using the Statistical Analysis System (SAS, Cary, NC) [55]

For greater accuracy of analysis, it is important to consider that the parameters A, B, C are not constant values but their behavior can be described by the following equations:

$$A = a_0 + a_1 N + a_2 N^2 \tag{5.3}$$

$$B = b_0 \tag{5.4}$$

$$C = (c_0 - c_1)/1 + exp[(N - c_2)/c_3] + c_1 \tag{5.5}$$

Values of the parameters $a_0, a_1, a_2, b_0, c_0, c_1, c_2$ are listed in the table 5.2.

$a_0 = -2.738$	$c_0 = -131.3$
$a_1 = 4.114 \times 10^{-2}$	$c_1 = 179.9$
$a_2 = -1.276 \times 10^{-4}$	$c_2 = -24.48$
$b_0 = 770.2$	$c_3 = 8.319$

Table 5.2 *Parameters of Eq 5.3, 5.4, 5.5*

As can be seen from the table 5.3, N oscillates between two ranges of values.

PEG	avg MW range	N	Calculated Viscosity at 298.15K	Calculated Viscosity at 372.15K
200	190-210	8	43.6	4.34
300	285-315	12-14	57.2-64.3	5.30-5.81
400	380-420	16-18	71.7-79.3	6.34-6.9
600	570-630	26-28	112.1-121.0	9.38-10.1
1000	950-1000	42-46	-	16.0-18.0
1500	1300-1500	58-68	-	25.2-32.4
2000	1900-2200	86-100	-	47.7-60.8

Table 5.3 *Relationship between N range, viscosity($10^{-6} m^2 s^{-1}$) and MW of the PEG*

For a greater accuracy of the final result, we then proceeded with a calculation of the values A, C (B does not show a dependence on N) for each value of N. At this point by replacing the obtained values of A, B, C we obtained various values of dynamic viscosity: This whole mathematical process was implemented in a script produced using the Matlab®software, thus obtaining the following graph that relates Temperature, Molecular weight, and kinematic viscosity.

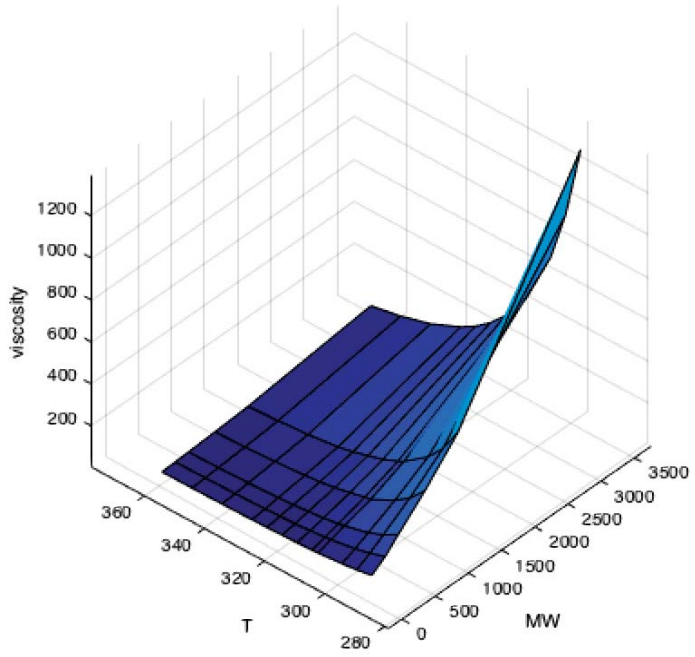

Fig. 5.1 *Graphic obtained with MatLab®representing molecular weight, viscosity, temperature relation*

However, the μ viscosity of the equation (Reference eq of stokes) is a dynamic viscosity; it is, therefore, necessary to use the following equation:

$$v = \frac{\mu}{\rho} \tag{5.6}$$

where:

- v is the kinematic viscosity
- μ is the dynamic viscosity
- ρ is the density

At this point it is necessary to make the following considerations:

- From literature, we know the density values of the various PEG at the process temperature (70°C)
- Pycnometer analysis allows us to obtain data on the density of the spheres
- The radius of the spheres can be considered constant only depending on the size of the pipette used

By fixing the Becher dimensions and measuring the time required for the sphere to reach the bottom in the various fluids, it is possible to obtain a determined value of the sedimentation speed through equation 5.1. Thus imposing a lower speed it is possible to find the optimum viscosity value that the fluid must have to obtain the most perfect spherical shapes possible. Therefore using the graph obtained with Matlab®it is possible to find the appropriate molecular weight. Based on all these considerations, it was decided to use PEG600. However, tests were also conducted using PEG400 and PEG1000 only as a countercheck.

5.3 Laboratory procedure

For the production of geopolymer spheres, the correct quantities of metakaolin and alkaline solution were first weighed; solutions already present in the laboratories of the University of Padua were used. The metakaolin powder was added to the alkaline solution and the whole system was mixed using an automatic mixer to set the speed at 1300rpm for a time of 10 minutes inside a plastic beaker (glass beakers are not used due to the strong basicity of the solution used). Subsequently, 8% by weight (compared to the solution) of SDS is added to the solution (8% takes into account the dilution already done with water, otherwise it is necessary to consider 0.8% of SDS in powder, without dilution) and the system it is left under mixing for another 5 minutes. It is advisable, during the last mixing phase, to shake the beaker to further encourage the formation of foam. The addition of the foaming agent as discussed in chapter 3, has the only purpose of increasing the superficial porosity of the final spheres, increasing the specific area and therefore improving the adsorption capacity. These steps allow to obtain the starting geopolymeric mixture and are represented in the Fig.5.2

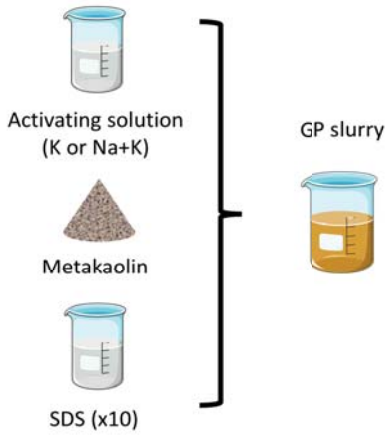

Fig. 5.2 *Schematic representation of the procedure used to obtain the geopolymer slurry*

Simultaneously with the mixing of the geopolymeric slurry, a beaker containing the PEG600 is heated inside a thermostatic bath at a temperature of 70°C. Everything is made through a ceramic bowl containing water positioned on a heating plate inside which, supported by support, the becker containing the PEG is positioned. Once the desired temperature has been reached, the geopolymer mixture is withdrawn through a plastic pipette and dropped into the PEG; every drop of slurry in contact with the PEG creates a sphere. The spheres thus formed are left inside the PEG for about 3/4 minutes, subsequently taken and placed inside a plastic container. We proceed in the same manner until the geopolymer solution reaches a viscosity such that it can no longer be withdrawn (as the geopolymerization reaction proceeds, the viscosity of the previously prepared mixture increases).

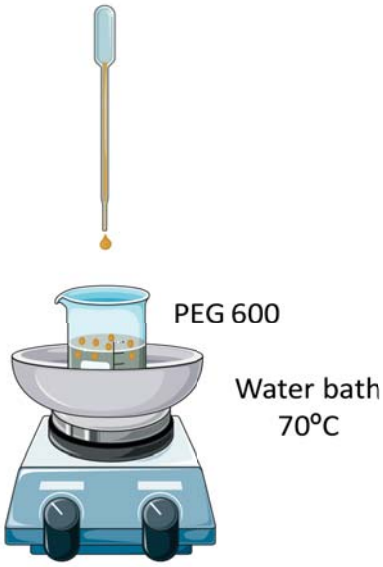

Fig. 5.3 *Schematic representation of the dropped operation*

The spheres thus obtained are washed with ethanol (it is preferable to use colorless ethanol to avoid unwanted colorations of the spheres), dried at room temperature for 24h then dried at 60°Cfor 24h. Some spheres thus produced are subjected to a surface modification treatment by immersion for 30 minutes in $C_9H_{24}Cl^{15}NO_3Si$ and then dried for 1h at room temperature and 2h at 60°C; this operation is performed to test anionic absorption.

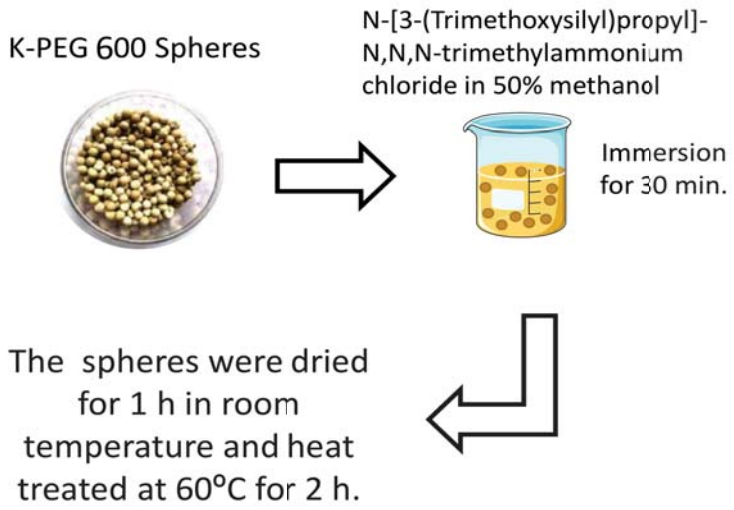

Fig. 5.4 *Schematic representation of surface modification procedure*

5.4 Characterization

The characterization of the spheres was made using the following analyzes:

- SEM analysis for surface porosity control (qualitative data); a microanalysis of the samples was also carried out to search for possible traces of PEG or residual ethanol
- XRD analysis. Although this type of analysis is no used for amorphous materials, this test was made for the detection of any unreacted material (unreacted material is represented by Si and Al peaks in the spectrum)
- Adsorption tests conducted by professor Mariella Bruzzoniti of the University of Turin.
- density measurements

As regards density measurements it is necessary to make some clarifications. Three density measurements are made: geometric density, apparent density and true density. The measurement of geometric density is obtained by dividing the mass of the sample by its geometric volume, calculated using a caliper. Apparent and true density measurements are obtained using a pycnometer. For each alkaline solution 4 spheres are randomly selected and for each its mass and diameter are measured. To obtain the geometric density value the ratio between mass and volume must be calculated

$$\rho_g = \frac{m}{V_g} \tag{5.7}$$

where:

- ρ_g is the geometric density
- m is the mass
- V_g is the geometric volume

The volume measured by the pycnometer is that of the bulk and closed porosities, therefore the open porosity where helium gas can enter is excluded. The apparent density value obtained is:

$$\rho_a = \frac{m}{V_g - V_{PA}} \tag{5.8}$$

where:

- ρ_a is the apparent density
- V_{PA} is the volume occupied by open porosity

Through the obtained density values it is possible to obtain the estimate of the porosity of each material. The geometric density takes into account the total porosity, that is open and closed one. The apparent density, measured starting from the scaffold with the pycnometer, takes into account only the closed porosity. Finally, the true density is the density of the powders, that is without porosity. Using the following formulas, after calculating the density values, it is possible to obtain information on the porosity of the samples:

$$P_{Open} = 1 - \frac{\rho_g}{\rho_a} \tag{5.9}$$

$$P_{Total} = 1 - \frac{\rho_g}{\rho_t} \tag{5.10}$$

$$P_{Close} = P_{Total} - P_{Open} \tag{5.11}$$

where:

- P_{Total} is the total porosity
- P_{Close} is the close porosity
- P_{Open} is the open porosity

The density values allow you to make observations on the materials taken into consideration. In fact, for example, a theoretical value of total porosity equal to zero indicates a completely dense material. The open (or effective) porosity is that which allows the passage of a fluid, it is, therefore, that related to the pores interconnected with each other. So if you want to get a permeable material, you need to have a high percentage of open porosity. Finally, the closed porosity is the non-interconnected one, which therefore does not allow the passage of fluids, but represents a discontinuity in the massive material.

5.5 DIW

5.5.1 Preparation of the ink

The process of ink preparation for DIW printing is extremely delicate since it requires important characteristics discussed in the chapter. First, a solution of sodium silicate, sodium hydroxide, and water were prepared with the following molar ratios:

- $\frac{Na_2O}{SiO_2} = 0.709$
- $\frac{H_2O}{Na_2O} = 13$

This solution had previously been prepared by other researchers and stored at 4°CThe ink formulation had the following molar ratios:

- $\frac{Na_2O}{SiO_2} = 0.263$
- $\frac{SiO_2}{Al_2O_3} = 3.8$
- $\frac{Na_2O}{Al_2O_3} = 1$
- $\frac{H_2O}{Na_2O} = 18$

To the mixture thus composed was added 5%wt of poly(ethylenglycole) PEG with an average molecular weight of 1000 g/mol (Sigma-Aldrich, St. Louis, MO) as a rheology modifier. PEG is frequently used as a thickening agent in aqueous-based systems as it creates an entanglement of polymer chains imparting a shear thinning behavior to the ink. Zeolites stored in ammonia (used as fillers) was added to this solution under mechanical stirring at 500rpm for 5 min at room temperature. Metakaolin powder was then added to the solution under mechanical stirring at 1000 rpm for 10 min at room temperature.

The formulation is summarized as follow:

- 32.26g of metakaolin powder
- 50g of alkaline solution
- 4.11g of PEG

Experimentally, it was found that the ink could be printed for ˜1.5 to 2h after mixing before it became too viscous. This limit depended from the equipment in use (for which no viscosity threshold was provided by the company). However, it was observed that extruding the ink at an advanced stage of reaction would result in a clumpy, disrupted filament which would not further rea

5.5.2 Generation of 3D model

As a 3D model was used a model designed by Ing.Giorgia Franchin and represented in the following figures

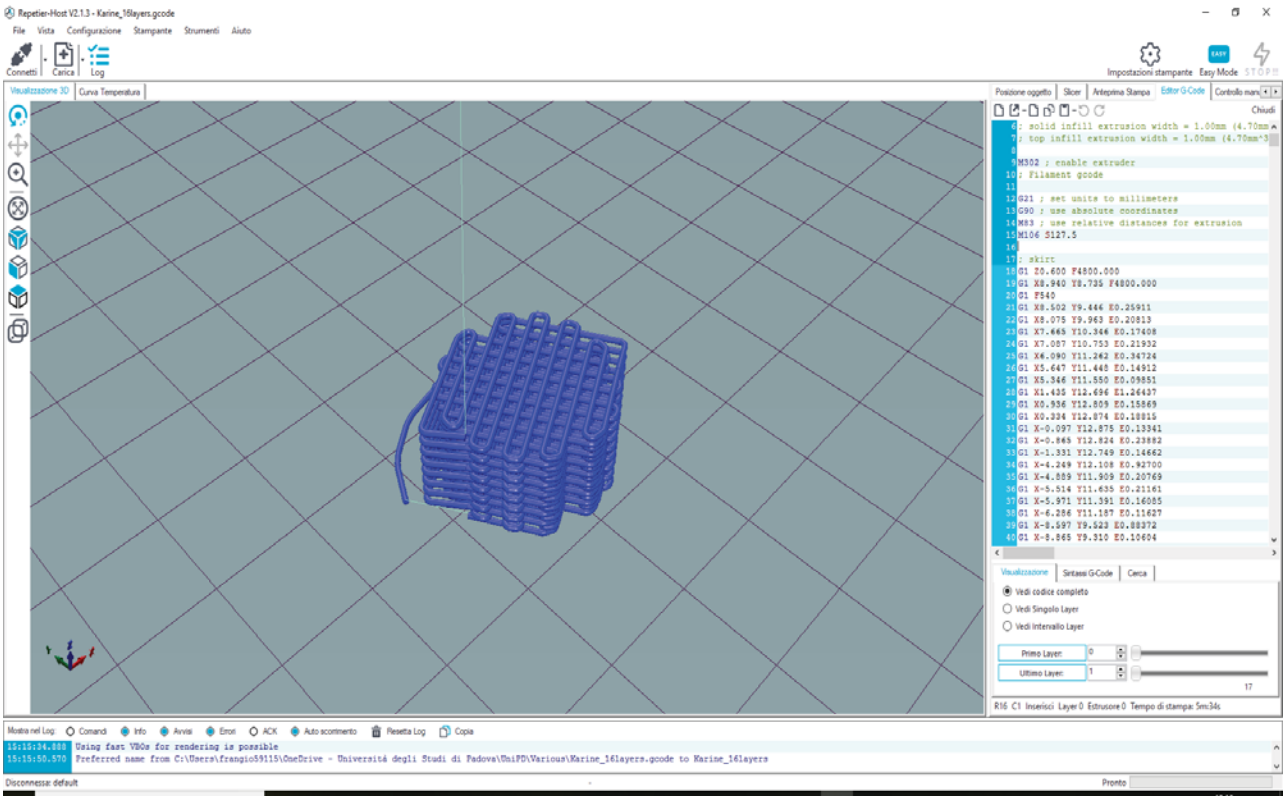

Fig. 5.5 *3D model visualization in the Solid Work®software*

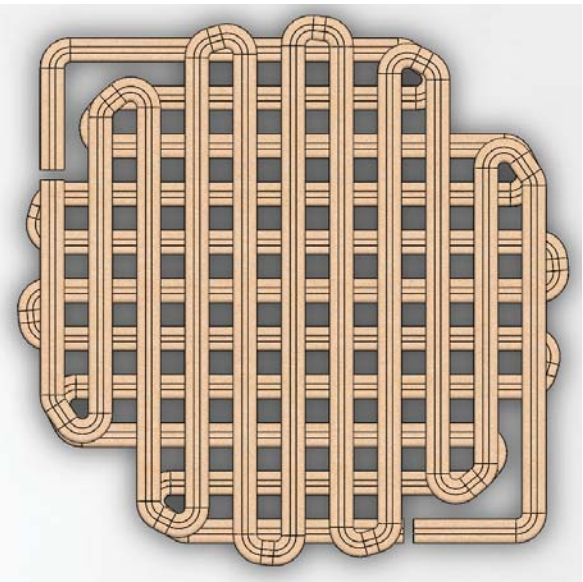

Fig. 5.6 *Top view of the 3D model*

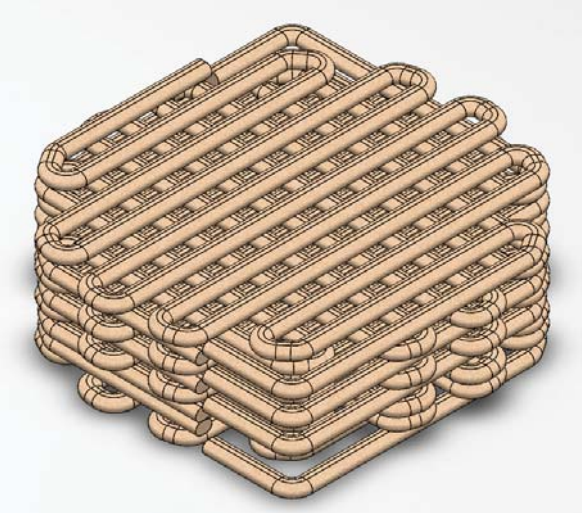

Fig. 5.7 *View from the side of the 3D model*

The lattice is composed of two filaments with the fist one oriented at 0° and the second at 90° to the horizontal, for a total of sixteen layers. The design is tetragonal with orthogonal layers of 0.8 mm wide parallel struts. The spanning distance between the struts was set at 1.6mm corresponding to a designed porosity of 59.16%.

Chapter 6

Result and discussion

The following chapter deals with the description and interpretation of the experimental results obtained by the characterization of the geopolymeric spheres.

6.1 Geopolymer spheres obtained

As can be seen from the Fig 6.1 the spheres obtained have a geometrically very accurate shape, demonstrating that the laboratory procedure chosen for their production is an extremely effective method. It can also be noted that the choice of the alkaline solution has no influence on the final shape of the spheres but that the spherical geometry depends only on the choice of the inert medium. Tests using PEG400 and PEG1000 confirms the above.

(a) **(b)**

Fig. 6.1 *K-based geopolymer spheres **(a)** and Na-Based **(b)***

6.2 Scanning Electron Microscopy (SEM)

For each sample, photos of the external and external surface were taken at 3 different magnifications (x100, x500, x2000); also, for each, microanalysis was provided to look for traces of PEG or ethanol.

6.2.1 Geopolymer K-Based

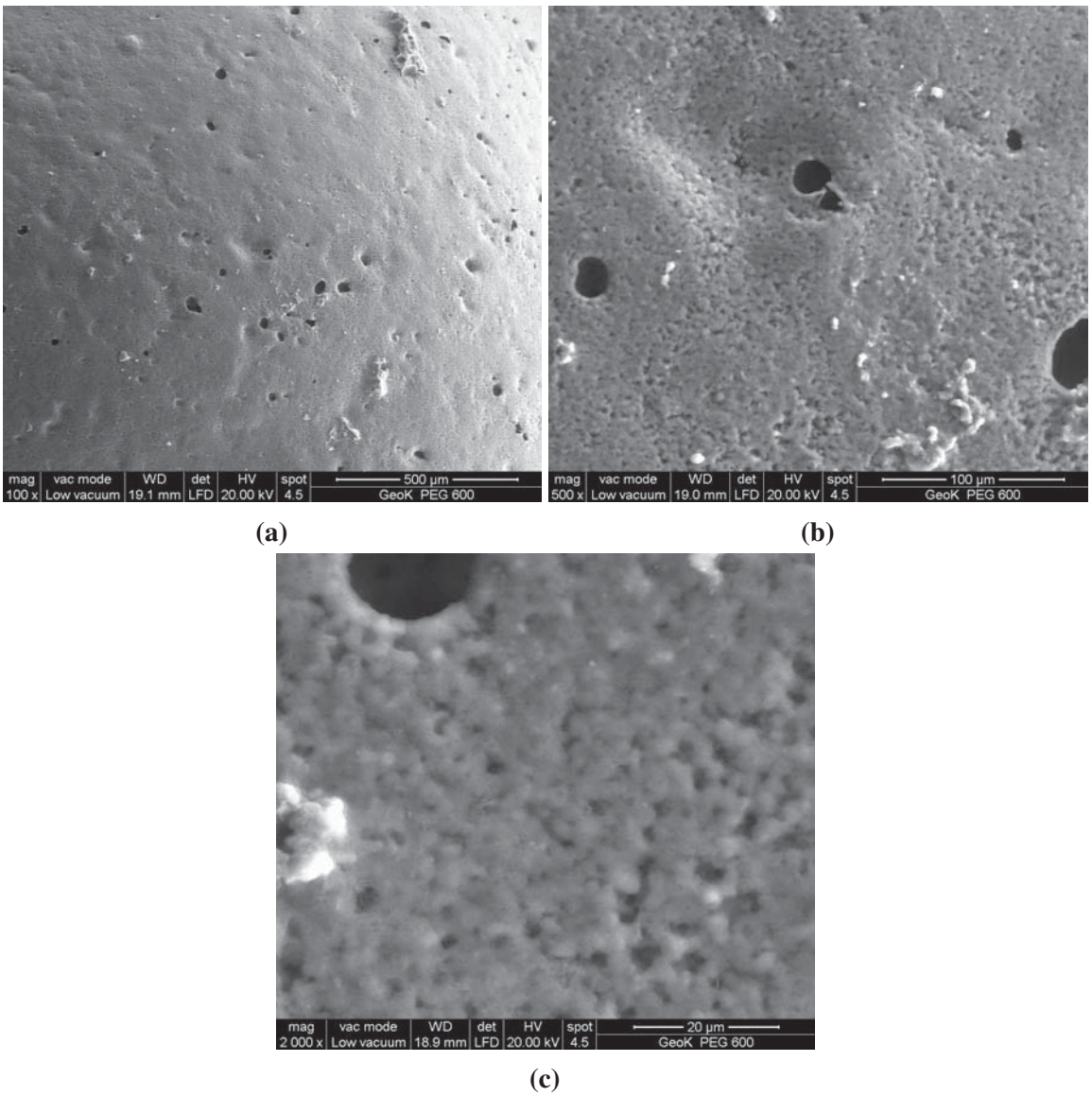

(a) **(b)**

(c)

Fig. 6.2 *SEM image external surface K-Based geopolymer, x100* ***(a)*** *x500* ***(b)*** *and x2000* ***(c)***

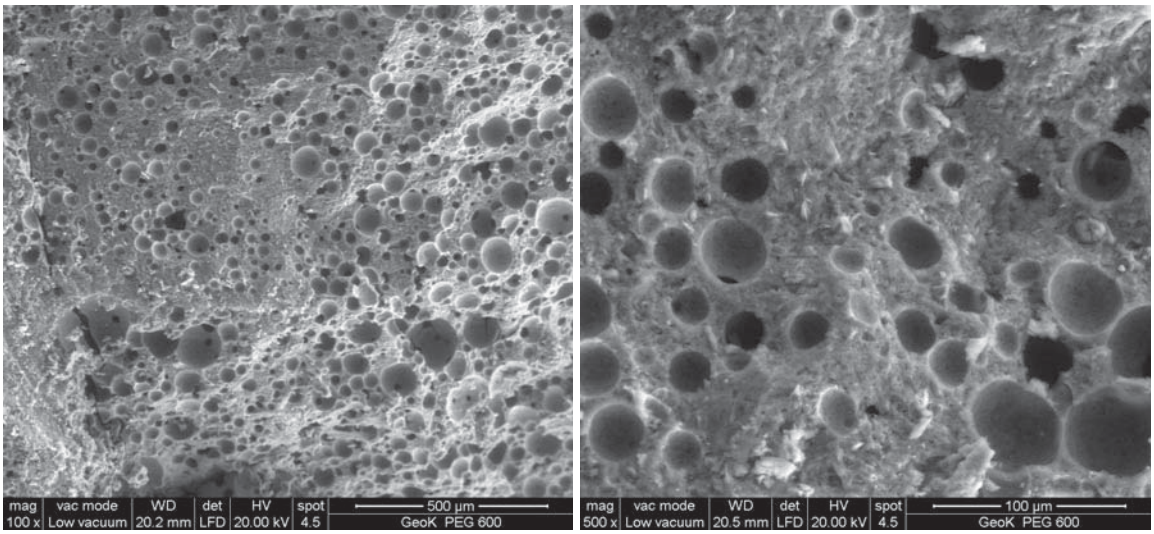

(a) *a* **(b)** *b*

(c) *c*

Fig. 6.3 *SEM image internal surface K-Based geopolymer, x100* ***(a)*** *x500* ***(b)*** *and x2000* ***(c)***

As you can see from the image 6.2 the use of the foaming agent allows to obtain external surface porosity(macro-type). This does not allow us to state that they will be permeable as it is not possible to determine, from the analysis of these photographs alone, the type of porosity obtained; however they justify the choice of more specific analysis (pycnometer). Also, the inner surface(Fig.6.3) has porosity and with comparison from the theory it can be assumed that it is meso-type (characteristic of geopolymeric materials)

6.2.2 Geopolymer Na-Based

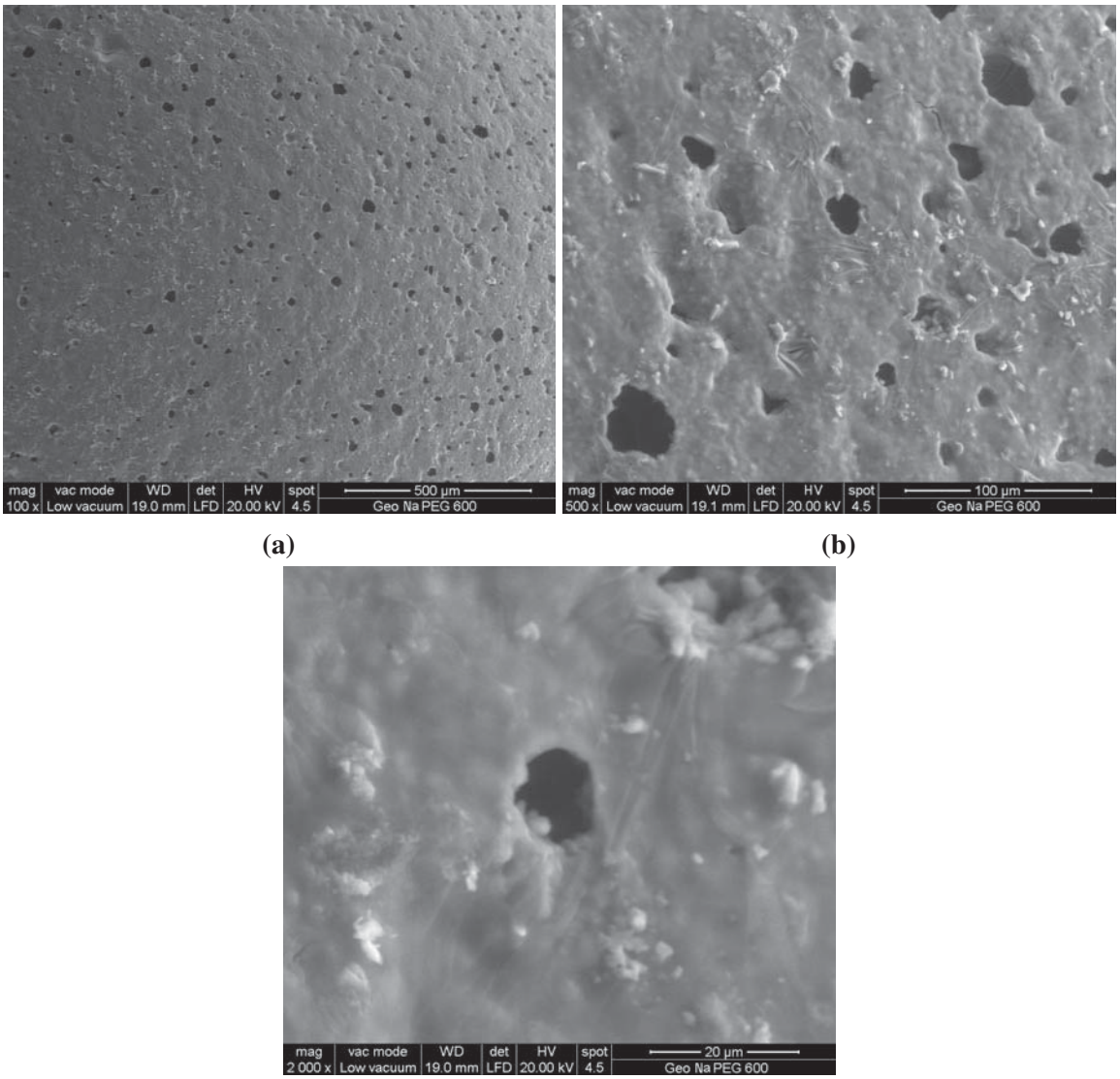

Fig. 6.4 *SEM image external surface Na-Based geopolymer, x100* ***(a)*** *x500* ***(b)*** *and x2000* ***(c)***

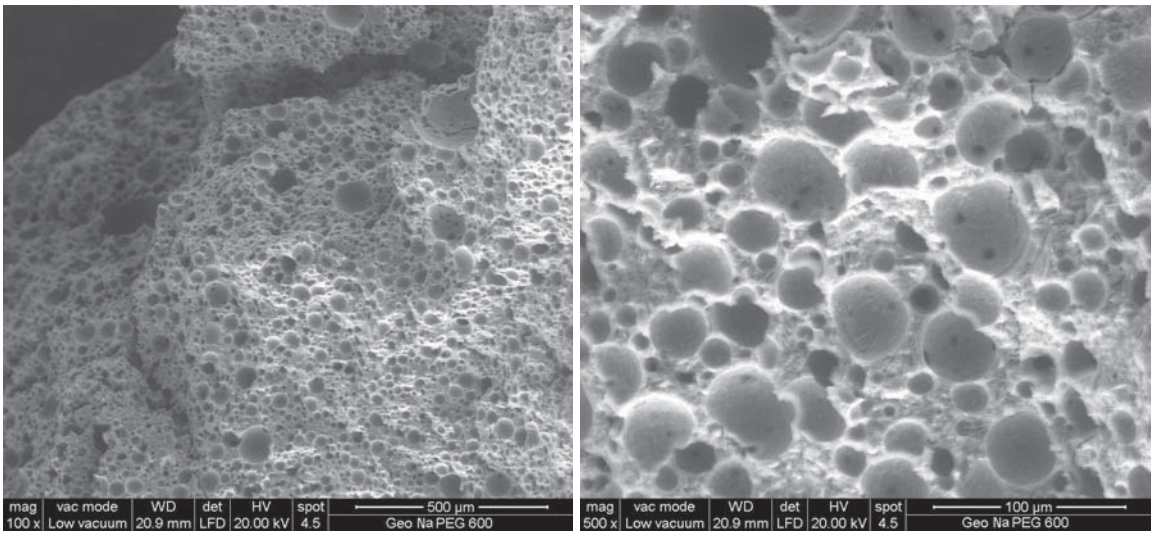

(a) **(b)**

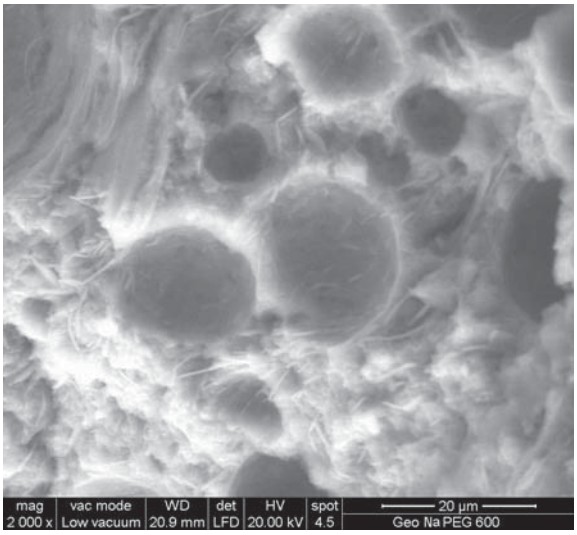

(c)

Fig. 6.5 *SEM image internal surface Na-Based geopolymer, x100* ***(a)*** *x500* ***(b)*** *and x2000* ***(c)***

Again as observable in Fig. 6.4 there is a presence of external surface porosity. The inner surface(Fig.6.5) has a porosity as well; there are no particular differences with the K-based spheres which suggest that there is no dependence between the porosity and the ions present inside the lattice.

6.2.3 Geopolymer mixed

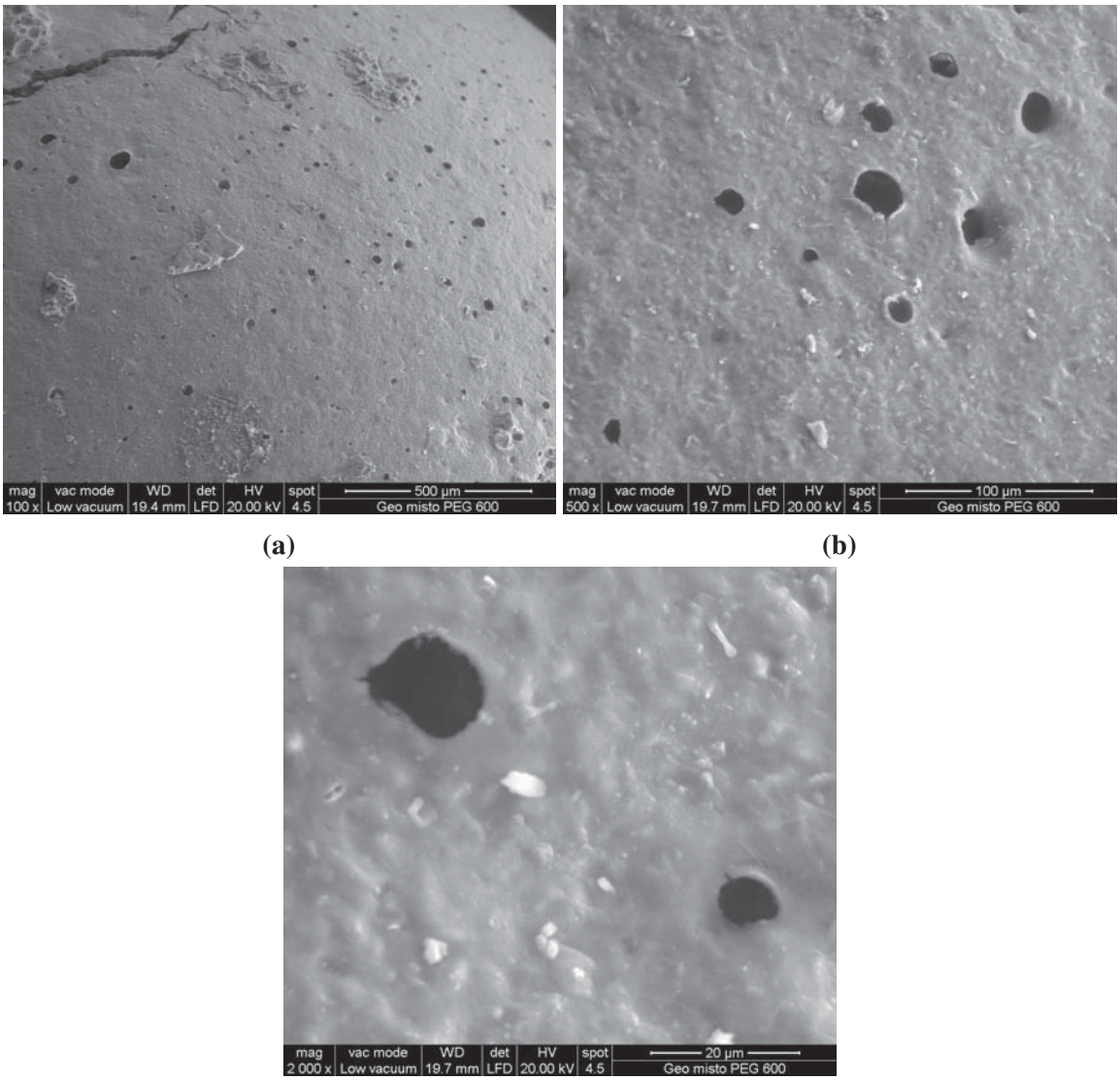

Fig. 6.6 *SEM image external surface Mixed geopolymer, x100* ***(a)*** *x500* ***(b)*** *and x2000* ***(c)***

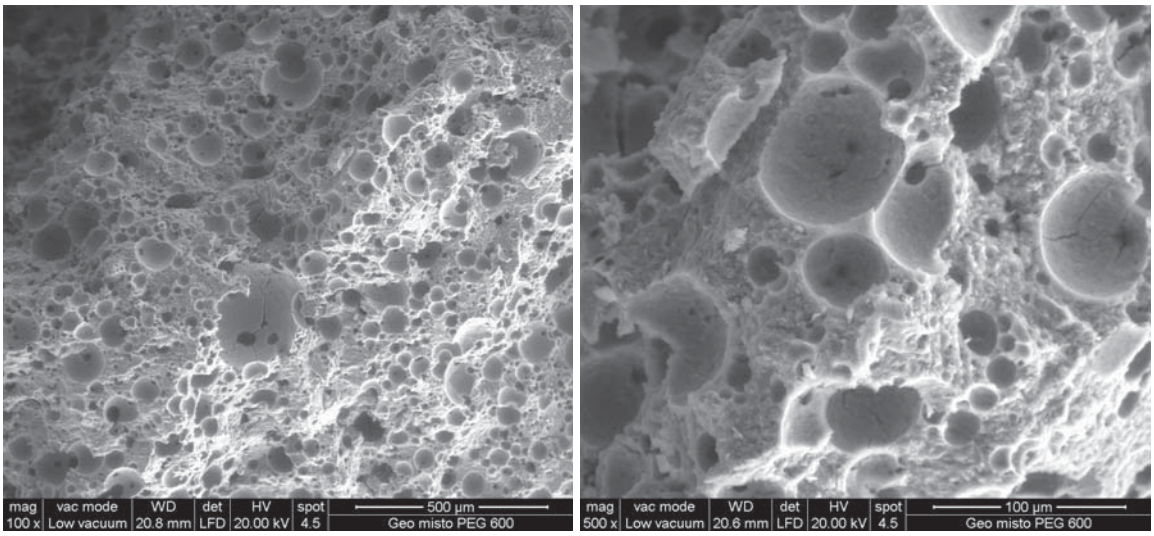

(a) **(b)**

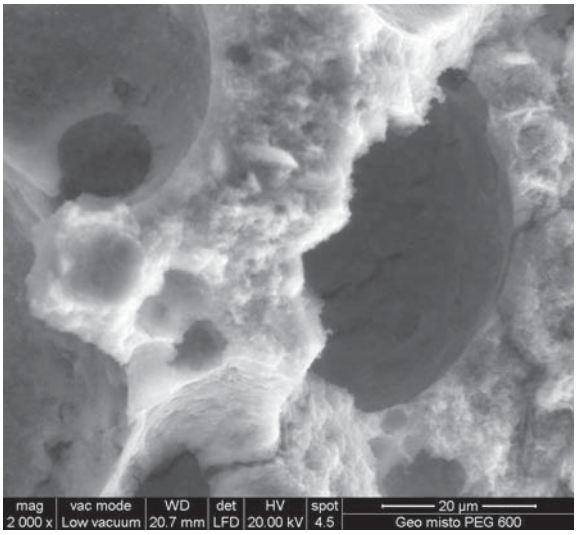

(c)

Fig. 6.7 *SEM image internal surface Mixed geopolymer, x100* ***(a)*** *x500* ***(b)*** *and x2000* ***(c)***

Regarding the spheres obtained with a mixed sodium-potassium solution, the images(Fig 6.10 & 6.11) do not show differences with the previous spheres. It is thus reasonable to assume that the porosity is influenced by the quantity of water present as a part of it is eliminated as a result of the geopolymerization reaction.

6.3 SEM mycroanalysis

Microanalyses using the electron microscope were carried out to search for any unreacted PEG or ethanol; the following results were found

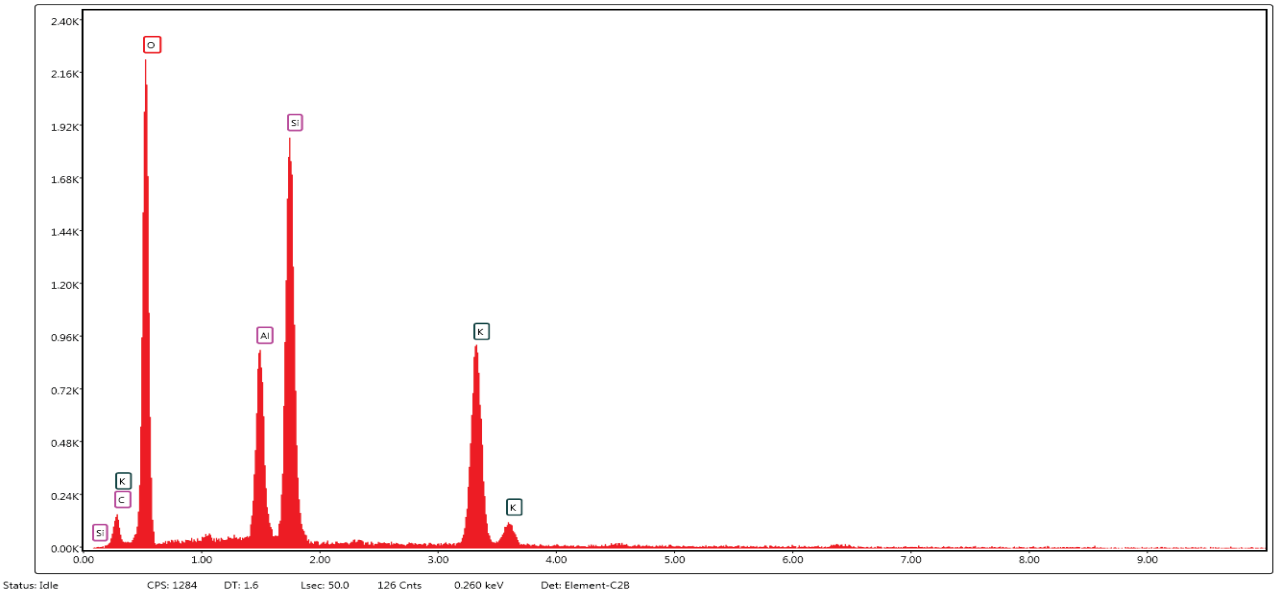

Fig. 6.8 *Microanalysis Geopolymer K-Based*

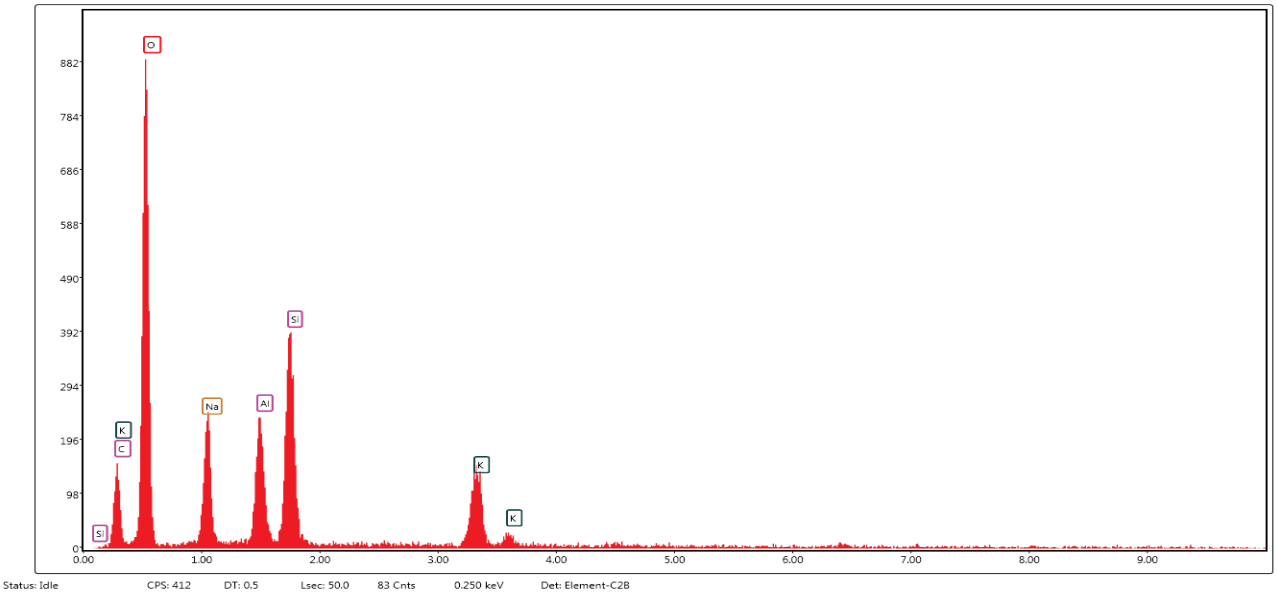

Fig. 6.9 *Microanalysis Geopolymer mixed solution*

The absence of traces of PEG is a guarantee of its inertia and of the effectiveness of using ethanol as a solution to perform spheres washing operations

6.4 Spheres with surface modification

Some spheres (K-Based) were coated by immersion for 30 minutes in $C_9H_{24}Cl^{15}NO_3Si$.

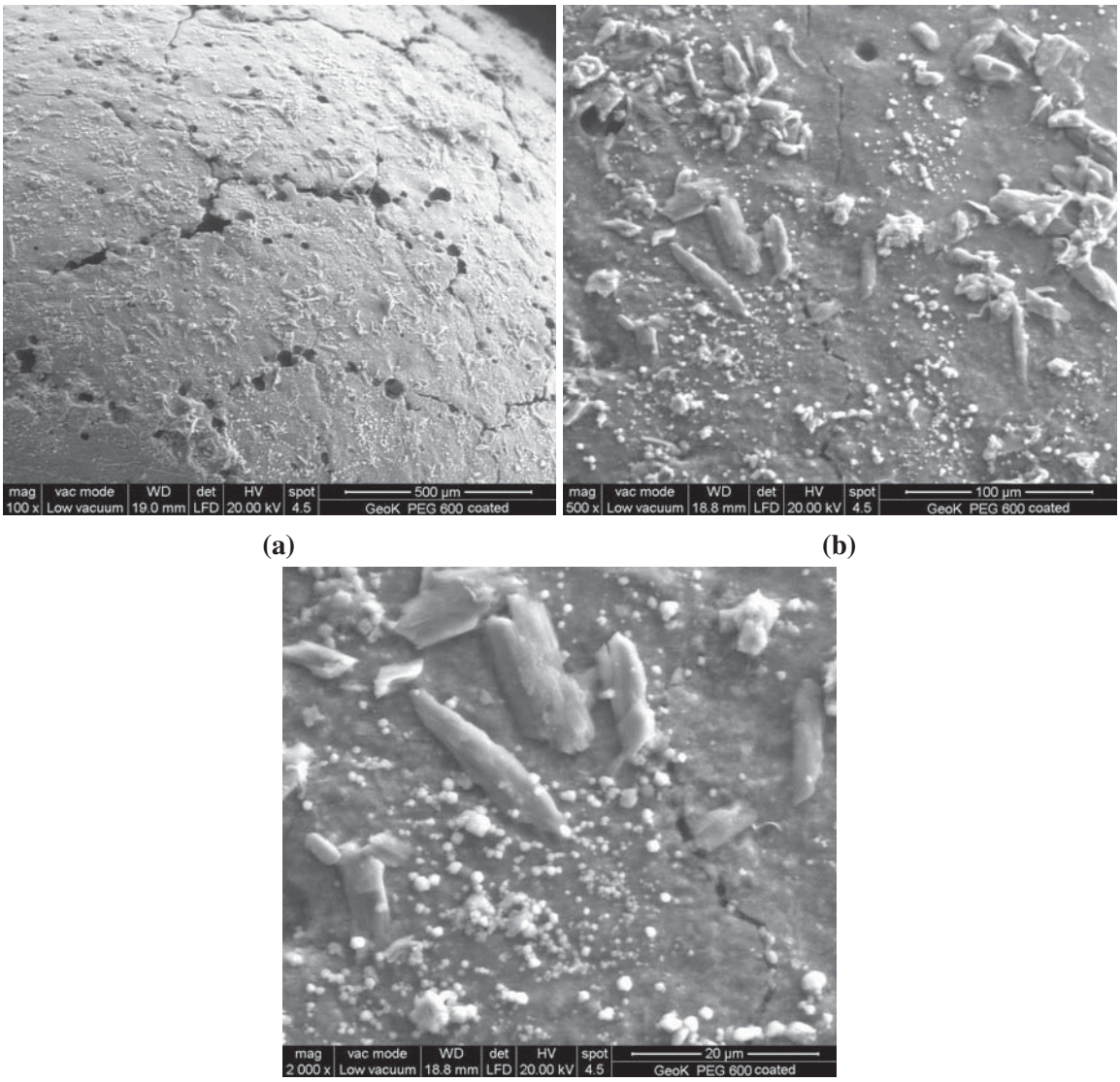

(a) **(b)**

(c)

Fig. 6.10 *SEM image external surface K-Based geopolymer modified by immersion in $C_9H_{24}Cl^{15}NO_3Si$, x100* ***(a)*** *x500* ***(b)*** *and x2000* ***(c)***

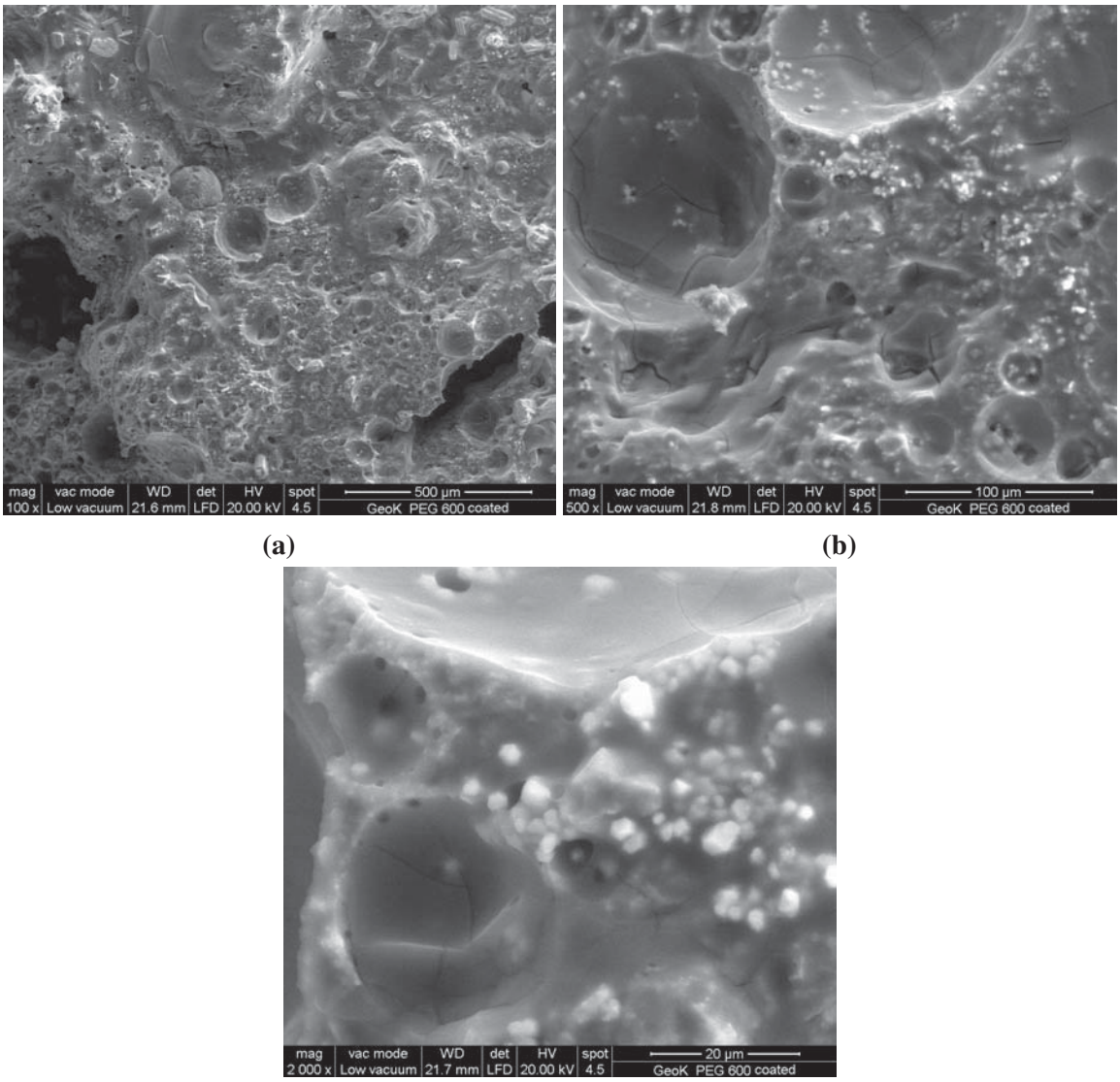

Fig. 6.11 *SEM image internal surface K-Based geopolymer modified by immersion in* $C_9H_{24}Cl^{15}NO_3Si$ *, x100* ***(a)*** *x500* ***(b)*** *and x2000* ***(c)***

It is possible to observe Cl residues in the internal and external structure of the coated spheres suggesting a probable infiltration through the mesopores of the geopolymer.

6.5 SEM Mycroanalysis of the coated spheres

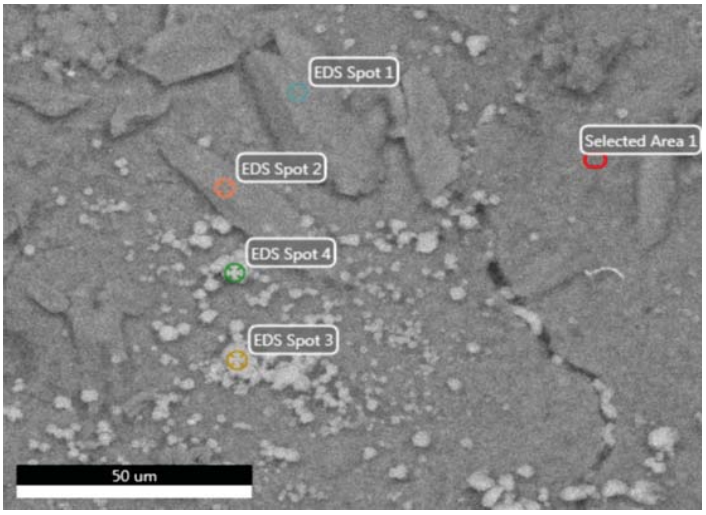

Fig. 6.12 *SEM image K-Based coated sphere with highlighted points chosen for microanalysis*

The figure 6.12 shows the 4 points for which the micro-analysis of the coated spheres have been carried out; only the results obtained from the analysis of point 1 and point 3 are reported, as points 2 and 4 show the same results:

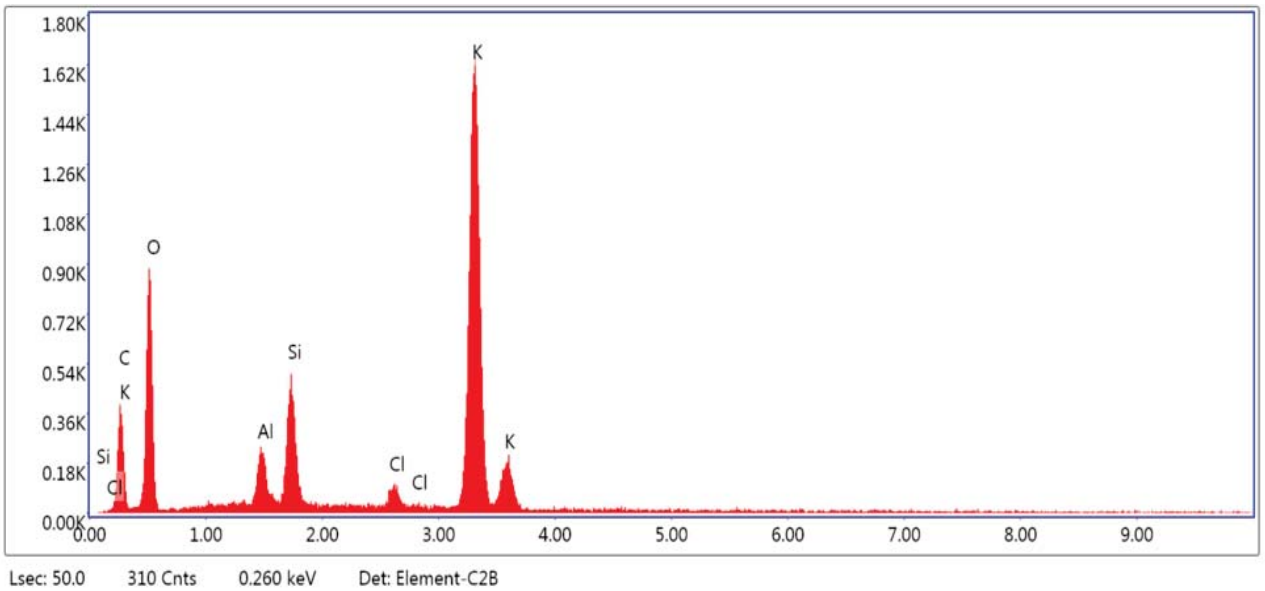

Fig. 6.13 *Microanalysis spectrum of point 1*

Element	Weight (%)	Atomic (%)	Net Int.	Error (%)	Kratio	Z	A	F
CK	9.36	16.74	32.96	11.41	0.0365	1.1147	0.3499	1.0000
OK	39.75	53.34	108.35	10.99	0.0723	1.0688	0.1704	1.0000
AlK	2.76	2.20	33.33	8.16	0.0192	0.9534	0.7273	1.0054
SiK	5.65	4.32	77.21	5.56	0.0448	0.9747	0.8091	1.0073
ClK	1.57	0.95	16.49	13.79	0.0198	0.9088	0.9435	1.0297
KK	40.92	22.47	22.47	351.52	2.18	0.3646	0.9048	1.0026

Table 6.1 *% Composition of point 1*

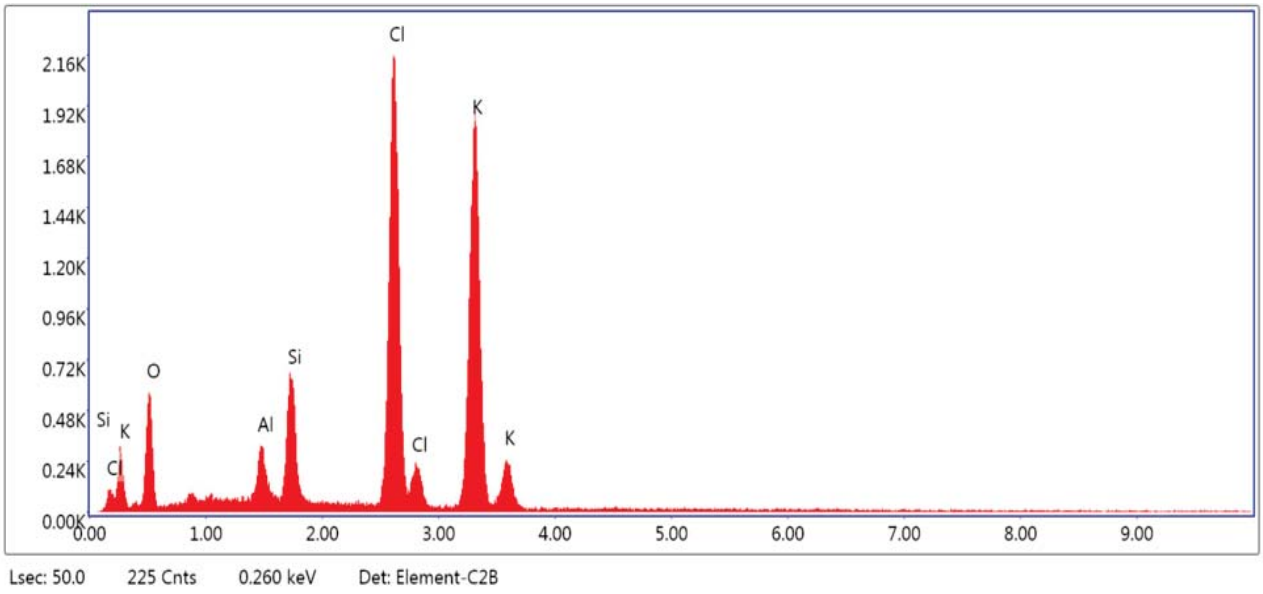

Fig. 6.14 *Microanalysis spectrum of point 3*

Element	Weight (%)	Atomic (%)	Net Int.	Error (%)	Kratio	Z	A	F
OK	23.90	41.38	73.05	11.56	0.0379	1.1189	0.1418	1.0000
AlK	2.91	2.99	48.96	7.13	0.0220	0.9998	0.7505	1.0064
SiK	5.75	5.67	108.31	4.76	0.0489	1.0223	0.8242	1.0091
ClK	30.11	23.52	424.03	2.39	0.2762	0.9538	0.9470	1.0154
KK	37.33	26.44	391.57	3.06	0.3158	0.9499	0.9499	1.0016

Table 6.2 *% Composition of point 3*

As can be seen from the Fig 6.13 6.14 and the respective tables 6.1 6.2 containing the % wt of each element present in the respective analysis areas, the white points visible from the previous SEM images, represent residual Cl.

6.6 XRD Analysis

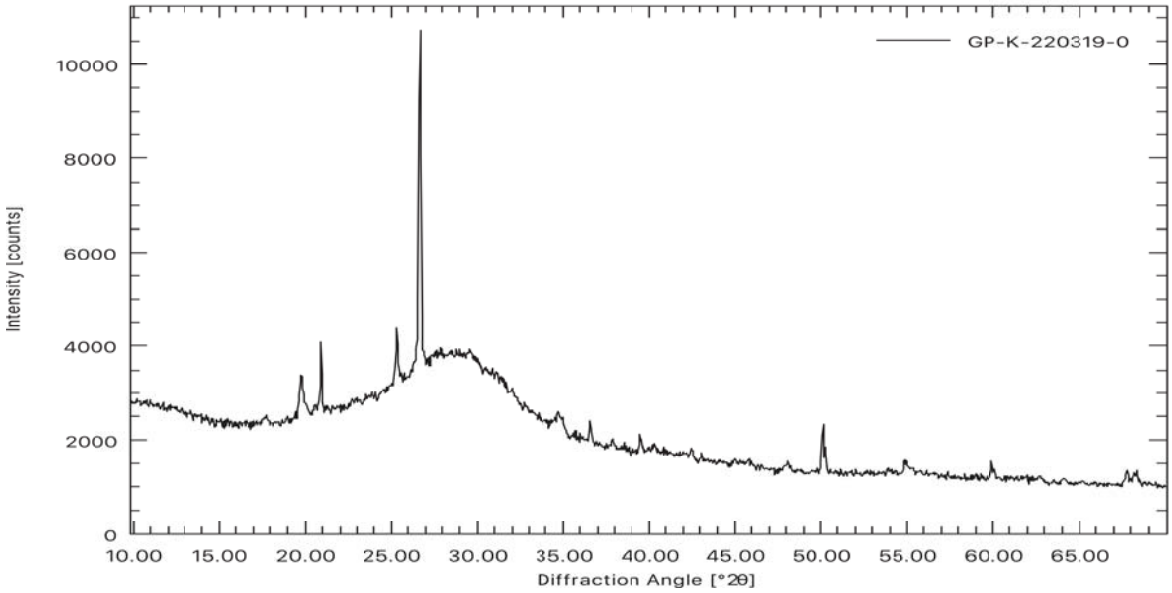

Fig. 6.15 *XRD K-Based Geopolymer*

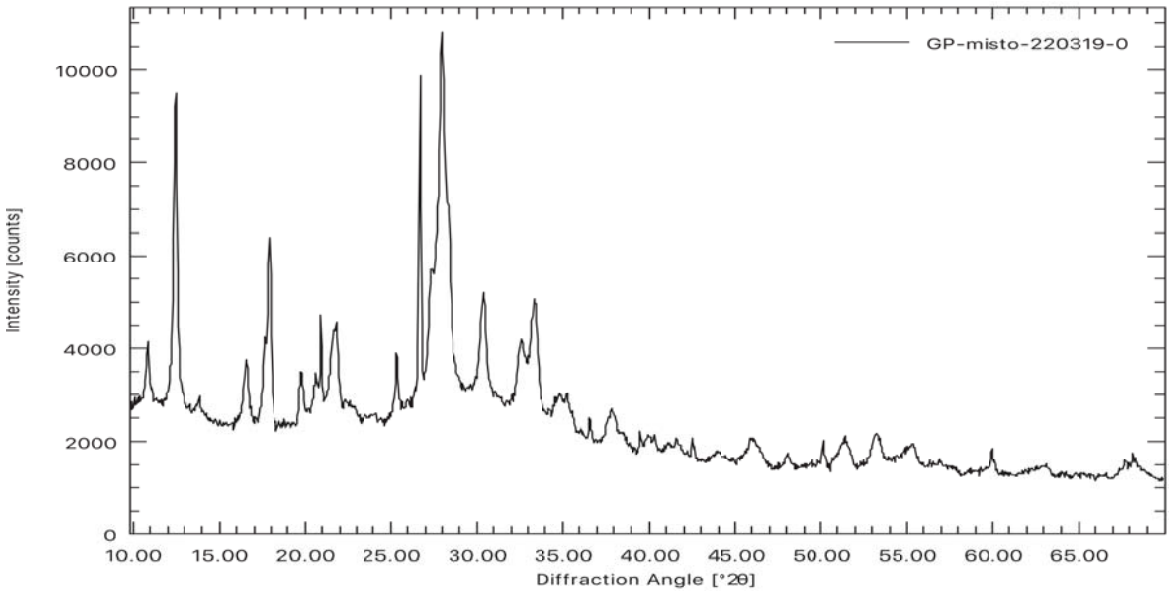

Fig. 6.16 *XRD mixed geopolymer*

In the XRD patterns (Fig 6.15 6.16) is possible to observe an amorphous matrix, with some peaks related to impurities typically found in metakaolin based geopolymers. The absence of further peaks related to any unreacted material shows that the reaction and treatment times have been chosen correctly.

6.7 Pycnometer data

Through density measurements carried out first on the spheres and then on the dust deriving from them, using the calculation method discussed in chapter 5 (about the porosity), it was possible to identify % and type of porosity. The following table shows the data obtained through the pycnometer analysis

K - based geopolimer spheres					
Run	**Volume** (cm^3)	**Deviation** (cm^3)	**Density** (g/cm^3)	**Deviation** (g/cm^3)	**Elapsed Time (h:m:s)**
1	0.2672	-0.0010	1.9110	0.0070	0:06:11
2	0.2688	0.0006	1.8997	-0.0043	0:08:04
3	0.2693	0.0011	1.8960	-0.0080	0:10:11
4	0.2682	0.0000	19039	-0.0001	0:12:40
5	0.2674	-0.0008	1.9095	0.0055	0:15:08
K-based geopolimer powder					
1	0.3483	0.0004	1.9620	-0.0024	0:06:43
2	0.3476	-0.0003	1.9643	-0.0001	0:11:43
3	0.3479	0.0000	1.9643	-0.0001	0:11:43
4	0.3476	-0.003	1.9661	0.0017	0:13:51
5	0.3480	0.0001	1.9636	-0.008	0:15:55

Table 6.3 *Pycnometer data of geopolymer K-Based*

Na-based geopolimer spheres					
Run	**Volume** (cm^3)	**Deviation** (cm^3)	**Density** (g/cm^3)	**Deviation** (g/cm^3)	**Elapsed Time (h:m:s)**
1	0.2338	-0.0009	2.0510	0.0084	0:05:12
2	0.2350	0.0002	2.0413	-0.0012	0:07:03
3	0.2356	0.0008	2.0361	-0.0015	0:08:44
4	0.2351	0.0003	2.0392	-0.0034	0:10:25
5	0.2344	-0.0004	2.0452	0.0274	0:12:12
Na-based geopolimer powder					
1	0.3036	0.1737	2.0643	-0.0002	0:04:35
2	0.3033	0.1737	2.0661	0.0016	0:06:25
3	0.3037	0.1740	2.0630	-0.0015	0:08:13
4	0.3034	0.1738	2.0652	0.0007	0:09:44
5	0.3036	0.1740	2.0639	0.0006	0:11:28

Table 6.4 *Pycnometer data of geopolymer Na-Based*

Mixed geopolimer spheres					
Run	**Volume** (cm^3)	**Deviation** (cm^3)	**Density** (g/cm^3)	**Deviation** (g/cm^3)	**Elapsed Time (h:m:s)**
1	0.2005	-0.0009	2.1910	0.0099	0:05:12
2	0.2013	-0.0002	2.1830	0.0019	0:07:03
3	0.2019	0.0005	2.1762	-0.0049	0:08:44
4	0.2021	0.0006	2.1745	-0.0067	0:10:25
5	0.2015	-0.0000	2.1809	-0.0002	0:12:12
Mixed geopolimer powder					
1	0.2590	-0.0002	2.1666	0.0020	0:04:35
2	0.2590	-0.0002	2.1662	0.0016	0:06:25
3	0.2596	0.0004	2.1617	-0.0029	0:08:13
4	0.2592	-0.000	2.1644	-0.0002	0:09:44
5	0.2593	0.0001	2.1642	-0.0005	0:11:28

Table 6.5 *Pycnometer data of mixed geopolymer*

The table 6.6 shows the average diameters of the balls measured using a caliper. The entire calculation process, already discussed in the chapter 5 was carried out using the Microsoft Excel®software; the calculation screen is shown below

	Mean diameter (mm)			
	Sphere 1	Sphere 2	Sphere 3	Sphere 4
K PEG 600	3.91	4.51	4.17	4.42
Na PEG 600	4.51	4.22	4.32	4.2
Mixed PEG 600	4.51	4.22	4.32	4.2

Table 6.6 *Spheres diameter measured*

K PEG 600		Diameter (mm)			
		Sphere 1	Sphere 2	Sphere 3	Sphere 4
Repetitions	1	3,91	4,51	4,17	4,42
	2	3,91	4,51	4,17	4,42
	3	3,91	4,51	4,17	4,42
	Mean Diameter (mm)	3,91	4,51	4,17	4,42
	Mean Ray (mm)	1,96	2,26	2,09	2,21
	Mass (g)	0,0351	0,0391	0,0309	0,0363
	Volume (cm^3)	0,0313	0,0480	0,0380	0,0452

ρa (g/cm^3)	1,9040
ρt (g/cm^3)	1,9644
ρg (g/cm^3)	0,8701
OP (%)	54,30
TP (%)	55,71
CP (%)	1,41

(a)

Na PEG 600		Diameter (mm)			
		Sphere 1	Sphere 2	Sphere 3	Sphere 4
Repetitions	1	4,48	3,97	4,47	4,09
	2	4,52	4,41	4,20	4,23
	3	4,54	4,29	4,3	4,28
	Mean Diameter (mm)	4,51	4,22	4,32	4,20
	Mean Ray (mm)	2,26	2,11	2,16	2,10
	Mass (g)	0,0405	0,0416	0,041	0,037
	Volume (cm^3)	0,0481	0,0394	0,0423	0,0388

ρa (g/cm^3)	1,8844
ρt (g/cm^3)	1,967
ρg (g/cm^3)	0,9491
OP (%)	49,63
TP (%)	51,75
CP (%)	2,12

(b)

MIxed PEG 600		Diameter (mm)			
		Sphere 1	Sphere 2	Sphere 3	Sphere 4
Repetitions	1	4,48	3,97	4,47	4,09
	2	4,52	4,41	4,20	4,23
	3	4,54	4,29	4,3	4,28
	Mean Diameter (mm)	4,51	4,22	4,32	4,20
	Mean Ray (mm)	2,26	2,11	2,16	2,10
	Mass (g)	0,0399	0,0391	0,04	0,037
	Volume (cm^3)	0,0481	0,0394	0,0423	0,0388

ρa (g/cm^3)	2,1811
ρt (g/cm^3)	2,1646
ρg (g/cm^3)	0,9248
OP (%)	57,60
TP (%)	57,28
CP (%)	-0,32

(c)

Fig. 6.17 *Porosity calculations of K-based* ***(a)*** *Na-based* ***(b)*** *and mixed geopolymer* ***(c)*** *through Microsft Excel®*

where:

- ρa = Apparent density : whole sphere (picnometer)
- ρt = Total density : dust (picnometer)
- ρg = Geometric density
- OP(%) = Open porosity
- TP(%) = Total porosity
- CP(%) = Closed porosity

As can be seen from the results shown in the figure, all the spheres obtained presented almost all of the open porosity which is exactly what we wanted to achieve to ensure their permeability. As for mixed geopolymer spheres, a negative value of CP has no physical meaning and is probably caused by some approximation error or some error in the measurement phase; it is, however, an extremely low value therefore negligible.

6.8 Adsorption test

As mentioned above, absorption tests were performed in the laboratories of the University of Turin thanks to the collaboration of professor Mariella Bruzzoniti. The following table shows the results obtained

Tested Samples	**Contaminants Removal(%)**					
	Cd	**Cr**	**Ni**	**Pb**	**As**	**Se**
Na (PEG 600)	44.3	65.0	66.3	93.2	-	-
K (PEG 600)	39.3	52.8	54.9	-	76.5	59.6
Mixed (PEG 600)	43.6	47.0	57.4	60.0	78.8	62.8

Table 6.7 *Removal percentage of contaminants to each type of spheres, after a contact time of 24 h in solutions with a concentration of 8 mg.L^{-1} for each contaminant.*

The absorption tests with metal ions were performed for the spheres, were cationic ion exchange occurred, as expected. The mixed spheres showed a removal for all ions, while for the K sphere with PEG 600, the greater removal was for Pb ions. So far, the obtained results were negative for adsorption of the anionic herbicide glyphosate, tested only with the coated spheres. Further work is undergoing to improve the results. The results for cationic removal were positive and its characterization was satisfactory, suggesting that these spheres can be used for water purification.

6.9 Mechanical properties

The machinery used for the compression tests on the samples is an INSTRON™Tensile Testing Machine model 1121. The instrument is formed by a vertical column with instrumentation for controlling the force and the speed of descent or ascent of the load cell. A digital system has been added to the original data acquisition system, connected to an electronic processor, so as to obtain the data supplied by the load cell in real time. The output of the force applied to the specimen during the test is obtained, through the specific software, through a graph in real time force / time generated by the computer. In this case the machinery is used in the compression test configuration, but it also has the possibility of carrying out tensile or bending tests. The following table shows the data obtained from the tests carried out on the spheres

	Sphere diameter (mm)	**Compressive strength (MPa)**
K PEG 600	4.32±0.14	0.48±0.19
Na PEG 600	4.44±0.2	0.87±0.22
Mixed PEG 600	4.11± 0.34	0.53± 0.25

Table 6.8 *Compression strength of the geopolymer spheres*

The compressive strength of the spheres is limited but, for this application, the values found are satisfactory.

6.10 3D filters

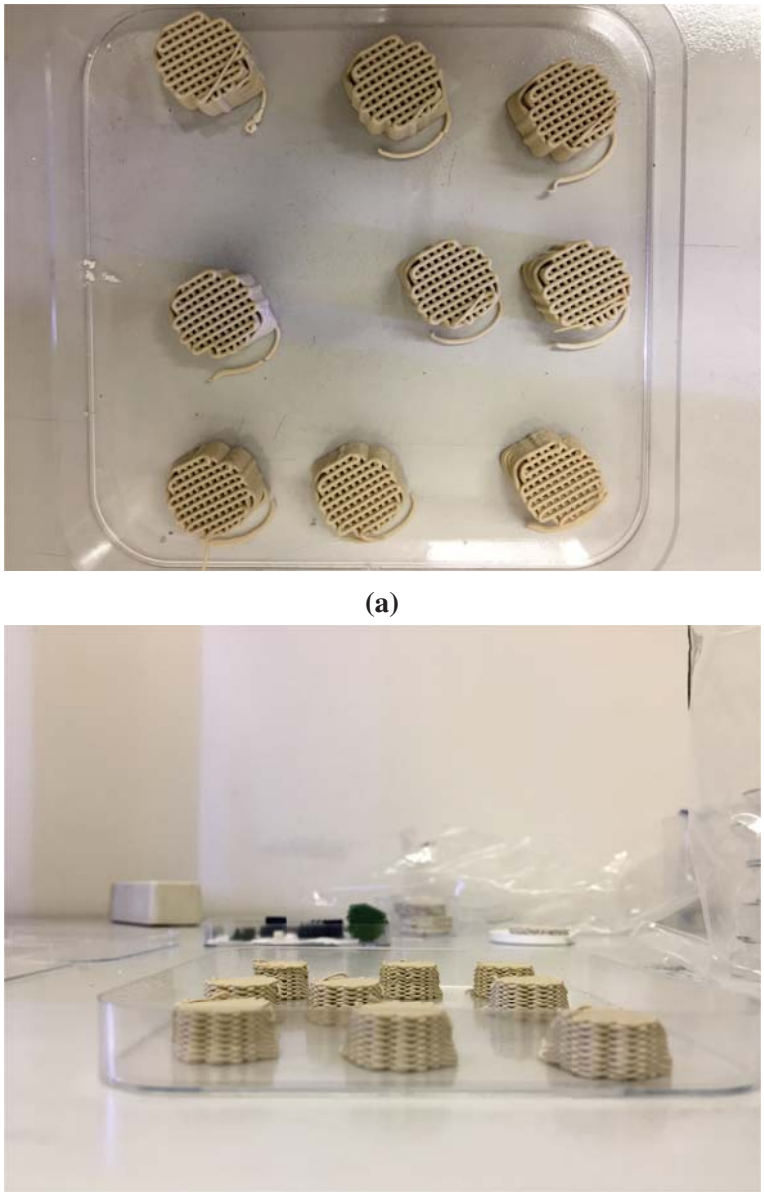

(a)

(b)

Fig. 6.18 *Images for the filters obtained from top view **(a)** and from the side **(b)***

As it is possible to observe (fig 6.18) the production of the 3D structures, using the geopolymer as the ink with the compositions already specified in chapter 4, took place successfully. These structures then subsequently have to be subjected to heat treatment and subsequent analyzes similar to those made for the spheres; however, due to lack of time, it was not possible to carry out these steps.

Conclusion

The present study was designed to manufacture and characterize porous geopolymer based material to be used in the water purification column. Three types of geopolymer have been considered to take into account the effect of the presence of different ions inside the lattice. The tests carried out on the spheres have not demonstrated substantial differences between the types of geopolymer analyzed, suggesting that the characteristics are only influenced by the original composition (obviously intended as molar relations). Open porosity was successfully obtained thus ensuring the permeability of the spheres. In conclusion, it can be stated that was possible to obtain geopolymeric spheres successfully. The results for cationic removal were positive and, even though the removal for anionic contaminant was negative for coated spheres, its characterization was satisfactory, suggesting that these spheres can be used for water purification. Also concerning the structures obtained with 3D printing, the results are satisfactory even if no characterization was made due to lack of time. Further works are still in progress.

References

[1] V. D. Glukhovsky. 'soil silicates'. *Gosstroyizdat Ukrainy Publishing (in Russian).*, 1959.

[2] D. M. Roy and C. A. Langton. Studies of ancient concretes as analogs of cementituos sealing materials for repository in tuff. *Los Alamos National Lab., NM (United States)*, (LA-11527-MS), 1989.

[3] J. Davidovits. Proc. 1st int. conf. on geopolymers. In *Soft mineralurgy and geopolymers*, volume 1, page 19– 23, Compiegne, France, June 1988.

[4] J. Davidovits. Geopolymers: Ceramic-like inorganic polymers. *Journal of Ceramic Science*, 2017.

[5] Hua Xu and J. S. J. van Deventer. The effect of alkali metals on the formation of geopolymeric gels from alkali feldspars. *Colloids Surf. A: Physiocochem. Eng. Aspects*, 216:27–44, 2003.

[6] J. S. J. Van Deventer J. G. S. Van Jaarsveld and L. Lorenzen. *Miner.Eng*, 10(7):659, 1997.

[7] J. Castro-Gomes F. Pacheco-Torgal and S. Jalali. Tungsten mine waste geopolymeric binder: preliminary hydration products inves- tigations.

[8] J.Davidovits. Chemistry of geopolymeric systems, terminology. *Proc. Int. Conf. Geopolymer*, pages 9–40, 1999.

[9] J.Davidovits. Proc. 1st int. conf. on alkaline cements and concretes. In *Properties of geopolymer cements*, pages 131–149, Kiev State Technical University, 1994.

[10] L. Maffucci R. Cioffi and L. Santoro. Optimisation of geopoly- mer synthesis by calcination and polycondensation of a kaolinitic residue.

[11] Glukhovsky VD. Soil silicates. page 154, 1959.

[12] Tregloan PA Swaddle TW Salerno J. Chem soc rev. 23, 1994.

[13] Nagy JB Crea F Derouane EG Dumont N Nastro A Subotic B Testa F Ivanova II, Aiello R. Micropor mater. 3, 1994.

[14] Faimon J. Geochim cosmochim acta. 60, 1996.

[15] Sobrados I Sanz J Fernandez-Jimenez A, Palomo A. Micropor mesopor mater. 91, 2006.

[16] Provis JL. Phd thesis, university of melbourne. 2006.

[17] Van Deventer JSJ Duxson P, Lukey GC. J mater sci. 2006.

[18] Hill F.C. Boisen Jr M.B. Downs R.T. Gibbs, G.V. *Molecules as a Basis for Modeling the Force Field of Silica*, chapter 6. R.A.B. Devine, J.-P. Duraud and E. Dooryhee, John Wiley and Sons Ltd, 2000.

[19] J.Davidovits. Iupac international symposium on macromolecules stockholm. In *Solid phase synthesis of a mineral block poly- mer by low temperature polycondensation of aluminosili- cate polymers*, September 1976.

[20] Swaddle T.W. North, M.R. Kinetics of silicate exchange in alkaline aluminosilicate solutions. *Inorg. Chem.*, 39:2661–2665, 2000.

[21] J. S. J. Van Deventer J. L. Provis, P. Duxson and G. C. Lukey. The role of mathematical modelling and gel chemistry in advancing geopolymer technology. *Chem. Eng. Res. Design*, 83:853–860, 2005.

[22] M. Biesemans J. Wastiels H. Rahier, B. Van Mele and X. Wu. Low- temperature reaction stoichiometry and structure of a model compound. *J. Mater. Sci*, 31:71–79, 1996.

[23] N. Sahai M. R. Anseau, J. P. Leung and T. W. Swaddle. Interactions of silicate ions with zinc (ii) and aluminium (iii) in alkali aqueous solution. *Inorg. Chem*, 44:8023–8032, 2005.

[24] Kinetics of silicate exchange in alkaline aluminosilicate solutions. *Inorg. Chem*, 39: 2661–2665, 2000.

[25] K. Sagoe-Crenstil P. De Silva and V. Sirivivatnanon. Kinetics of geopolymerisation: role of Al_2O_3 and SiO_2. *Cement Concrete Res.*, 37:512–518, 2007.

[26] J. L. Provis and J. S. J. van Deventer. Geopolymerisation kinetics. 1. in situ energy-dispersive x-ray diffractometry. *Chem. Eng. Sci.*

[27] T. Brown L. Weng, K. Sagoe-Crentsil and S. Song. Effects of aluminates on the formation of geopolymers. *Mater. Sci. Eng. B*, 117:163–168, 2005.

[28] J. L. Provis and J. S. J. van Deventer. Geopolymerisation kinetics. 2. reaction kinetic modelling. *Chem. Eng. Sci*, 62:2318–2329, 2007.

[29] J. Faimon. Oscillatory silicon and aluminum aqueous concentra- tions during experimental aluminosilicate weathering. *Geochim. Cosmochim. Acta*, 60:2901–2907, 1996.

[30] Bell J. Gordon M Kriven, W.M. Microstructure and micro- chemistry of fully-reacted geopolymers and geopolymer matrix composites. *Ceram. Trans.*, 153:227–250, 2003.

[31] Zongjin Li Yunsheng Zhang. Synthesis and microstructural characterization of fully reacted potassium poly(sialate-siloxo) geopolymeric cement matrix. *Aci Materials Journal*, page 161, 2008.

[32] J.S.J. Lukey G.C. Xu H. Sindhunata, van Deventer. Effect of curing temperature and silicate concentration on fly ash-based geopolymerization. *Ind. Eng. Chem. Res.*, 45: 3559 – 3568, 2006.

[33] MacKenzie K.J.D. Thaumaturgo C. Barbosa, V.F.F. Synthe- sis and characterization of materials based on inorganic poly- mers of alumina and silica: sodium polysialate polymers. *Int. J. Inorg. Mater.*, 2:309–317, 2000.

[34] M.R. Rowles. *The structural nature of aluminosilicate inor- ganic polymers: A macro to nanoscale study.* Phd Thesis, Curtin University of Technology, Perth, Australia, 2004.

[35] Z. Huajun C. Yue Z. Zuhua, Y. Xiao. Role of water in the synthesis of calcined kaolin based geopolymer. *Appl. Clay Sci*.

[36] F. Yan H. Wang, H. Li. Synthesis and mechanical properties of metakaolinite based geopolymer. *Colloids Surf. A: Physicochem. Eng. Aspects*, 268:1–6, 2005.

[37] D. Zaharaki K. Komnitsas and V. Perdikatsis. Effect of synthesis parameters on the compressive strength of low-calcium ferronickel slag inorganic polymers. *J. Haz. Mater*, 161:760–768, 2009.

[38] A. van Riessen J. Temuujin and R. Williams. Influence of calcium compounds on the mechanical properties of fly ash geopolymer pastes. *J. Haz. Mater*.

[39] Framework-type determination for zeolite structures in the inorganic crystal structure database, shujiang yang and mohammed lach-hab iosif i. vaisman estela.

[40] Porosity, characterization and structural proposities of natural zeolite–clinoptilolite-as a sorbent, m. mansouri,n. rikhtegar, h. ahmad pabahi, .

[41] Ion exchange in geopolymers,jose ramon gasca-tiradoalejandro manzano-ramirezalejandro manzano-ramirezeric m. riveramunozshow, .

[42] Metal ions as probes for characterization of geopolymer materials, oleg bortnovskyjiri dedecekjiri dedecekzdenka tvaruzkovashow, .

[43] Adsorption processes for water treatment and purification, adrian bonilla-petriciolet didilia ileana mendoza-castillo hildaelizabethreynel-avila, .

[44] Giles ch, macewan th, nakhwa sn, smith d (1960) studies in adsorption. part xi. a system of classification of solution adsorption isotherms, and its use in diagnosis of adsorption mechanisms and in measurement of specific surface areas of solids. j chem soc 3973–3993, .

[45] The heavy metal adsorption characteristics on metakaolin-based geopolymer,t.w. cheng m.l.lee m.s.ko t.h.ueng s.f.yang, .

[46] Purkait, m.k., gusain, d.s., dasgupta, s., de, s., 2004. adsorption behavior of chrysoi- dine dye on activated charcoal and its regeneration characteristics using different surfactants. separation science and technology 39 (10), 2419–2440.

[47] Flow of fluids through granular beds and packed columns, chapter 4.

[48] Mccabe w, smith jc, harriot p (2005) unit operations of chemical engineering. mcgraw-hill, new york.

[49] Foust as, wenzel la, clump cw, maus l, andersen bl (1980) principles of unit operations. wiley, new york.

[50] Richardson et al., 2000.

[51] Giani et al., 2005.

[52] Pressure drop measurements and modeling on sic foams, maxime lacroix, patrick nguyen, daniel schweich, cuong pham huu, sabine savin-poncet, david edouarda.

[53] J. choi, o.-c. kwon, w. jo, h.j. lee, m.-w. moon, 4d printing technology: a review, 3d print, addit. manuf. 2 (2015) 159–167, http://dx.doi.org/10.1089/ 3dp.2015.0039.

[54] Direct ink writing of geopolymeric inks, giorgia franchin, paolo scanferla, luca zeffiro, hamada elsayeda, andrea baliello, giovanni giacomello, marco pasetto, paolo colombo.

[55] Jose Guilherme L. F. Alves Kinematic Viscosities of Poly(ethylene glycols) Marina S. Cruz, Lucy D. A. Chumpitaz and State University of Campinas (UNICAMP) P.O. Box 6121 Campinas SP 13083-970 Brazil Antonio J. A. Meirelles LASEFI, Food Engineering DepartmentsFEA, 2017.

[56] J. Faimon. Oscillatory silicon and aluminum aqueous concentrations during experimental aluminosilicate weathering. *Department of Mineralogy, Petrography, and Geochemistry, Masaryk University.*, 1995.

[57] Jose Guilherme L. F. Alves Marina S. Cruz, Lucy D. A. Chumpitaz and Antonio J. A. Meirelles. Kinematic viscosities of poly(ethylene glycols). *State University of Campinas (UNICAMP),Brazil*, 2000.

[58] Rubina Chaudhary Divya Khale. Mechanism of geopolymerization and factors influencing its development: a review. *Springer Science*, 2007.

[59] Joseph Davidovits. 30 years of successes and failures in geopolymer applications. market trends and potential breakthroughs. *Geopolymer Conference, Melbourne, Australia*, 2002.

[60] Joseph Davidovits. Geopolymer chemistry and applications. *Institut geopolymere*, 2000.

[61] J.S.J. van Deventer J.L. Provis. Geopolymerisation kinetics,2 reaction kinetic modelling. *Department of Chemical and Biomolecular Engineering, The University of Melbourne,Australia*, 2006.

[62] J.S J. Van Deventer J.L. Provis, P. Duxson and G. C. Luke. The role of mathematical modelling and gel chemistry in advancing geopolymer technology. *Department of Chemical and Biomolecular Engineering, The University of Melbourne, Victoria, Australia*, 2005.

[63] Jose Guilherme L. F. Alves Marina S. Cruz, Lucy D. A. Chumpitaz and Antonio J. A. Meirelles. Kinematic viscosities of poly(ethylene glycols). *State University of Campinas (UNICAMP),Brazil*, 2000.

[64] Joseph Davidovits and Michel Davidovics. Geoplymer ultra high temperature tooling materal for the manufacture of advanced composites. *Geopolymer Institute, Cordi-Geopolymere SA*, 1991.

[65] Hanna Runtti Janne Pesonen Juho Yliniemi Ulla Lassi Tero Luukkonen, Anne Heponiemi. Application of alkali activated materials for water and wastewater treatment a review. *Reviews in Environmental Science and Bio Technology*, 2019.

[66] K Afshar E. Abkar H. Kister, J. Scherffius. Realistically predict capacity and pressure drop for packed columns. 2007.

[67] Daniel Schweichc Maxime Lacroixa, Patrick Nguyenb. Pressure drop measurements and modeling on sic foams. *Chemical Engineering Science*, 2007.

[68] D.G. Kroger K.G. Allen, T.W. von Backstrom. Packed bed pressure drop dependence on particle shape, size distribution, packing arrangement and roughness. *Department of Mechanical and Mechatronic Engineering, University of Stellenbosch,South Africa*, 2013.

[69] Nikolai Kolev. Packed bed columns. for absorption, desorption, rectification and direct heat transfert.

[70] Jonathan Worstell. Fixed bed reactor. 2014.

[71] Jacques J. G. M. van Bokhoven Freek Kapteijn Marco J. G. Linders, Martijn B. L. van der Weijst and Jacob A. Moulijn. Design of an industrial adsorption process with activated carbon for the removal of hexafluoropropylene from wet air. *Chemical Engineering Department, Industrial Catalysis Section, Delft University of Technology*, 2001.

[72] Barry Crittenden W. J. Thomas. Adsorption technology and design. *Elsevier Science and Technology Books*, 1998.

[73] Long Fumei Hu Mingyu, Zhu Xiaomin. Alkali activated fly ash based geopolymers with zeolite or bentonite as additives. *College of Civil Engineering, Nanchang University, Nanchang, Jiangxi, China*, 2009.

[74] Yuelian Peng Shaobin Wanga. Natural zeolites as effective adsorbents in water and wastewater treatment. *Chemical Engineering Journal*, 2009.

[75] Mohd Mustafa Al Bakri Abdullah Nurliyana Ariffin. Review on adsorption of heavy metal in wastewater by using geopolymer. 2016.

[76] R. Torres L. Gomez C. Villa, E.T. Pecine. Geopolymer synthesis using alkaline activation of natural zeolite. 2010.

[77] Henk Nugteren Aleksandar Nikolova, Ivan Rostovsky. Geopolymer materials based on natural zeolite. 2017.